AUSTRAL
JOURNAL OF IMAGING
REVISTA CHILENA DE RADIOLOGÍA

Indexed in: SciELO, Scopus, EMBASE, DOAJ, LATINDEX Catálogo 2.0, MIAR, Bibliovigilance, Dialnet
ISSN: 2810-6954 / e-ISSN: 2810-708X
VOLUME 32. ISSUE 3, JULY-SEPTEMBER 2026

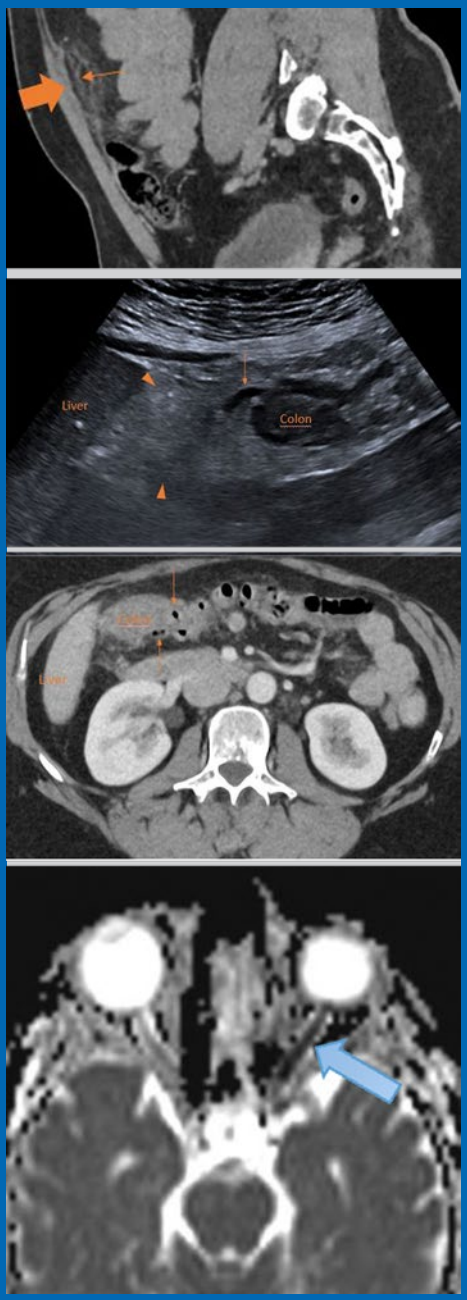

PERMANYER
www.permanyer.com

www.resochradi.com

AUSTRAL
JOURNAL OF IMAGING
REVISTA CHILENA DE RADIOLOGÍA

Indexed in: SciELO, Scopus, EMBASE, DOAJ, LATINDEX Catálogo 2.0, MIAR, Bibliovigilance, Dialnet
ISSN: 2810-6954 / e-ISSN: 2810-708X
VOLUME 32. ISSUE 3, JULY-SEPTEMBER 2026

Editorial Board

PERMANYER
www.permanyer.com

www.resochradi.com

11902ACHI263

AUSTRAL JOURNAL OF IMAGING
REVISTA CHILENA DE RADIOLOGÍA

PERMANYER

Check for updates

EDITORIAL

«The secret of change is to concentrate all your energy not on fighting the old, but on building the new.» (Socrates, 470 BC - 399 BC)

«El secreto del cambio es concentrar toda tu energía no en luchar contra lo viejo, sino en construir lo nuevo» (Sócrates, 470 a.C. - 399 a.C.)

David Ladrón de Guevara-Hernández

Editor in Chief, Austral Journal of Imaging/Revista Chilena de Radiología, Santiago, Chile

In 2022, when I accepted the challenge of leading the editorial direction of our *Revista Chilena de Radiología*, I honestly didn't quite know what I was getting myself into, since the work of an associate editor – which I had been doing for several years – is objectively quite different from that of editor-in-chief. After this period of hard work, I understand the importance of the position, which is not limited only to reading and correcting articles, but also involves leading a multi- and transdisciplinary human team as effectively as possible, and shaping and guiding the development of a journal with a history and prestige like ours.

I believe we have succeeded in creating a more global journal with a greater international presence, due both to its bilingual nature and the diverse platforms on which it is available: SOCHRADI (*Sociedad Chilena de Radiología*/Chilean Society of Radiology), with the complete collection dating back to 1992; SciELO, which serves as our regional showcase with issues from 2002 onward; and Permanyer, our window to the world with issues in English and Spanish available since 2022. A dedicated journal website, with direct access from the web and links to these platforms, is a logical step in this development and remains a goal for future challenges.

In 2024, our journal debuted its new name, *Austral Journal of Imaging*, a name with a global and international identity, focused on increasing circulation through a primary English version that includes articles with DOIs in the universal language of science. The choice of the new name was the result of an interesting and prolific forum, including brainstorming, carried out between historical editors, associate editors of that time and contributors to the journal, in which the *Austral Journal of Imaging* prevailed by majority vote.

With the aim of improving the quality of articles, the first reviewer training course was held in 2025, which focused on the multidimensional optimization of the peer review process, a critical element in the task of improving the articles. The course successfully ushered in the era of *e-learning*, becoming the first of its kind offered by SOCHRADI. It had over 50 participants, and with the possibility of being repeated at discretion to train new teams of reviewers who join the journal. Today, our editorial team has managed to establish itself as a solid and functional group of people, with extensive experience and suitable preparation. We also currently have an advisory editorial committee comprised of specialists in statistics, radiation protection, and other non-medical areas who have completed this

Correspondence:
David Ladrón de Guevara-Hernández
E-mail: humdavidhm@hotmail.com

Date of reception: 27-03-2026
Date of accptance: 13-04-2026
DOI: 10.24875/AJI.M26000040

Available online: 14-07-2026
Austral J. Imaging. (Engl. ed.). 2026;32(3):101-102
www.resochradi.com

Table 1. Progress achieved in the last 4 and a half years

Progress	Date
First bilingual issue in Spanish and English	January 2022
DOAJ indexing	March 2022
Digitization of the complete collection dating from 1995	November 2022
Formation of the international editorial committee	June 2023
SOCHRADI 80th anniversary of printed edition	October 2023
Strategic meeting of the journal with historical editors, contributors, and the editorial committee	October 2023
ORCID code for each author	October 2023
Forum for name change: prevailing *Austral Journal of Imaging* (AJI)	October 2023
Incorporation of AJI to social media	November 2023
Name change to AJI is implemented: English-language journal	January 2024
Single DOI in English	January 2024
AJI editorial committee attends the "Publications in Radiodiagnosis 2024 SERAM" course sponsored by SOCHRADI	March 2024
AJI re-indexed in SciELO	June 2024
Acquisition of anti-plagiarism software	June 2024
Journal's 30th anniversary of printed edition	October 2024
AJI re-indexed in Scopus	October 2024
Use of *software* for detection of generative artificial intelligence	January 2025
Restructuring of the editorial committee's organizational chart (co-editor and advisory editorial committee: statistics, radiation protection, etc.)	March 2025
First AJI/SOCHRADI reviewers' course	September 2025
Indexing in Bibliovigilance	March 2026

course and who will undoubtedly contribute to further improving the quality of the articles.

The consolidation of an international editorial team in addition to the national one, the systematic use of the ORCID code with its icon at the bottom of each author's profile, transparency in the authorship declarations, the implementation of anti-plagiarism software and generative artificial intelligence detectors in the editorial process, the appropriate implementation of marketing and scientific dissemination, and the important DOAJ (Directory of Open Access Journals) indexing, all point to the development of a modern journal that meets the current editorial guidelines of excellence.

It is noteworthy that following the name change from *Revista Chilena de Radiología* to *Austral Journal of Imaging*, which occurred at the beginning of 2024 (Table 1), with the loss of rankings and a fresh start to accumulate citations from scratch, the current SJR index is significantly higher than it was in the last year of *Revista Chilena de Radiología*, with the consequent improvement in our position relative to other national medical journals. This remarkable increase in readership and citations is undoubtedly due in large part to greater visibility and, especially, the global access inherent in an English-language journal.

We believe that the quality of published texts is the critical factor that must be improved today, essential for reaching higher levels of recognition. How can we achieve this? By further improving our editorial and peer-review processes, opening ourselves up to the world to increase the number of readers and authors interested in submitting manuscripts to our journal, and, of course, encouraging regional research and, consequently, the production of original articles.

Today, as I conclude my term as editor-in-chief, I believe I am leaving the journal in good standing and prepared to face the challenges that will undoubtedly come in the future. I sincerely thank the three boards of directors of SOCHRADI with whom I had the privilege of working, and especially the invaluable help of Carmen, Andrea, Pablo, and Gabriela, always willing to lend a hand in any way they could. I also thank and acknowledge the tremendous work of Permanyer, especially of María and Silvia, without whom this journal could not have faced the changes and transformations that have taken place. I will continue to contribute from the editorial committee and also as an author of articles for our journal, a task I certainly miss.

I therefore welcome Dr. Patricia Guzmán, a radiologist specializing in abdominal and pelvic imaging, with a master's degree in Health Sciences Education, and a long history as a contributor and also as co-editor of our journal, who will now lead the team and guide the future steps of the *Austral Journal of Imaging*. I am confident that her leadership and incredible work ethic will boost the growth and development of our beloved magazine.

AUSTRAL JOURNAL OF IMAGING
REVISTA CHILENA DE RADIOLOGÍA

PERMANYER

Check for updates

LETTER TO THE EDITOR

Simple X-rays, complex responsibility: an ongoing dilemma

Radiografías «simples», responsabilidad compleja: un dilema vigente

Luis Canales-Franco

Imaging Unit, Hospital Regional de Ñuble, Chillán; Faculty of Medicine, Universidad Católica de la Santísima Concepción, Concepción. Chile

Dear Editor:

X-rays are the foundational technique of imaging, and despite the development of computed tomography (CT), magnetic resonance imaging (MRI), hybrid imaging, and interventional radiology, they remain the most frequently requested examination in most healthcare systems. However, a progressive disengagement of radiologists from their interpretation has taken hold in the Chilean public sector, primarily to delegate functions of the specialist to other, "more complex" methods. This trend has become normalized under the erroneous notion that simple radiography is an "easy" or low-complexity technique, which has justified its delegation to non-radiologist physicians without sufficient training.

In Europe, conventional radiology represents between 60 and 75% of the total activity of imaging services.[1] Despite this, a significant portion of the reports are not submitted by radiologists, a phenomenon that stems not only from resource limitations, but also from a mindset that underestimates the complexity of the method. North American evidence is even more categorical: almost half of the radiographs performed by non-radiologists lack an adequate report, with omissions in findings, diagnostic conclusions, or insufficient documentation to allow for a follow-up or re-evaluation.[2]

In Chile, although formal studies do not exist, the reality is evident: the vast majority of radiographs in the public healthcare system are interpreted by non-radiologist physicians, often without the necessary training in technique, radiological anatomy, or semiology. International evidence confirms that this practice is not harmless: almost half of the radiographs evaluated by non-radiologists have incomplete or insufficient reports[2], and significant diagnostic omissions have been described, such as pulmonary nodules or unstable fractures overlooked in initial readings.[3] This problem is exacerbated because, at the undergraduate level, radiology instruction is often minimal and frequently delivered by non-radiologist professionals, creating a vicious cycle: the "simple" is taught in a simplified way, the simplified is interpreted without method, and the misinterpreted is normalized as adequate. Thus, a quality standard lower than the actual potential is legitimized. The result of this practice is the training of generations who lack the necessary conceptual understanding to interpret a technique that forms the very basis of radiology. This raises the question: are these colleagues aware of the responsibility they bear when interpreting such a demanding method such as this? And, similarly, when expanding the availability of equipment in hospitals, family health centers (*centros de salud familiar – CESFAM in Chile*), or high-resolution emergency services (*servicios de alta resolución de urgencia – SAR in Chile*), does the healthcare authority consider this human factor in its attempt to increase diagnostic capacity by delegating a critical examination to those who have not been adequately trained?

A second, distinct but complementary phenomenon is the progressive distancing of the radiologists themselves from radiography. Although often perceived as "basic," radiography is a demanding technique: multiple structures are superimposed in one or two projections, and the diagnosis depends on the interpretation of shadows, densities, and contours in a two-dimensional image. This inherent ambiguity requires a deep knowledge of three-dimensional anatomy and a tolerance for uncertainty that

Correspondence:
Luis Canales-Franco
E-mail: luiscanalesf@gmail.com

Date of reception: 21-12-2025
Date of acceptance: 21-02-2026
DOI: 10.24875/AJI.25000083
Available online: 14-07-2026
Austral J. Imaging. (Engl. ed.). 2026;32(3):103-104
www.resochradi.com

not all modalities demand. For many young or trainee radiologists, this complex interpretive terrain generates insecurity and fosters a preference for sectional methods such as CT or MRI, where anatomy is displayed in a more orderly manner. This shift, while understandable, impoverishes the specialist's cognitive foundation, whose radiological reasoning is based on the integration between anatomy, projection, and semiology.

A third problem, strictly related to training, is the progressive decrease in exposure to radiographs in residency programs. In public hospitals, the volume of patient care and the prioritization of advanced techniques significantly reduce the time dedicated to radiography. When the residents train in environments where this technique is considered secondary, their interpretive skills are weakened. This training deficit not only limits the competence of future radiologists but also deepens the dependence on more complex methods to solve problems that could be adequately addressed with a well-executed and well-interpreted radiograph. In this context, are we tacitly accepting that a 21st-century radiologist cannot properly interpret a radiograph?

The clinical repercussions of this phenomenon are widely documented. Discrepancies of up to 19% exist in chest radiographs interpreted by emergency physicians,[4] along with significant diagnostic variability among experienced observers,[5] and low diagnostic accuracy for common thoracic pathologies when the reading is performed outside of radiology.[6] These errors not only affect the clinical course but also increase the repetition of studies, radiation exposure, and system costs.[3]

The legal dimension is also not minor. In countries with explicit regulations, the radiology report is considered an integral part of the imaging procedure, and its omission has resulted in legal sanctions.[1] Although Chile lacks specific regulations, professional liability arising from incorrect or incomplete interpretation remains in effect, especially when the reading is delegated without criteria or institutional support.

In this context, artificial intelligence (AI) emerges as a promising tool, particularly in emergency medicine. Algorithms can support the detection of pneumonia, fractures, or pneumothorax with good performance. However, uncritical reliance on these tools could exacerbate the decline in interpretive skills, as AI does not replace anatomical understanding or the ability to integrate variations, artifacts, or clinical context.

Something similar could occur with the increasing widespread use of simplified ultrasound or echoscopy. Its use outside of radiology departments, with less standardization and without solid training, could replicate the trivialization observed in simple radiography. Ultrasound, even more dependent on the operator, risks losing diagnostic value if it becomes an examination without structure, criteria, or adequate supervision.

In short, reinstating simple radiography at the heart of clinical practice requires concrete and feasible measures, such as ensuring the radiologist's participation in its interpretation in emergency and inpatient settings, strengthening its systematic teaching at the undergraduate level, and guaranteeing structured exposure during residency. Recognizing the complexity of the technique and explicitly assuming professional responsibility for its interpretation not only strengthens the specialty, but also improves the quality of care and directly contributes to patient safety.

Funding

The author declares that he have not received funding.

Conflicts of interest

The author declares no conflicts of interest.

Ethical considerations

Protection of human subjects and animals. The author declares that no experiments on humans or animals were performed for this research.

Confidentiality, informed consent, and ethical approval. The study does not involve personal data, medical records, or human biological samples; therefore, ethical approval is not required. The SAGER guidelines do not apply.

Declaration on the use of artificial intelligence. The author declares that Chat GPT was used for editorial support in grammatical review, verification of formal consistency, and word count, without generating original scientific content for the manuscript.

References

1. Valdés Solís P, Morales Santos Á, González Álvarez I, Martínez Serrano C. El informe de la radiología simple: algo más que un imperativo legal. Radiología. 2013;55(4):279-82.
2. Weiner SN. Radiology by nonradiologists: is report documentation adequate? Am J Manag Care. 2005;11(12):781-5.
3. Pérez-Peña del Llano M, Llavona Amor JA, González Huerta C, Gutiérrez Pérez I, Quispe León C, Guerra del Barrio E. El informe de la radiología simple de urgencias: más que una buena práctica, nuestra obligación [Internet]. Seram; 2015. Disponible en: https://piper.espacio-seram.com/index.php/seram/article/view/516/332
4. Eng J, Mysko WK, Weller GE, Renard R, Gitlin JN, Bluemke DA, et al. Interpretation of Emergency Department Radiographs. AJR Am J Roent-genol. 2000;175:1233-8.
5. Robinson P, Wilson D, Coral A, Murphy A, Verow P. Variation between experienced observers in interpretation of A&E radiographs. Br J Radiol. 1999;72:323-30.
6. Alaseri ZM. Accuracy of chest radiograph interpretation by emergency physicians. Emerg Radiol. 2009;16:111-4.

AUSTRAL JOURNAL OF IMAGING
REVISTA CHILENA DE RADIOLOGÍA

PERMANYER

Check for updates

ORIGINAL ARTICLE

Contrast-enhanced mammography-guided biopsy: initial experience

Biopsia bajo guía de mamografía con contraste: experiencia inicial

Paulina Neira-Vallejos, María C. Vial, Carolina Behnke, and Rodrigo Herrmann*

Radiology Department, Centro de la Mama de Clínica MEDS La Dehesa, Santiago, Chile

Abstract

Introduction: *Contrast-enhanced mammography (CEM) is a breast imaging technique which displays suspicious lesions that enhance with iodinated contrast, similar to magnetic resonance imaging (MRI), detecting lesions that may not be represented on conventional techniques such as mammography and breast ultrasound.* **Objective:** *To evaluate the feasibility and performance of CEM-guided percutaneous biopsy and compare these results with those of MRI-guided biopsy.* **Materials and methods***: A prospective observational study of lesions diagnosed as suspicious by CEM or breast MRI, which underwent CEM biopsy. Patients and their lesion characteristics, procedural details, histopathological results, and procedural success, were recorded.* **Results:** *A total of 43 patients, with a median age of 50 years, were referred for CEM biopsy during the study period. The lesion type was primarily non-enhancing mass (72%) with a median size of 12 mm. The biopsy success rate was 40/43 (93%). In more than half of the cases, the procedure was performed based on the MRI finding, without CEM prior to the biopsy. The median procedure time was 17 minutes. The malignancy rate was 15%, and the high-risk lesion rate was 30%, with one case of underdiagnosis (2.5%).* **Conclusion:** *CEM biopsy is a safe and reliable procedure as an alternative to MRI-guided biopsy.*

Keywords: *Percutaneous biopsies. Contrast-enhanced mammography. Breast neoplasia. Breast MRI.*

Resumen

Introducción: *La mamografía con contraste (CEM) es una modalidad de imagen mamaria que muestra lesiones sospechosas que realzan con el contraste iodado, en forma similar a la resonancia, detectando lesiones que pueden no tener representación en las modalidades convencionales como la mamografía y la ecografía mamaria.* **Objetivo:** *Evaluar factibilidad y rendimiento de la biopsia percutánea bajo guía de CEM y comparar estos resultados con los de la biopsia bajo resonancia.* **Material y métodos:** *Estudio observacional prospectivo de lesiones diagnosticadas como sospechosas por CEM o resonancia mamaria, a las que se les realizó biopsia CEM. Se registraron las características de las pacientes y sus lesiones, detalles del procedimiento, resultados histopatológicos y éxito del procedimiento.* **Resultados:** *Un total de 43 pacientes, con una mediana de edad de 50 años, fueron referidas para biopsia CEM en el periodo estudiado. El tipo de lesión fue principalmente realce no masa (72%) con una mediana de tamaño de 12 mm. La tasa de éxito de las biopsias fue de 40/43 (93%). En más de la mitad de los casos el procedimiento se hizo sobre la base del hallazgo diagnosticado en resonancia, sin CEM previa a la biopsia. La mediana de tiempo del procedimiento fue de 17 minutos. La tasa de malignidad fue del 15% y la tasa de lesiones de alto riesgo un 30%, con un caso de subdiagnóstico (2.5%).* **Conclusión:** *La biopsia CEM es un procedimiento seguro y confiable como una alternativa a la biopsia bajo guía de resonancia.*

Palabras clave: *Biopsias percutáneas. Mamografía con contraste. Neoplasia mamaria. Resonancia mamaria.*

***Correspondence:**
Paulina Neira-Vallejos
E-mail: paulina.neira@meds.cl

Date of reception: 28-08-2025
Date of acceptance: 12-11-2025
DOI: 10.24875/AJI.25000064

Available online: 14-07-2026
Austral J. Imaging. (Engl. ed.). 2026;32(3):105-113
www.resochradi.com

Introduction

Contrast-enhanced mammography (CEM) is a breast imaging modality which shows suspicious lesions that enhance with iodinated contrast, attributed to the neovascularization of these. It is a technique called dual, because it combines a low-energy image, similar to 2D mammography, and a second high-energy image to show the distribution of the iodinated contrast in the breast, in which a recombined image is obtained through subtraction processing to visualize only the distribution of the iodinated contrast. It evaluates both morphology and enhancement, similarly to MRI, detecting lesions that may not be represented by conventional techniques such as mammography and breast ultrasound, and consequently improving sensitivity for cancer detection[1-6]. Its indications include characterization of lesions with inconclusive findings, preoperative staging, monitoring of response to neoadjuvant chemotherapy, and screening in women with increased risk[7-11].

The results of CEM studies in screening and diagnosis are very similar to those known for breast MRI, with high sensitivity and specificity for breast cancer detection[12-15], with the advantage of being less expensive and requiring less time to acquire, making it preferable for patients when comparing both modalities[16-19]. A specific lexicon for CEM has recently been incorporated[20-22], although in general, in the description of findings it uses parameters similar to those of breast MRI, which facilitates its interpretation by radiologists.

For lesions that are only seen in contrast studies, the only option until recently was MRI guided biopsy, but this type of biopsy has disadvantages, as it is expensive, it is obtained with specific equipment, takes a long time to perform, requires well-trained personnel, is very unaffordable and has some contraindications, such as claustrophobia, anthropometric limitations or metallic devices[23,24].

CEM biopsy is a novel technique that uses stereotactic imaging to locate the enhancing lesion and a vacuum system, via a dedicated biopsy system attached to the mammography unit, and it can be an alternative to breast MRI for guiding procedures in lesions visible only on contrast-enhanced examinations[25]. Since 2022, several articles have been published showing encouraging results with this biopsy modality[26-33].

This study presents the first experience in a Chilean center with CEM-guided biopsy and its results, and has as its objective to evaluate the feasibility and performance of CEM-guided biopsies of lesions visualized on both CEM and MRI and to compare these results with those published for MRI-guided biopsy.

Materials and methods

Study design and included population

This was a prospective observational study of diagnostic tests for lesions diagnosed as suspicious by CEM or breast MRI, not present on previous mammography or breast ultrasound, in which CEM biopsy was performed between July 2023 and April 2025. It was approved by the scientific ethics committee, reference number SSM Oriente 010425-4.

Included in this study were all patients over 18 years of age with lesions detected by CEM or breast MRI without representation on ultrasound or tomosynthesis, and with a CEM biopsy requested by their attending physician.

Pregnant patients, patients with iodine allergy, and those with a history of renal insufficiency or abnormal creatinine levels were excluded.

Procedure description

Before performing the procedure, the CEM or MRI in which the lesion was diagnosed, was reviewed, and informed consent was obtained from the patient. The biopsies were performed by five radiologists specializing in breast cancer, with 10 to 25 years of experience.

The CEM biopsy procedures were performed using a GE HealthCare Senographe Pristina system with its Serena Bright contrast-guided biopsy system, as follows: 350 mg/l (300-370) iodinated nonionic low-osmolarity contrast agent is administered using an injection pump at 1.5 ml/kg at 3 ml/s, followed by a 10-30 ml saline bolus. Depending on the lesion location and aiming for the shortest path from the skin to the lesion, the patient can be in a seated or lateral decubitus position, and the needle can be inserted laterally or vertically relative to the mammography detector. The breast is positioned 2 minutes after the start of the contrast injection, in the target area, and the image is acquired using tomosynthesis and dual-energy imaging at 0° (scout). Underlying recognizable findings are identified using low-energy or tomosynthesis imaging, and enhancement is confirmed on the scout. Next, a pair of angled views are obtained, and the target is marked for localization using the three coordinates (X, Y, and Z), and the device is then automatically positioned. The skin is disinfected, local anesthetic is applied, and the

needle is inserted into the breast until it reaches the point defined by the holder where the needle tip aligns with the target confirmed in the pre-shot dual-energy views. The shot is then activated, and sampling is performed using the vacuum-assisted device (we use EnCor Enspire), yielding 8 to 12 samples. At this stage of the procedure, an X-ray of the specimens is obtained after they have been washed to remove any blood, in order to identify samples with increased density due to the iodinated contrast. Finally, a marker is inserted at the biopsy site, and its location is checked, usually with a tomosynthesis projection. After the procedure, usual mammographic projections (mediolateral oblique [MLO] and craniocaudal [CC]) of the biopsied breast are obtained and post-procedure instructions are given to the patient.

Suspicious lesions on MRI that did not have prior CEM, with benign histological results on the CEM biopsy, classified as B1 and B2 lesions according to needle biopsy pathology classification of the European Working Group for Breast Screening Pathology (EWP)[34], underwent a non-contrast T1 gradient sequence post-biopsy to ensure that the susceptibility artifact produced by the marker coincided with the location of the lesion site originally visible on MRI.

Data collection and analyzed variables

The following variables were recorded: age, breast density according to ACR-BIRADS[21] on mammography, lesion size, background enhancement on CEM according to ACR-BIRADS[22], presence of lesion enhancement on scout scans, scout number, lesion representation type on contrast-enhanced examination according to ACR-BIRADS[22], biopsy duration, biopsy success (defined as obtaining samples from the target lesion), presence of iodine in the samples obtained during the biopsy (determined by the radiologist performing the procedure), measurement of the regions of interest (ROIs) of the densest and least dense samples, and histological results of the biopsies. Complications were also recorded, regarding vasovagal reactions, hematomas larger than 20 mm, and allergic reactions. The time taken to perform the biopsy was measured in minutes, from the acquisition of the first scout scan until breast decompression after marker localization. Finally, the marker location coincidence between pre- and post-biopsy MRI scans was documented in cases of benign results without pre-procedure CEM.

Statistical analysis

Data were recorded in a Microsoft Excel spreadsheet. The median was calculated for continuous quantitative variables. A biopsy yield rate was calculated based on the percentage weight in the biopsies performed; from this, the positive predictive value (PPV) of the biopsies was calculated.

The SPSS statistical software was used for normality analysis of the data from dense and non-dense specimens obtained in the biopsy, and the Shapiro-Wilk test was applied. Student's t and Wilcoxon tests were used for significance analysis.

Results

A total of 43 patients, with a median age of 50 years (range 32–79), were referred for CEM biopsy during the study period. They presented with a mammographic density pattern of 72% ACR C or heterogeneously dense according to the ACR-BIRADS classification[21] and background parenchymal enhancement on diagnostic CEM or during CEM biopsy, minimal and mild in half of the patients (25.6% each) and moderate and marked in the other half (39.5% and 9.3% respectively) according to the ACR-BIRADS CEM lexicon[22]. The indications for those that had contrast-enhanced examinations which detected the suspicious lesion were, firstly, for local staging in 47% of cases and, secondly, for lesion characterization in 26%. Sixty-three percent of the patients had their biopsied suspicious lesion diagnosed on breast MRI and did not have a diagnostic CEM prior to the biopsy. The lesion type studied by biopsy was primarily non-mass enhancement (31/43, 72%), as seen on either CEM or MRI (whose classification was concordant when both were available), with a median lesion size of 12 mm (ranging from 5 to 84 mm). Detailed clinical characteristics of the included patients and the suspicious lesions that underwent CEM biopsy are shown in tables 1 and 2.

The biopsy success rate was 40/43 (93%). Only one biopsy was performed per patient; no duplicate biopsies were performed. Three patients could not undergo biopsy because the lesion did not enhance during the procedure, and there were no associated findings on tomosynthesis. These were classified as unsuccessful or canceled procedures.

The positioning was in a seated position in all patients and most by horizontal approach (85%).

The median procedure time was 17 minutes (range 11-32 minutes). The median number of scouts used to

locate the target lesion was 2 (range 1-5). Three patients had faint enhancement (low conspicuity) of the lesion in whom an enhancement-related finding, such as density or calcifications, was identified, so the biopsy continued to be converted to tomosynthesis-guided or 2D stereotactic biopsy modality. In only two patients was the clip used to mark the sampling site displaced, by distances of 18 mm and 48 mm, respectively. Post-biopsy hematomas occurred in four patients (10%), and there were no vasovagal or allergic reactions.

Each radiologist recorded their impression of the presence of iodine in the samples obtained, which reached a rate of 95% (38/40). To try to objectify this finding, we measured the density of one of the samples using Hounsfield units, with a region of interest (ROI) in the area that appeared to contain iodine, yielding an average of 1.228 (standard deviation [SD]: 0.1840) and we located another ROI in the less dense but non-adipose area of a sample, with an average of 1.057 (SD: 0.1678), with a statistically significant difference ($p < 0.05$). The details of the procedures are described in table 3.

Histologically, the benign lesion rate was 85%, with 30% corresponding to high-risk lesions. The malignancy rate was 15%, which corresponds to the positive predictive value (PPV) of the biopsies. Of the 12 patients with high-risk lesions, five were kept under observation and seven underwent surgery. Among the latter, there was one case diagnosed as atypical ductal hyperplasia on the CEM biopsy which was found to be ductal carcinoma *in situ* during surgery, corresponding to an underdiagnosis (2.5% of all biopsies). All six cases with a malignant result on the CEM biopsy underwent surgery. The details of the pathological diagnoses of the biopsies are shown in table 4.

Surgical interventions included conservative surgery in 16 patients (40%), mastectomy in four patients (10%), and follow-up in 20 patients (50%).

Of the three patients in whom the biopsy was canceled because the lesions did not enhance during the procedure, in two of them the suspicious lesion was diagnosed on MRI, and in one on both, CEM and MRI, and all were non-mass type lesions. They were followed up with contrast-enhanced examinations performed between 1 and 4 weeks after the biopsy attempt; two were performed with CEM and one with MRI, with no evidence of abnormal enhancement.

Table 5 presents a sub-analysis of the histological results and management of the group of patients who underwent biopsy for lesions diagnosed on MRI without having previously undergone a CEM. This group comprised 27 patients, 25 of whom showed enhancement during the procedure (93% success rate), and two of whom did not. The malignancy rate in this subgroup was 24%. Figure 1 illustrates one such case.

There were 13 patients who underwent CEM biopsy directly from an MRI finding that had a benign pathological diagnosis, classified as B1 and B2 lesions. These patients were offered a post-biopsy T1-weighted MRI sequence without contrast, which was performed in 10 of the 13, and in all of these cases the marker location was concordant with the site of the suspicious lesion on MRI. Of the three patients in whom the biopsy was not performed, one underwent surgical excision of the area, which yielded no findings other than those of the percutaneous biopsy; in the second, the biopsy was

Table 1. Patient characteristics

Variables	(n = 43)
Age in years, median, (min-max)	50 (32-79)
Breast density*, n (%)	
A	0 (0%)
B	9 (20.9%)
C	31 (72.1%)
D	3 (7%)
Background parenchymal enhancement, n (%)	
Minimal	11 (25.6%)
Mild Moderate	11 (25.6%)
Marked	17 (39.5%)
	4 (9.3%)
Clinical indication for contrast-enhanced examination	
Lesion characterization	11 (25.6%)
Staging	20 (46.5%)
Post-neoadjuvant chemotherapy	2 (4.6%)
Screening	7 (16.3%)
Symptomatic	3 (7%)

*According to the ACR-BIRADS® classification of breast density composition.

Table 2. Characteristics of the lesions

Variables	(n = 43)
Suspicious finding detected in:	
MRI	27 (62.8%)
CEM	6 (14%)
Both	10 (23.2%)
Type of suspicious lesion on CEM and/or MRI*	
Mass	12 (27.9%)
Non-mass enhancement	31 (72.1%)
Size of suspicious lesion, median, mm (min-max)	12 (5-84)

*According to the MRI and ACR-BIRADS® CEM lexicon.
CEM: contrast-enhanced mammography.

Table 3. Procedures under CEM guidance

Variables	CEM biopsies (n = 43)
Success rate, n (%) Yes No	 40 (93.02%) 3 (6.98%)
	CEM biopsies performed (n = 40)
Total time per procedure in min, median, (min-max)	17 (11-32)
Number of scouts per procedure, median, (min-max)	2 (1-5)
Number of procedures converted to volume	2 (5%)
Number of procedures converted to DSB	1 (2.5%)
Position in chair, n (%) Seated Lying down	 40 (100%) 0 (%)
Approach, n (%) Horizontal Vertical	 34 (85%) 6 (15%)
Needle gauge, n (%) 10 G	 40 (100%)
Visualization of increased density attributed to iodine in samples Yes No	 38 (95%) 2 (5%)
Displaced clip Yes No	 2 (5%) 38 (95%)
Biopsy complications Vasovagal reaction Hematomas Allergic reactions	 0 (0%) 4 (10%) 0 (0%)

CEM: contrast enhanced mammography; DSB: 2D digital stereotactic biopsy.

Table 4. Pathological results of biopsies under CEM guidance

Pathology in biopsy specimen*, n (%)	(n = 40)
B1. Normotypical breast tissue, adipose tissue, areas of fibrosis, secretory changes	8 (20%)
B2. Fibroadenoma, columnar changes, fibrocystic changes, inflammatory lesions, usual ductal hyperplasia, fat necrosis, pseudoangiomatous hyperplasia	14 (35%)
B3. Flat epithelial atypia, atypical ductal hyperplasia, lobular neoplasia, papillary lesions, radial scar	12 (30%)
B5. Malignant: Ductal carcinomal *in situ* Invasive ducal carcinoma Invasive lobular carcinoma	6 (15%) 2 (5%) 3 (7.5%) 1 (2.5%)

*Pathological classification of needle breast biopsies according to the European Working Group for Breast Screening Pathology (EWGBSP)
CEM: contrast enhanced mammography.

converted to 2D stereotactic guidance due to the presence of faint calcifications in the same area as the enhancement, and calcifications were obtained in the samples; and a third patient, whose biopsy result was a fibroadenoma, did not attend for the procedure.

Discussion

Success and cancellation rates

Our CEM biopsy results showed a 93% success rate and a 7% cancellation rate due to lack of enhancement, similar to that described in other studies using this guidance method[26-33] and in MRI-guided biopsies, which in the publications have a success rate of 85 to 98% and a biopsy cancellation rate due to lack of lesion visualization of 8 to 13%[35-41]. We had three patients in whom we changed the biopsy guidance modality during the procedure, since the target lesion showed faint enhancement (low conspicuity according to ACR-BIRADS), obscured by background enhancement, but with some finding on tomosynthesis or 2D technique that allowed for obtaining adequate samples of the target lesion, so they were considered successful, with a concept similar to that defined in the Kornecki study[28]. The three patients whose lesions were not visualized at the time of the biopsy, and who were therefore excluded, subsequently underwent a contrast-enhanced examination, with no abnormal findings. One explanation for this could have been transient enhancement related to hormonal changes, similar to what occurs on MRI[23].

Positive predictive value

In our series, the positive predictive value (PPV) of CEM biopsies was 15%, compared to other published studies of CEM biopsies that range from 24% to 67%[26-32] and within the PPV range described for MRI-guided biopsies, which ranges from 14% to 61%[23,38]. PPV depends largely on the study population[23], and only two of the CEM biopsy studies that we know of having been published mention the indications for contrast-enhanced examination. In our series, we had a lower percentage of patients with an indication for local staging and symptomatic patients, which is a population with a higher

Table 5. CEM guided biopsies performed based on MRI findings

CEM biopsies based solely on MRI findings	(n = 27) (100%)	Management after CEM biopsy
Canceled biopsies without enhancement	(n = 2) (7.4%)	
Successful biopsies	(n = 25) (92.6%)	
Histopathological finding*	(n = 25) (100%)	
B1: nonspecific	5 (20%)	Follow-up with T1-weighted MRI sequence post-biopsy: 4 (80%) Follow-up without T1-weighted MRI sequence post-biopsy: 1 (20%)†
B2: columnar changes, usual ductal hiperplasia, fibroadenoma, pseudoangiomatous stromal hyperplasia	8 (32%)	Follow-up with T1-weighted MRI sequence post-biopsy: 6 (75%) Follow-up without T1-weighted MRI sequence post-biopsy: 2 (25%)‡
B3: radiating scar, papilloma, atypical ductal hyperplasia	7 (28%)	Surgery: 5 (71.4%) Follow-up: 2 (28.6%)§
B5: malignant (carcinomas *in situ* and infiltrating)	5 (20%)	Surgery: 5 (100%)

*Pathological classification of needle breast biopsies according to the European Working Group for Breast Screening Pathology (EWGBSP).
†One patient with benign surgery.
‡One patient with calcifications in digital stereotactic biopsy (DSB) and another patient with fibroadenoma.
§Two patients with radiation scarring.
CEM: contrast-enhanced mammography; DSB: 2D digital stereotactic biopsy.

probability of cancer, compared to these other two series that reported the indication[26,31].

Procedure time

We had a median duration of 17 minutes for CEM biopsies, similar to other publications, which range from 10 to 22 minutes[26-32], and shorter than the time required for biopsies under MRI guidance, which last between 35 and 41 minutes if we consider only the procedure time with image acquisition, and 60 to 70 minutes if we consider the total time spent in the MRI room[38,42].

CEM biopsies based on breast MRI findings

It is important to highlight that in our biopsies, in more than half of the cases, the procedure was performed based on the finding diagnosed on MRI, without prior CEM testing, with a success rate of 93%. Patients in this group with benign results were mostly studied with a non-contrast T1-weighted sequence after the biopsy, and the location of the marker coincided with the site of the initial MRI finding.

There is a study with a similar flow to our last group, in which 29 lesions were studied under CEM guidance based on findings detected on breast MRI, without prior CEM, with 27 of the 29 lesions presenting as non-mass findings and with a biopsy success rate of 93%, similar to ours. The study concluded that MRI guidance of lesions visible on MRI can be replaced by CEM guidance, without the need for a prior CEM[32].

There is another recent publication in which the patients with suspicious lesions diagnosed on MRI were offered the option of CEM biopsy. These patients underwent a diagnostic CEM, and if a lesion was identified, a CEM-guided biopsy was performed immediately, which occurred in only six of the 21 patients, all with benign results and biopsy sites concordant with the initial MRI lesion[33]. Among the limitations of this study, the authors mention the readers' lack of experience with the method and the use of a new, single-vendor mammography system, different from the equipment used in most CEM biopsy publications, including our own.

Biopsy specimens

Among our results, it is also interesting to note that we took a radiograph of the specimens obtained during the procedure, and in almost all cases (38/40), the radiologists recorded the presence of samples with areas of increased density, which was attributed to the presence of iodine. This finding is mentioned in Kowalski's research article[27]. Attempting to objectify the radiologists' impression, we measured the density of

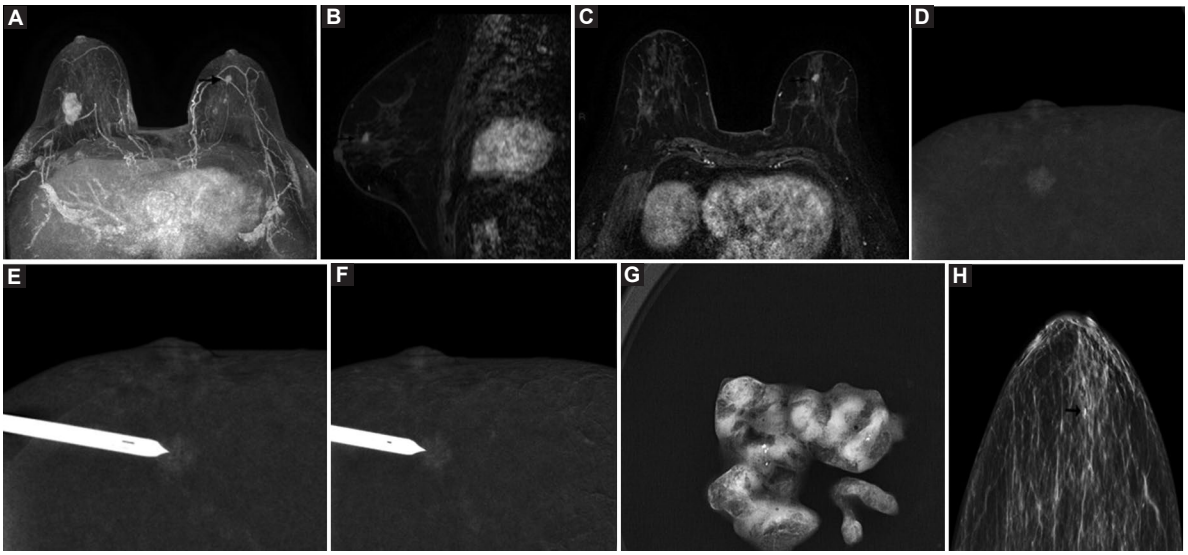

Figure 1. A 75-year-old patient diagnosed with invasive ductal carcinoma of the right breast, underwent breast MRI for local staging, which detected a mass-like lesion in the contralateral breast suspicious for neoplasia, but not reflected on mammography or ultrasound. She was referred for CEM-guided percutaneous biopsy of the left breast lesion. **A:** MIP showing a right mass diagnosed as invasive ductal carcinoma and a 9 mm left retroareolar nodule (arrow) with other smaller posterior nodules suspicious for neoplasia. **B:** left nodule visible on a dynamic T1-weighted contrast-enhanced sequence (arrow). **C:** Sagittal MPR of the left nodule (arrow). **D:** CEM biopsy scout of the left breast, positioned in the retroareolar region with a nodule concordant to the location seen on previous MRI. **E-F:** pre-firing stereotactic needle projections in CEM biopsy. **G:** radiograph of the CEM biopsy samples. **H:** post-biopsy CC projection with marker at the sampling site (arrow), corresponding to the same location of the nodule on breast MRI. The histological result of the contrast-enhanced mammography CEM biopsy was moderate to poorly differentiated invasive ductal carcinoma, Elston and Ellis grade 3. Surgical biopsy: invasive ductal carcinoma with an *in situ* component, 7 mm, and foci of papillomatosis; sentinel lymph node with no evidence of neoplasia (0/2). CC: craniocaudal; CEM: contrast-enhanced mammography; MIP: maximum intensity projection; MPR: multiplanar reconstruction.

the samples with Hounsfield unitsm with one region of interest (ROI) located in an area of higher density, which appeared to be secondary to the presence of iodine, and another ROI located in the less dense but non-adipose area, with a statistically significant difference ($p < 0.05$) (Fig. 2).

Disadvantages and complications of CEM biopsy

One disadvantage of the CEM biopsy compared to MRI-guided biopsy is that it irradiates the breast. In this regard, the publications that reported the dose per procedure averaged between 14 and 21 mGy, similar to a dose for 2D biopsy under stereotactic guidance[29-31]. Another disadvantage is the use of iodinated contrast medium and the possibility of an allergic reaction. This is a very rare event, described in less than 1% of cases, and most are mild[1,16]. Among the reported complications of CEM biopsies, the most frequent are hematomas and vasovagal reactions[26-32]. In our series, hematomas larger than 20 mm were observed in only 10% of patients, a common occurrence with 10-gauge needle biopsies, which is the needle we used, and there were no vasovagal or allergic reactions.

Study limitations

Among the limitations of our study is the small sample size. We also did not measure the radiation dose of the procedure; however, it is worth noting that the median number of scouts was only 2 per procedure. We also assumed that the samples with areas of higher density were due to the presence of iodine. In the group of patients in whom we performed CEM biopsy due to a suspicious finding on MRI, without prior diagnostic

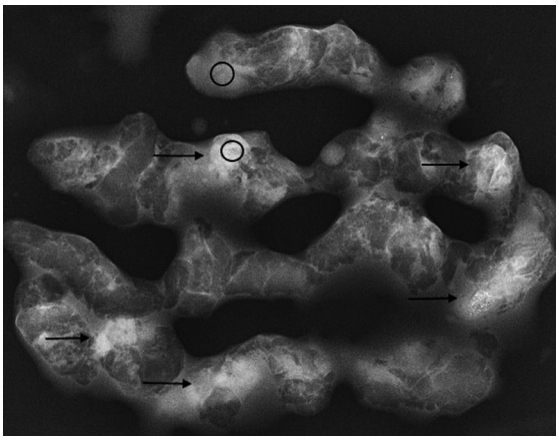

Figure 2. Example of a radiograph of samples obtained from a CEM biopsy. The arrows indicate dense areas that appear to contain iodine. The circles indicate where the densities were measured, with one region of interest (ROI) in the dense area and another in the less dense, but non-adipose area.

CEM, the optimal approach would have been to perform a non-contrast T1 sequence in all of them to confirm that the area studied corresponded exactly to the MRI finding. However, we did so in the 77% of the benign B1 and B2 type cases, and in the cases where a malignant lesion or high-risk lesions such as radiation scars were found, it seems clear that our objective was correct. We still need to follow up with all of the patients with benign results, which is currently underway.

In this study, we demonstrated the feasibility of performing biopsies under CEM in suspicious lesions diagnosed on CEM or breast MRI, with a similar success rate and positive predictive value to MRI-guided biopsy, and with the benefit of shorter execution time and, in our country, at a cost of less than half that of MRI-guided biopsy.

Conclusion

CEM biopsy is a fast, safe, and reliable procedure as an alternative to MRI-guided biopsy for lesions that enhance without representation on conventional methods, for lesions diagnosed by both CEM and MRI.

Funding

The authors declare that they have not received funding.

Conflicts of interest

The authors declare no conflicts of interest.

Ethical considerations

Protection of human subjects and animals. The authors declare that no experiments on humans or animals were performed for this research.

Confidentiality, informed consent, and ethical approval. The authors have followed their institution's confidentiality protocols, obtained informed consent from all patients, and secured approval from the Ethics Committee. SAGER guidelines have been followed as applicable to the nature of the study.

Declaration on the use of artificial intelligence. The authors declare that no generative artificial intelligence was used in the writing or creation of the content of this manuscript.

References

1. Zanardo M, Cozzi A, Trimboli RM, Labaj O, Monti CB, Schiaffino S, et al. Technique, protocols and adverse reactions for contrast-enhanced spectral mammography (CESM): a systematic review. Insights Imaging. 2019;10(1):76.
2. Dromain C, Thibault F, Diekmann F, Fallenberg EM, Jong RA, Koomen M, et al. Dual-energy contrast-enhanced digital mammography: initial clinical results of a multireader, multicase study. Breast Cancer Res. 2012;14(3):R94.
3. Cheung YC, Lin YC, Wan YL, Yeow KM, Huang PC, Lo YF, et al. Diagnostic performance of dual-energy contrast-enhanced subtracted mammography in dense breasts compared to mammography alone: interobserver blind-reading analysis. Eur Radiol. 2014;24(10):2394-403.
4. Lobbes MB, Lalji U, Houwers J, Nijssen EC, Nelemans PJ, van Roozendaal L, et al. Contrast-enhanced spectral mammography in patients referred from the breast cancer screening programme. Eur Radiol. 2014;24(7):1668-76.
5. Luczyńska E, Heinze-Paluchowska S, Dyczek S, Blecharz P, Rys J, Reinfuss M. Contrast-enhanced spectral mammography: comparison with conventional mammography and histopathology in 152 women. Korean J Radiol. 2014;15(6):689-96.
6. Lalji UC, Houben IP, Prevos R, Gommers S, van Goethem M, Vanwetswinkel S, et al. Contrast-enhanced spectral mammography in recalls from the Dutch breast cancer screening program: validation of results in a large multireader, multicase study. Eur Radiol. 2016;26(12):4371-9.
7. Kim EY, Youn I, Lee KH, Yun JS, Park YL, Park Ch, et al. Diagnostic value of contrast-enhanced digital mammography versus contrast-enhanced magnetic resonance imaging for the preoperative evaluation of breast cancer. J Breast Cancer. 2018;21(4):453-62.
8. Iotti V, Ravaioli S, Vacondio R, Coriani C, Caffarri S, Sghedoni R, et al. Contrast-enhanced spectral mammography in neoadjuvant chemotherapy monitoring: a comparison with breast magnetic resonance imaging. Breast Cancer Res. 2017;19(1):106.
9. Jochelson MS, Pinker K, Dershaw DD, Hughes M, Gibbons GF, Rahbar K, et al. Comparison of screening CEDM and MRI for women at increased risk for breast cancer: a pilot study. Eur J Radiol. 2017; 97:37-43.
10. Sorin V, Yagil Y, Yosepovich A, Shalmon A, Gotlieb M, Neiman OH, et al. Contrast-enhanced spectral mammography in women with intermediate breast cancer risk and dense breasts. AJR Am J Roentgenol. 2018;211(5):W267-W274.
11. Sung JS, Lebron L, Keating D, D'Alessio D, Comstock CE, Lee CH, et al. Performance of dual-energy contrast-enhanced digital mammography for screening women at increased risk of breast cancer. Radiology. 2019;293(1):81-8.
12. Fallenberg EM, Schmitzberger FF, Amer H, Ingold-Heppner B, Balleyguier C, Diekmann F, et al. Contrast-enhanced spectral mammo-graphy vs. mammography and MRI - clinical performance in a multi-reader evaluation. Eur Radiol. 2017;27(7):2752-64.

13. Chou CP, Lewin JM, Chiang CL, Hung BH, Yang TL, Huang JS, et al. Clinical evaluation of contrast-enhanced digital mammography and contrast enhanced tomosynthesis-Comparison to contrast-enhanced breast MRI. Eur J Radiol. 2015;84(12):2501-8.
14. Li L, Roth R, Germaine P, Ren S, Lee M, Hunter K, et al. Contrast-enhanced spectral mammography (CESM) versus breast magnetic resonance imaging (MRI): a retrospective comparison in 66 breast lesions. Diagn Interv Imaging. 2017;98(2):113-23.
15. Clauser P, Baltzer PAT, Kapetas P, Hoernig M, Weber M, Leone F, et al. Low-dose, contrast-enhanced mammography compared to contrast-enhanced breast MRI: a feasibility study. J Magn Reson Imaging. 2020;52(2):589-95.
16. Patel BK, Gray RJ, Pockaj BA. Potential cost savings of contrast-enhanced digital mammography. AJR Am J Roentgenol. 2017;208(6):W231-W237.
17. Sumkin JH, Berg WA, Carter GJ, Bandos AI, Chough DM, Ganott MA, et al. Diagnostic performance of MRI, molecular breast imaging, and contrast-enhanced mammography in women with newly diagnosed breast cancer. Radiology. 2019;293(3):531-40.
18. Hobbs MM, Taylor DB, Buzynski S, Peake RE. Contrast-enhanced spectral mammography (CESM) and contrast enhanced MRI (CEMRI): patient preferences and tolerance. J Med Imaging Radiat Oncol. 2015;59(3):300-5.
19. Phillips J, Miller MM, Mehta TS, Fein-Zachary V, Nathanson A, Hori W, et al. Contrast-enhanced spectral mammography (CESM) versus MRI in the high-risk screening setting: patient preferences and attitudes. Clin Imaging. 2017;42:193-7.
20. Perry H, Phillips J, Dialani V, Slanetz PJ, Fein-Zachary VJ, Karimova EJ, et al. Contrast-enhanced mammography: a systematic guide to interpretation and reporting. AJR Am J Roentgenol. 2019;212(1):222-31.
21. D'Orsi CJ, Sickles EA, Mendelson EB, Morris EA. ACR BI-RADS® atlas: breast imaging reporting and data system. Reston (VA): American College of Radiology; 2013.
22. Lee CH, Philips J, Sung JS, Lewin JM, Newell MS. Contrast-enhanced mammography (CEM): a supplement to ACR BI-RADS® mammography 2013 [Internet]. Reston (VA): American College of Radiology; 2022 [citado 27 jun 2022]. Disponible en: https://www.acr.org/-/media/ACR/Files/RADS/BI-RADS/BIRADS_CEM_2022.pdf
23. Han BK, Schnall MD, Orel SG, Rosen M. Outcome of MRI-guided breast biopsy. AJR Am J Roentgenol. 2008;191(6):1798-804.
24. Malhaire C, El Khoury C, Thibault F, Athanasiou A, Petrow P, Ollivier L, et al. Vacuum-assisted biopsies under MR guidance: results of 72 pro-cedures. Eur Radiol. 2010;20(7):1554-62.
25. James J. Contrast-enhanced spectral mammography (CESM)-guided breast biopsy as an alternative to MRI-guided biopsy. Br J Radiol. 2022;95(1132):20211287.
26. Alcantara R, Posso M, Pitarch M, Arenas N, Ejarque B, Iotti V, et al. Contrast-enhanced mammography-guided biopsy: technical feasibility and first outcomes. Eur Radiol. 2023;33(1):417-28.
27. Kowalski A, Arefan D, Ganott MA, Harnist K, Kelly AE, Lu A, et al. Contrast-enhanced mammography-guided biopsy: initial trial and experience. J Breast Imaging. 2023;5(2):148-58.
28. Kornecki A, Bhaduri M, Khan N, Nachum IB, Muscedere G, Shmuilovich O, et al. Contrast-enhanced mammography-guided breast biopsy: single-center experience. AJR Am J Roentgenol. 2023;220(6):826-7.
29. Sammarra M, Piccolo CL, Sarli M, Stefanucci R, Tommasiello M, Orsaria P, et al. Contrast-enhanced mammography-guided biopsy: preliminary results of a single-center retrospective experience. J Clin Med. 2024;13(4):933.
30. Tang YC, Cheung YC. Contrast-enhanced mammography-guided biopsy: technique and initial outcomes. Quant Imaging Med Surg. 2023;13(8):5349-54.
31. Layden N, Sesnan G, Kessell M, Hardie M, Taylor D. Stereotactic biopsy with contrast-enhanced mammography: the initial Australian experience. J Med Imaging Radiat Oncol. 2024;68(4):393-400.
32. Aribal E, Guldogan N, Seker ME, Yilmaz E, Turk EB. MRI only detected lesions: can contrast enhanced mammography guided biopsy be an alternative method: Initial clinical findings. Eur J Radiol. 2024;173:111373.
33. Morris MF, Summers D, Welk LA, Harrison M, Johnston B, Rangan P, et al. Initial attempted contrast-enhanced mammography-guided biopsy for suspicious breast MRI findings: a single institution's experience. AJR Am J Roentgenol. 2025;224(1):e2431940.
34. Perry N, Broeders M, de Wolf C, Törnberg S, Holland R, von Karsa L. European guidelines for quality assurance in breast cancer screening and diagnosis. Fourth edition-summary document. Ann Oncol. 2008;19(4):614-22.
35. Han BK, Schnall MD, Orel SG, Rosen M. Outcome of MRI-guided breast biopsy. AJR Am J Roentgenol. 2008;191(6):1798-804.
36. Malhaire C, El Khoury C, Thibault F, Athanasiou A, Petrow P, Ollivier L, et al. Vacuum-assisted biopsies under MR guidance: results of 72 procedures. Eur Radiol. 2010;20(7):1554-62.
37. Heywang-Köbrunner SH, Heinig A, Schaumlöffel U, Viehweg P, Buchmann J, Lampe D, et al. MR-guided percutaneous excisional and incisional biopsy of breast lesions. Eur Radiol. 1999;9(8):1656-65.
38. Imschweiler T, Haueisen H, Kampmann G, Rageth L, Seifert B, Rageth C, et al. MRI-guided vacuum-assisted breast biopsy: comparison with stereotactically guided and ultrasound-guided techniques. Eur Radiol. 2014;24(1):128-35.
39. McGrath AL, Price ER, Eby PR, Rahbar H. MRI-guided breast interventions. J Magn Reson Imaging. 2017;46(3):631-45.
40. Hefler L, Casselman J, Amaya B, Heinig A, Alberich T, Koelbl H, et al. Follow-up of breast lesions detected by MRI not biopsied due to absent enhancement of contrast medium. Eur Radiol. 2003;13(2):344-6.
41. Brennan SB, Sung JS, Dershaw DD, Liberman L, Morris EA. Cancellation of MR imaging-guided breast biopsy due to lesion nonvisualization: frequency and follow-up. Radiology. 2011;261(1):92-9.
42. Rauch GM, Dogan BE, Smith TB, Liu P, Yang WT. Outcome analysis of 9-gauge MRI-guided vacuum-assisted core needle breast biopsies. AJR Am J Roentgenol. 2012;198(2):292

AUSTRAL JOURNAL OF IMAGING
REVISTA CHILENA DE RADIOLOGÍA

PERMANYER

Check for updates

ORIGINAL ARTICLE

SimuTC: a didactic tool for learning image reconstruction in computed tomography

SimuTC: una herramienta didáctica para el aprendizaje de reconstrucción de imágenes por tomografía computarizada

Angélica Valdés[1], Cristián Arellano[1], Claudio Cuellar-Fritis[1], and Marvin Querales[2]*

[1]Faculty of Medicine, School of Medical Technology, Universidad de Valparaíso, Viña del Mar; [2]Institute of Mathematics, Physics and Statistics, Universidad de Las Américas, Sede Providencia, Santiago. Chile

Abstract

Introduction: *Computed tomography (CT) is a crucial tool in modern medical diagnosis; however, teaching it poses challenges due to the limited availability of equipment and high operating costs.* **Objective:** *In response, SimuTC was developed, an educational simulator designed to enhance learning in CT image reconstruction.* **Material and methods:** *Development was structured in three stages: 1) collection of representative clinical images, 2) design of the digital environment, and 3) technical and educational validation by medical technology students and teachers.* **Results:** *SimuTC enables the selection of anatomical regions, adjustment of technical parameters, and visualization of the resulting set of images, providing warnings when the configuration does not align with the diagnostic objective. The perception survey showed high acceptance. The most valued dimensions were improved learning, understanding of reconstruction parameters, and usefulness as a teaching supplement. Qualitative comments highlighted aspects such as usefulness, ease of use, and clinical applicability in a positive manner.* **Conclusions:** *SimuTC is a tool that promotes active learning. Its implementation complements theoretical training, improves accessibility to simulated experiences, and strengthens key technical skills in training environments with limited resources.*

Keywords: *Computed tomography. Image reconstruction. Computer simulation. Health education.*

Resumen

Introducción: *La tomografía computarizada (TC) es clave en el diagnóstico médico actual; sin embargo, su enseñanza enfrenta desafíos debido a la limitada disponibilidad de equipos y el alto costo operacional.* **Objetivo:** *En respuesta, se desarrolló SimuTC, un simulador educativo orientado a fortalecer el aprendizaje de reconstrucción de im.genes por TC.* **Material y métodos:** *El desarrollo se estructuró en tres etapas: 1) recopilación de imágenes clínicas representativas, 2) diseño del entorno digital y 3) validación técnica y educativa por estudiantes y docentes de tecnología médica.* **Resultados:** *SimuTC permite seleccionar la región anatómica, ajustar parámetros técnicos y visualizar el conjunto de imégenes resultantes, entregando advertencias cuando la configuración no se ajusta al objetivo diagnóstico. La encuesta de percepción mostró una alta aceptación. Las dimensiones más valoradas fueron la mejora del aprendizaje, la comprensión de los parámetros de reconstrucción y la utilidad como complemento docente. Los comentarios cualitativos destacaron positivamente aspectos como la utilidad, la facilidad de uso y la aplicabilidad clínica.* **Conclusiones:** *SimuTC es una herramienta que favorece el aprendizaje activo. Su implementación complementa la formación teórica, mejora la accesibilidad a experiencias simuladas y fortalece competencias técnicas clave en entornos de formación con recursos limitados.*

Palabras clave: *Tomografía computarizada. Reconstrucción de imágenes. Simulación por computador. Educación en salud.*

Correspondence:
Cristián Arellano
E-mail: cristian.arellano@uv.cl

Date of reception: 28-07-2025
Daste of acceptance: 12-11-2025
DOI: 10.24875/AJI.25000057

Available online: 14-07-2026
Austral J. Imaging. (Engl. ed.). 2026;32(3):114-123
www.resochradi.com

Introduction

Computed tomography (CT) is a complex imaging modality that has become an essential tool for the diagnosis and monitoring of various pathologies, therapeutic planning, and screening studies in healthy subpopulations with specific risk factors.[1,2] Its growing relevance in the clinical setting has driven the need to train highly skilled professionals in the use and management of this technology. In medical technology academic programs, CT instruction encompasses both the physical and technical principles as well as the development of fundamental practical skills for operating the equipment and interpreting the images obtained. However, CT training faces several challenges, among which limited access to practical experiences stands out. This problem stems primarily from the high cost of equipment and its maintenance, which restricts its availability for educational purposes and hinders the implementation of clinical practices.[3,4] Added to this is the heavy workload and staff shortages in many imaging departments, which further reduces the availability of *in situ* training spaces for the students. Furthermore, teaching the image acquisition and reconstruction process presents an additional didactic challenge in this area, as it involves data acquisition, its processing, and understanding the impact of the technical parameters on image quality and the radiation dose.[5]

Given this scenario, educational simulators have emerged as innovative and effective pedagogical tools that allow us to complement traditional training and strengthen teaching and learning processes in safe and controlled environments.[6] These simulators allow students to practice repeatedly and experiment with diverse clinical scenarios[6,7] without compromising patient safety.[8,9] As Lee et al.[10] highlight, simulation promotes model-based learning, allowing students to formulate questions, construct hypotheses, and evaluate them in a dynamic and risk-free environment, thus facilitating a deeper understanding of complex concepts.

The effectiveness of simulation in healthcare education has been widely supported by the literature. Rodríguez et al.[11] point out that its use fosters the development of skills in realistic contexts, promotes interprofessional learning and decision-making in complex scenarios, as well as stimulating self-reflection and improving feedback. Brim et al.,[12] for their part, state that teaching in simulated environments improves long-term knowledge retention and better prepares students to face real clinical scenarios compared to purely theoretical instruction. Likewise, Yin Mar and Nataraja[13] indicate that simulation can be adapted to prevalent health problems in local contexts, which reinforces its relevance and effectiveness in professional training.

Despite its multiple benefits, the implementation of simulators in healthcare education is not yet widespread.[10,14] In particular, the teaching of CT image reconstruction in undergraduate contexts continues to be under-represented in the literature, especially in Latin American countries, which limits the development of key technical skills in students. In response to this need, this study describes the development of SimuTC, an accessible and functional educational simulator, designed to facilitate the practice of the CT image reconstruction process for medical technology students. This tool aims to strengthen the theoretical and practical understanding of the reconstruction process, overcome limitations of access to real equipment, and contribute innovatively and safely to the training process, in accordance with the current challenges of the healthcare system and professional training in imaging.

Material and methods

The development of SimuTC was carried out in three main stages: 1) collection and processing of clinical images, 2) design and implementation of the digital environment, and 3) technical and educational evaluation of the tool.

Collection and processing of clinical images

The initial stage involved presenting the educational project to the Bioethics Committee of the Faculty of Medicine at the Universidad de Valparaíso, Chile, obtaining their approval through minutes No. 24/2024. Once the initiative was authorized, representative tomographic images were selected and processed. To do this, the necessary permission was obtained from the medical director of a clinic in the Valparaíso region to use previously acquired clinical studies of real patients. All studies were selected and anonymized according to ethical standards. The inclusion criteria were: 1) absence of structural or pathological alterations, and 2) availability of raw data on the CT scanner, an essential requirement to allow reconstruction using multiple technical combinations.

Processing was performed on a Siemens Somatom Definition CT scanner, generating reconstructed image volumes from combinations of technical parameters, such as:

– Reconstruction algorithm or *kernel*: standard or custom.
– Slice thickness: 1 or 3 mm.
– Viewing window (width/level): 150/50, 400/40, 1500/-500, and 2500/500.

This strategy enabled the creation of a structured collection of studies, systematically organized into folders according to anatomical region and technical parameters. The anatomical areas included were:
– Thorax: reconstructions of soft tissues, lung parenchyma, and bone structures.
– Brain: reconstructions of brain parenchyma and skull bone structures.
– Abdomen: reconstructions of soft tissues and bone components.

Design and implementation of the digital environment

The simulator design was based on a series of technical and functional requirements (Table 1), defined from an analysis of the actual operating dynamics of CT equipment in the clinical setting.

The simulator allows the user to select an anatomical segment, adjust the technical parameters, and view the corresponding set of images. This functional logic simulates the actual image reconstruction process in a clinical CT scanner, thus facilitating the understanding of the impact of each parameter on diagnostic quality. For educational purposes, an automatic feedback system was incorporated to evaluate the consistency between the selected parameters and the defined diagnostic objective.

The technical development was carried out in Python 3.12, using the Tkinter and Pillow (PIL) libraries to implement an interactive and user-friendly graphical user interface. To ensure offline operation (without Internet connection), the images used are stored locally on the computer where the application is running, organized in a hierarchical folder system according to anatomical region and the reconstruction parameters. This organization allows for efficient access and rapid retrieval of the datasets corresponding to each selected combination. The storage system enables efficient navigation through drop-down menus and dynamic scrolling for visual exploration of the reconstructed images.

Technical and educational evaluation

With the aim to assess the usefulness of SimuTC as an educational tool, a perception survey was administered to students and faculty of the Medical Technology program at the Universidad de Valparaíso. Participation was voluntary, in response to an open call made by the research team via email and word of mouth. In the case of the students, all those enrolled in the CT course during the first semester of 2025 agreed to complete the survey (29 in total). Regarding the faculty, 8 of the 12 available professors (all medical technologists specializing in imaging and medical physics) participated in the study by answering the questionnaire.

Table 1. Technical and functional requirements of SimuTC

No.	Requirements
1	It must have an interactive visualization of the images according to the anatomical region and the selected technical parameters.
2	It must generate automatic feedback that warns of inconsistencies between the parameters and the diagnostic objective.
3	It must allow exploration of the selected images with scroll navigation.
4	It must allow for offline operation.

The instruments were designed using a focus group methodology with two iterations, which included both the research team and three experts in the field (not surveyed, from another institution). This allowed for the collection of participants' perceptions, experiences, and suggestions regarding the topic of study. This strategy facilitated the identification of relevant dimensions and the formulation of items pertinent to the research context. Thus, the final instrument comprised nine questions with responses on a five-point Likert type scale, where 1 represented "strongly disagree" and 5 "strongly agree." The instrument was administered anonymously and voluntarily, guaranteeing the confidentiality of the participants, in accordance with the ethical principles of educational research. The survey addressed three key dimensions:
– Functionality and usefulness: evaluation of the simulator's contribution to understanding reconstruction parameters and their impact on image quality.
– Usability: assessment of accessibility, ease of navigation, and the intuitiveness of the digital environment.
– Reliability and applicability: degree of coherence of the simulator with other learning environments used in the program, as well as its potential value as a complementary pedagogical resource.

The analysis of each question was performed using descriptive statistics, obtaining the average responses and representing them in a bar chart to facilitate interpretation. Given the limited size of the student and faculty group, a separate pilot study was deemed unnecessary. However, the wording of the items was carefully reviewed to ensure clarity and relevance. Reliability was also verified using Cronbach's alpha coefficient, yielding a result of 0.687, indicating an acceptable, but moderate, internal consistency. As the context of this research is exploratory, the result was considered adequate.

Finally, the survey included an open comments section where participants could express general observations, highlight positive aspects, and propose suggestions for improving the tool. To evaluate these comments, an automated sentiment analysis was applied using a multilingual language model based on *transformers* (CardiffNLP Twitter XLM-RoBERTa). The data was processed with Python and the *transformers* library, classifying each comment into the categories of positive, negative, or neutral sentiment.

Results

SimuTC structure and functionality

SimuTC presents an interface structured in sequential stages that simulate the logical operation flow of a CT scanner. The interaction begins with an initial menu where the user must select the anatomical segment to be evaluated (Fig. 1), a fundamental decision as it determines the available structure options in the next stage.

Once the anatomical region is defined, a set of dropdown menus appears, allowing the selection of both the specific structure to be studied and the technical reconstruction parameters (Fig. 2). These parameters include the reconstruction algorithm (*kernel*), slice thickness, and display window values (width and level). The interface incorporates a confirmation button (Perform reconstruction) that loads the images corresponding to the selected parameter combination, and a navigation button (Back) that allows users to return to the previous menu and modify the selection if needed. This structure promotes smooth and intuitive navigation within the simulator, facilitating the exploration of different technical combinations based on the user's defined diagnostic objective.

After confirming the reconstruction, a feedback pop-up window appears, evaluating the consistency of the selected parameters with the established diagnostic objective. If an inappropriate configuration is detected, the tool does not specify which parameter is incorrect, thus encouraging critical analysis by the student. Therefore, regardless of the feedback result, SimuTC always displays the set of images corresponding to the selected parameter combination (figure 3 and 4), allowing for exploration via scrolling. This functional logic aims to replicate real clinical experience, allowing students to actively experiment with technical parameters and observe their direct impact on the quality and diagnostic usefulness of the reconstructed images.

SimuTC evaluation

The overall perception of the students who used the SimuTC tool is presented in figure 5A, which shows the average student responses to the evaluated statements. All items achieved averages above 4, and most exceeded 4.5 points, demonstrating high overall acceptance of the tool. The highest-rated dimensions were improved learning, understanding of reconstruction parameters, and usefulness as a teaching aid. In contrast, the items with relatively lower scores, although still within the positive range, were intuitive navigation and ease of use.

Regarding faculty perceptions, responses were collected from eight academics in the same program. The results showed a highly positive assessment, with averages above 4.5 for all items considered. Four statements received the highest average score (5.0): fostering critical thinking, enriching the learning process, understanding the reconstruction parameters, and potential future use in teaching (Fig. 5B). These results indicate a high degree of validation by the faculty, in both pedagogical and technical terms.

The qualitative results obtained from the students' open-ended comments are summarized in figure 6, which represents a word cloud generated from the most frequent responses given by students in the open-ended comments, excluding empty or neutral terms. Terms such as "liked," "excellent," "easy," "useful," "perhaps," and "should" stand out, reflecting a combination of highly positive assessments along with constructive suggestions for improving the tool. Terms like "improve" and "should" suggest areas for development, while expressions like "excellent," "useful," and "liked" reinforce the positive perception of the simulator. On the other hand, sentiment analysis of each comment revealed that 75.9% were classified as positive, 13.8%

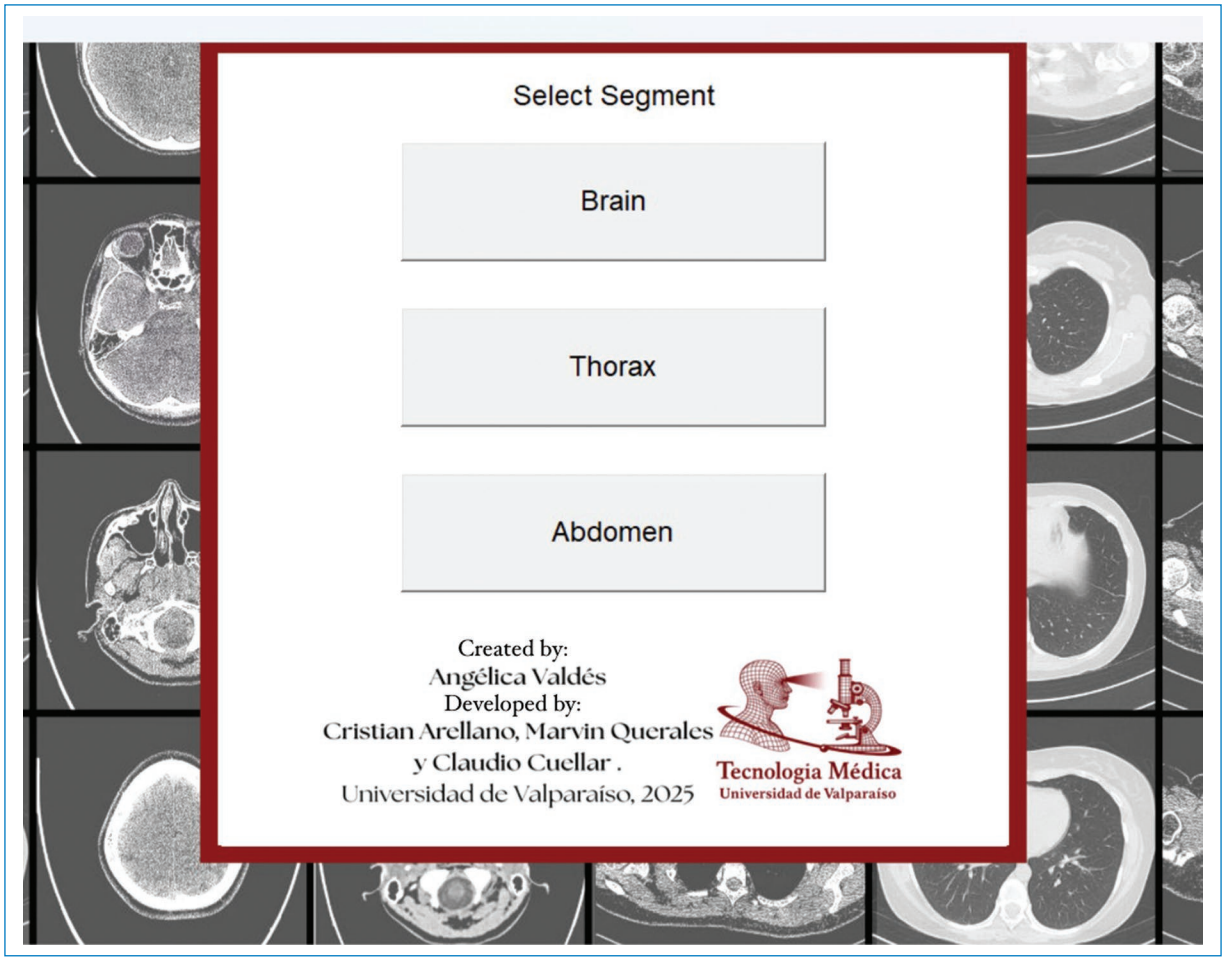

Figure 1. SimuTC's initial menu, where the anatomical segment to be evaluated is selected.

as neutral, and the remainder as negative, indicating good user acceptance.

The general comments provided by the instructors are summarized in table 2. These comments highlight strengths such as academic usefulness and pedagogical relevance, as well as opportunities for improvement related to the simulator's aesthetic design and the incorporation of new functions or anatomical regions. Sentiment analysis revealed that 6 of the 8 comments (75%) were positive, and the remainder were neutral (similar to the results obtained from the students).

Discussion

The development and preliminary validation of the SimuTC educational simulator is part of a growing trend toward the incorporation of digital technologies in medical science education, particularly in the field of imaging. In this context, educational simulators represent effective tools for facilitating the understanding of complex clinical processes in a safe, repeatable, and accessible environment.[15]

Unlike other existing tools, SimuTC is presented as an accessible simulator specifically designed for teaching the CT image reconstruction process, with an emphasis on the selection and combination of technical parameters. Other simulators, such as CTSim[15] and DukeSim,[16] operate using advanced mathematical models to generate simulated data or sinograms, but their use requires specialized technical knowledge and they are not designed for the undergraduate training of medical technologists. Meanwhile, platforms like NETRAD CT[17] and Virtual CT Trainer[18] allow for complex simulations that reproduce more complete acquisition processes, even with remote operation of CT equipment, but access is restricted by high costs and dependence on institutional infrastructure.

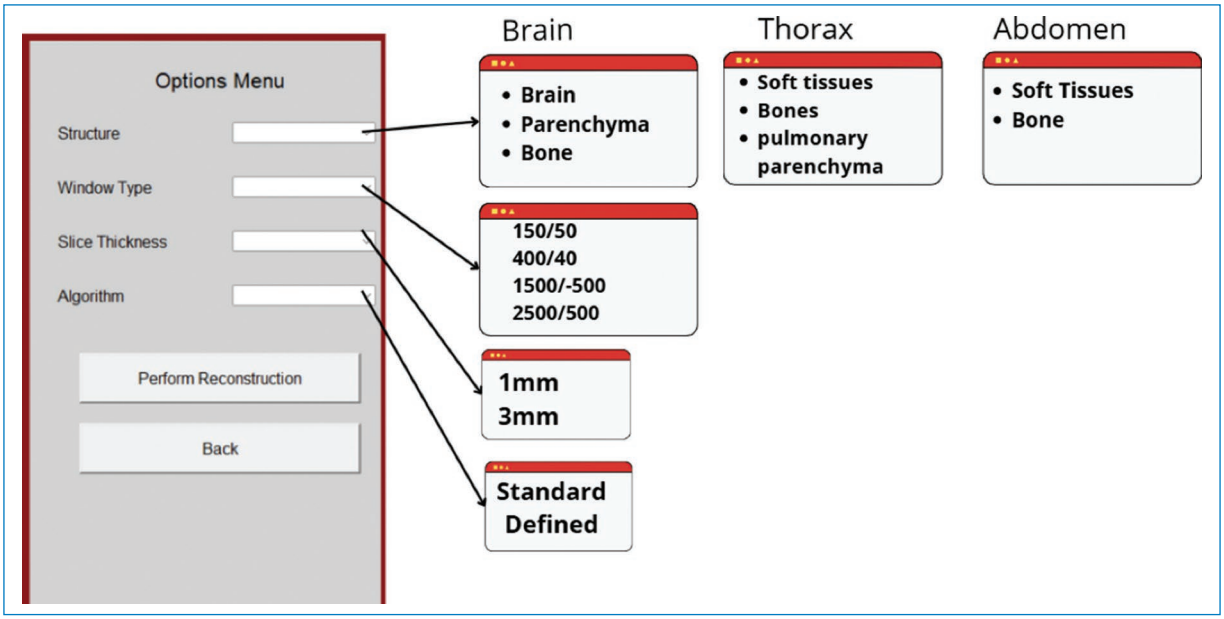

Figure 2. SimuTC options menu for image reconstruction.

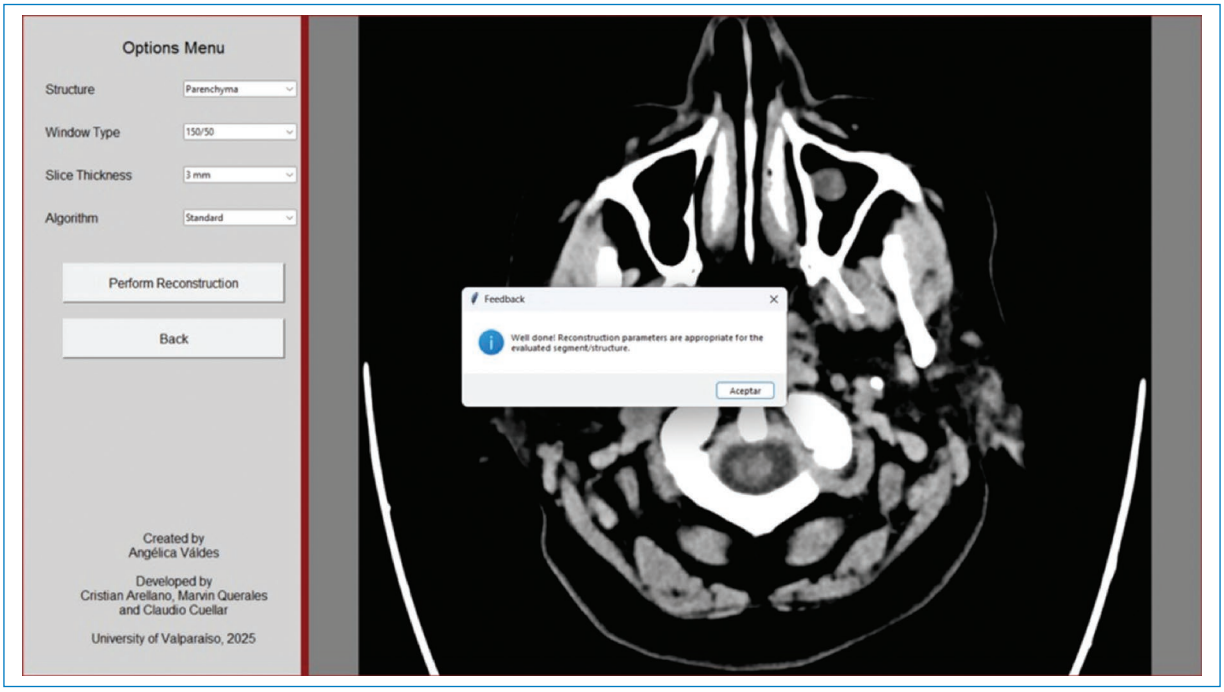

Figure 3. Visualization of the images associated with the correctly selected reconstruction parameters and anatomical structure.

In 2021, Siemens Healthineers introduced a simulator for common CT protocols, including the image acquisition and post-processing phases, called SmartSimultor.[19] This tool has a user-friendly interface and high user satisfaction, according to research conducted by Chau and Arruza.[20] On the other hand, Stowe et al.[21] presented CTSim, a name similar to that presented by He et al.[15], which allows users to freely explore the parameters that affect reconstruction, in addition to having knowledge questions about particular cases,

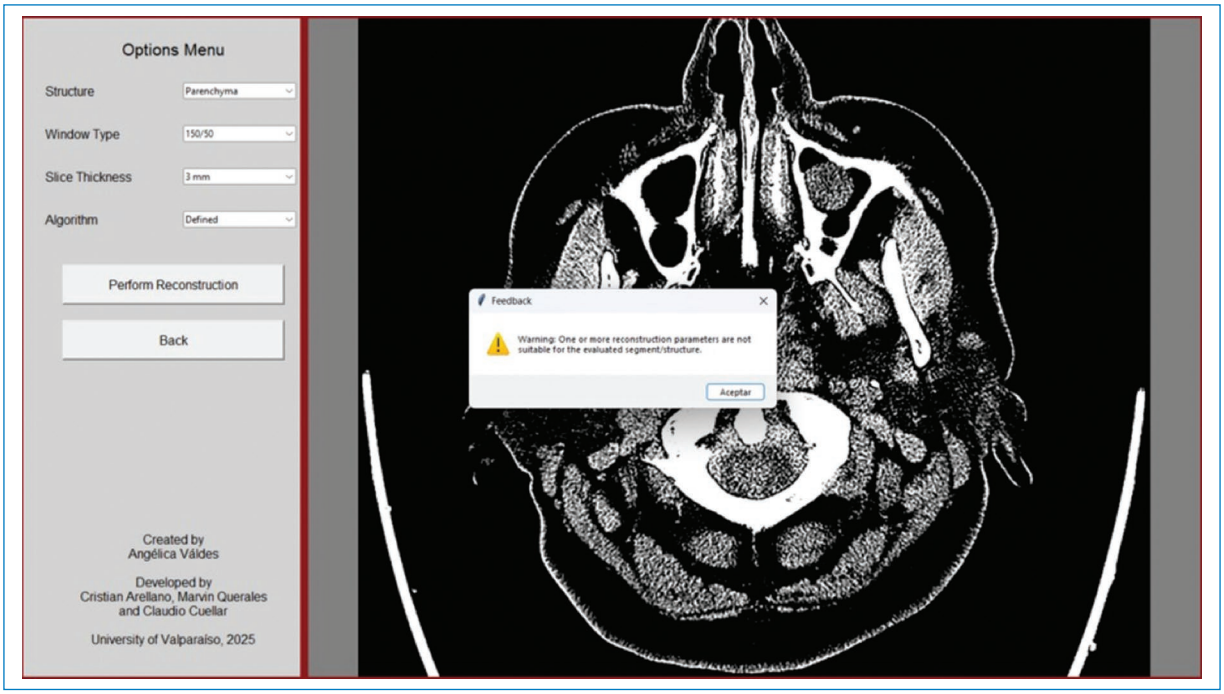

Figure 4. Visualization of the images associated with the incorrectly selected reconstruction parameters and anatomical structure.

with immediate feedback on them. While SimuTC shares many similarities in its overall visual format and functionality, the main difference lies in the feedback provided during parameter selection. By allowing the exploration of multiple technical combinations and offering automatic feedback on the diagnostic coherence of the user's decisions, it promotes active learning, critical thinking, and informed decision-making. The deliberate design of non-specific feedback, which avoids directly pointing out errors, aims to stimulate individual reflection, in line with the principles of reflective simulation.

In the context in which the first version of SimuTC was developed, the requirements of open-source (free) software and the ability to function offline were addressed, making it a valuable tool in undergraduate educational contexts with limited resources or logistical constraints. However, the simulator has some limitations. Firstly, it is restricted to images of patients without structural abnormalities, which prevents the exploration of pathological cases. Secondly, its scope is limited to the reconstruction stage, without including simulation of the clinical environment or the complete acquisition process. Furthermore, the evaluation was based on the perceptions of students and teachers, without including objective measures of impact on academic performance or the transfer of knowledge to clinical contexts. This situation reflects one of the main criticisms of most existing simulators, where qualitative studies based on self-reports predominate.[22]

Despite this, both students and teachers highlighted the usefulness of SimuTC as a training supplement, especially in technical subjects such as CT. Its ease of use, intuitive visualization, and ability to freely navigate the images were valued. Nevertheless, improvements were proposed focusing on the visual aspect, the inclusion of more anatomical structures, and additional parameters such as the angiographic window or iterative adjustments, suggesting a high potential for scalability of the system.

In this scenario, it is essential to consider not only the technical and pedagogical validation of the simulator, but also its integration within the career curriculum. At the Universidad de Valparaíso, SimuTC has been systematically implemented in the CT course, corresponding to the seventh semester, particularly in the initial modules focused on the conceptual foundations of the modality, although its use can be extended to other course content. Its incorporation is currently formative, given that the current version does not record values or store individual performance responses;

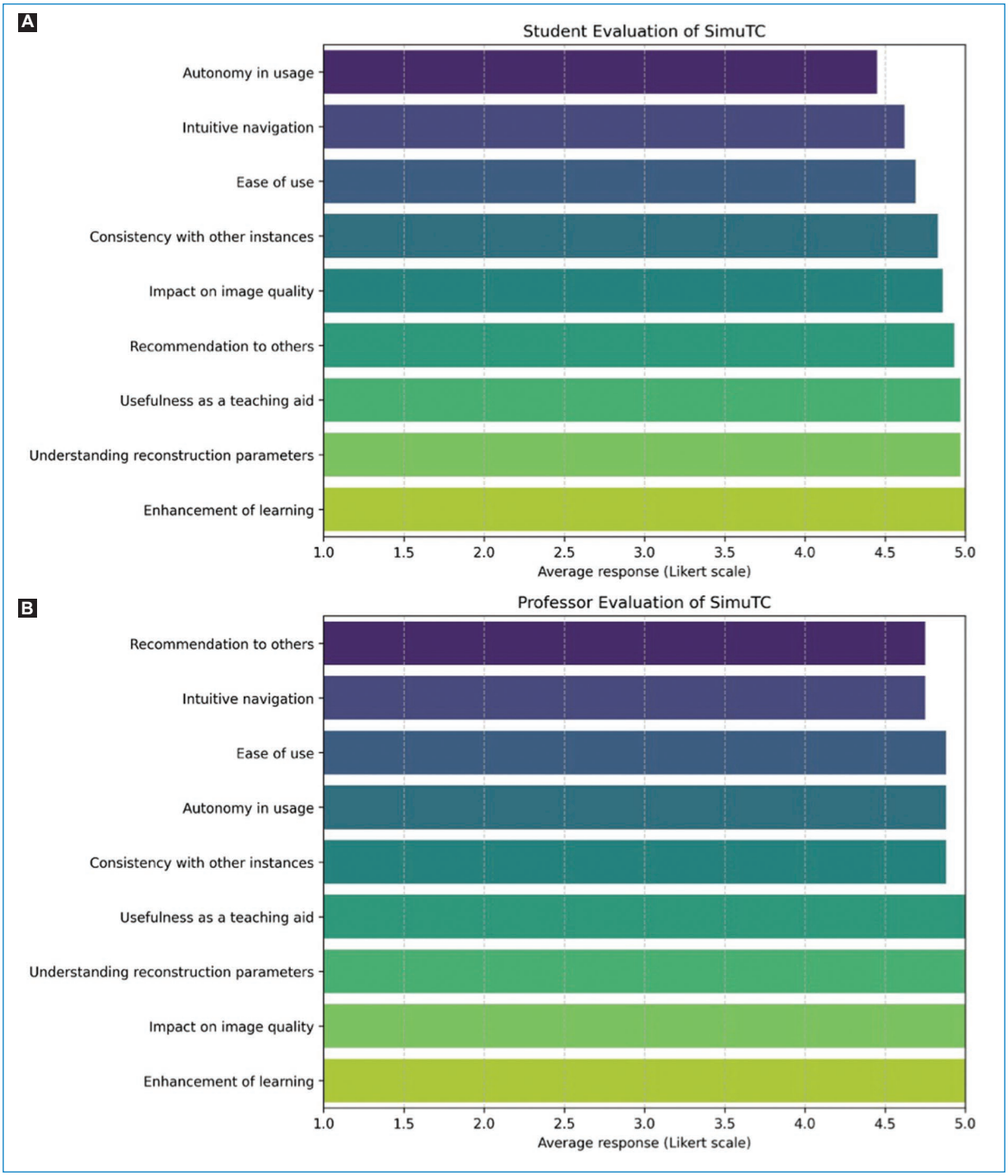

Figure 5. Overall results of the perception survey on SimuTC by students **(A)** and faculty **(B)** of the School of Medical Technology (*Escuela de Tecnología Médica*).

however, practical activities have been designed that encourage experimentation with different parameter combinations, complemented by the tool's automatic feedback and group discussions guided by the teaching team.

The simulator has been used in teacher-led workshops, which foster group reflection and critical discussion of the results, as well as in individual self-assessment activities, reinforcing learning autonomy. This dual feedback approach (teacher and automated) aims to enhance

Figure 6. Word cloud of free-form comments about SimuTC by students.

both deliberate practice and subsequent reflection, essential aspects of simulation-based learning.

Based on these findings, several lines of future work are envisioned, with a projection of the tool's progressive evolution. Priorities include improving the visual design of the user interface, incorporating new image sets from different anatomical regions, including images from contrast studies, and adding other technical parameters of the reconstruction process, such as intensity or percentage of iterative reconstruction and other window combinations, such as for example, the angiographic window. In parallel, the development of a more specific feedback system is planned, capable of identifying the inappropriate parameter and justifying why it does not align with the diagnostic objective, along with the development of a usage logging system that allows for tracking individual student responses and obtaining objective learning metrics that will enable the use of SimuTC within summative assessments.

Another relevant aspect is quantitative pedagogical validation, through studies with pre- and post-test designs, comparative analyses between groups, or longitudinal studies that measure knowledge retention. Finally, creating a multiplatform or web-based version would expand its reach and accessibility, facilitate its integration into educational platforms, allowing for resource sharing between institutions, integration with educational platforms, and even incorporate interactive assessment modules and AI-based personalization.

Conclusions

The SimuTC educational simulator is an innovative, accessible, and highly accepted proposal aimed at strengthening the teaching of CT image reconstruction in undergraduate contexts. Its pedagogical design focused on parametric analysis, its offline functionality, and its low technical requirements make it a particularly relevant tool for institutions with limited resources or restricted access to clinical equipment.

Funding

The authors declare that they have not received funding.

Conflicts of interest

The authors declare no conflicts of interest.

Ethical considerations

Protection of human subjects and animals. The authors declare that no experiments on humans or animals were performed for this research.

Table 2. General comments from faculty members on the SimuTC evaluation

Faculty member	General comment
1	"For future versions, I would improve the interface to make it more modern and intuitive, to better suit current users (students)."
2	"Excellent tool for students! For future versions, please include skeletal muscle and an angiographic window. Congratulations!"
3	"The user interface is aesthetically pleasing."
4	"It's a very good tool. An angiographic window and reconstruction types with different levels of iteration could be added."
5	"The aesthetics could be improved to be more similar to GE or Siemens medical platforms."
6	"I think it's an excellent tool! Learning by doing! Congratulations to the team that worked on this project. It certainly contributes greatly to the training of medical technology students."
7	"I believe it is an excellent contribution to the teaching and learning process for students. I can see that it's a user-friendly platform and I believe it will be an excellent support tool for this important subject."
8	"I think the application is fantastic, and as a suggestion, I'd like to add a test bank so students can check their learning level. This might be included in version 2 of the application, which we're eagerly awaiting, and I want to reiterate that I really liked it."

Confidentiality, informed consent, and ethical approval. The authors have obtained approval from the Ethics Committee for the analysis of routinely collected and anonymized clinical data; therefore, individual informed consent was not required. Relevant ethical recommendations have been followed.

Declaration on the use of artificial intelligence. The authors declare that no generative artificial intelligence was used in the writing or creation of the content of this manuscript.

References

1. Withers PJ, Bouman C, Carmignato S, Cnudde V, Grimaldi D, Hagen CK, et al. X-ray computed tomography. Nat Rev Methods Primers. 2021;1:18.
2. Al-Hayek Y, Ofori-Manteaw B, Frame N, Spuur K, Zheng X, Rose L, et al. Localiser radiographs in CT: current practice, radiation dose, image quality and clinical applications. Radiography. 2024;30:1546-55.
3. Lopez DR, Crosetti B de B. Diseño de una propuesta didáctica para el uso de simuladores virtuales en la rama sanitaria de formación profesional. RiiTE Rev Interuniv Investig Tecnol Educ. 2020;(8):1-16.
4. Ketterer SJ, Callender J, Warren M, Al-Samarraie F, Ball B, Calder KA, et al. Simulated versus traditional therapeutic radiography placements: a randomised controlled trial. Radiography. 2020;26:140-6.
5. Willemink MJ, De Jong PA, Leiner T, De Heer LM, Nievelstein RAJ, Budde RPJ, et al. Iterative reconstruction techniques for computed tomography. Part 1: technical principles. Eur Radiol. 2013;23:1623-31.
6. Chaka B, Hardy M. Computer based simulation in CT and MRI radiography education: current role and future opportunities. Radiography. 2021;27:733-9.
7. Contreras Olive Y, Reyes Fournier M, Nates Reyes AB, Pérez Arbolay MD. Los simuladores como medios de enseñanza en la docencia médica. Rev Cub Med Mil. 2018;47:1-11.
8. Ruiz-Parra AI, Angel-Müller E, Guevara O. La simulación clínica y el aprendizaje virtual. Tecnologías complementarias para la educación médica. Rev Fac Med (Bogota). 2009;57:67-79.
9. Falloon G. Using simulations to teach young students science concepts: an experiential learning theoretical analysis. Comput Educ. 2019;135:138-59.
10. Lee WC, Neo WL, Chen DT, Lin TB. Fostering changes in teacher attitudes toward the use of computer simulations: flexibility, pedagogy, usability and needs. Educ Inf Technol. 2021;26:4905-23.
11. Rodríguez-Torres AF, Orozco-Alarcón KE, Delgado-Campoverde ME, Curay-Carrera PA, Barros-Castro HA. La simulación clínica en la formación de profesionales de la salud: una oportunidad para aprender a aprender. Dominio Cienc. 2023;9:438-54.
12. Brim NM, Venkatan SK, Gordon JA, Alexander EK. Long-term educational impact of a simulator curriculum on medical student education in an internal medicine clerkship. Simul Healthc. 2010;5:75-81.
13. Yin Mar Oo, Nataraja RM. The application of simulation-based medical education in low- and middle-income countries: the Myanmar experience. Semin Pediatr Surg. 2020;29:150910.
14. Stinken-Rösner L. Simulations in science education: status quo. Prog Sci Educ (PriSE). 2020;3:26-34.
15. He L, Lu W, Wang Z, Wang S, Xue M. CTSim: a numerical simulator of computed tomography for high-quality radiological education. Int J CARS. 2022;17:1257-69.
16. Abadi E, Harrawood B, Sharma S, Kapadia A, Segars WP, Samei E. DukeSim: a realistic, rapid, and scanner-specific simulation framework in computed tomography. IEEE Trans Med Imaging. 2019;38:1457-65.
17. NETRAD CT-Scanner opens at University of Sydney. OzTREKK; 2014 Mar 20. (Consultado el 18-06-2025.) Disponible en: https://oztrekk.com/news/netrad-ct-scanner-opens-at-university-of-sydney/.
18. Virtual CT Trainer - computerized tomography training. RadTechEdU; 2021. (Consultado el 18-06-2025.) Disponible en: https://radtechedu.com/vct/.
19. Siemens Healthcare. SmartSimulator. 2021 (Consultado el 14-10-2025.) Disponible en: https://www.siemens-healthineers.com/de-ch/services/customer-services/connect-platforms-and-smartenablers/smart-simulator.
20. Chau M, Arruza E. Maximising undergraduate medical radiation students' learning experiences using cloud-based computed tomography (CT) software. Simul Gaming. 2023;54:447-60.
21. Stowe J, O'Hallora C, Photopoulos G, Lia A, Quinn M, Tschan F, et al. CTSim: changing teaching practice in radiography with simulation. Radiography (Lond). 2021;27:490-8.
22. McInerney N, Nally D, Khan MF, Heneghan H, Cahill RA. Performance effects of simulation training for medical students - a systematic review. GMS J Med Educ. 2022;39:Doc51.

AUSTRAL JOURNAL OF IMAGING
REVISTA CHILENA DE RADIOLOGÍA

PERMANYER

Check for updates

ORIGINAL ARTICLE

Percutaneous ultrasound-guided intrahepatic portosystemic shunt (TIPS)

Derivación portosistémica intrahepática (TIPS) guiado por ultrasonido por vía percutánea

Patricio Vargas-Hudson, Roberto Muñoz-Estrada, Benjamín Horwitz-Zanolli, Juan Niedmann-Espinosa, Gian Zamboni-Torres, Sebastián Glaria-Grego, Antonio Vallejos-Cabezas, and Nicolas Radic-González*

Imaging Department, Clínica Alemana-Universidad del Desarrollo, Santiago, Chile

Abstract

Introduction: *The transjugular intrahepatic portosystemic shunt (TIPS) is a procedure used to reduce portal system pressure. The main difficulty of the conventional technique lies in accessing the portal vein from the hepatic vein.* **Objective:** *To evaluate the technical feasibility, safety, and clinical outcomes of TIPS creation using an ultrasound-guided percutaneous transhepatic approach in an institutional case series.* **Material and methods:** *A retrospective study was conducted including patients between 2007 and 2024, who underwent a technical variant of the TIPS procedure consisting of a percutaneous transhepatic parietal access guided by ultrasound.* **Results:** *The technique achieved 100% technical success and single-attempt portal access, leading to low fluoroscopy times and radiation doses. Portal gradient reduced by 10 mmHg average. The technique overcomes the "blind" access limitation, optimizing safety and radiation exposure. Complications and patency are consistent with the literature.* **Conclusions:** *The ultrasound-guided percutaneous transhepatic approach for TIPS creation is safe and effective in our institutional experience, allowing for reduced puncture times and radiation exposure.*

Keywords: *Transjugular intrahepatic portosystemic shunt. TIPS. Portal hypertension. Ultrasound. Percutaneous procedures.*

Resumen

Introducción: *La derivación portosistémica intrahepática transyugular (TIPS) es un procedimiento utilizado para reducir la presión del sistema portal. La dificultad de la técnica convencional radica principalmente en el acceso a la porta desde la vena hepática.* **Objetivo:** *Evaluar la factibilidad técnica, la seguridad y los resultados clínicos de la realización de TIPS mediante técnica percutánea transparietohepática guiada por ultrasonido, en una serie institucional.* **Material y métodos:** *Se realizó un estudio retrospectivo que incluyó pacientes entre 2007 y 2024 que fueron sometidos a una variante técnica del TIPS consistente en un acceso percutáneo transparietohepático guiado por ultrasonido.* **Resultados:** *La técnica tuvo un 100% de éxito técnico y acceso portal en un solo intento, resultando en bajos tiempos de fluoroscopia y dosis de radiación. Gradiente portal reducido en 10 mmHg en promedio. La técnica supera la limitación del acceso «a ciegas», optimizando la seguridad y la exposición radiológica. Las complicaciones y la permeabilidad son concordantes con las descritas en la literatura.* **Conclusiones:** *La técnica percutánea transparietohepática guiada por ultrasonido para la creación de TIPS es segura y eficaz en nuestra experiencia institucional, permitiendo reducir los tiempos de punción y de exposición radiológica.*

Palabras clave: *Derivación portosistémica intrahepática. TIPS. Hipertensión portal. Ultrasonido. Procedimientos percutáneos.*

***Correspondence:**
Roberto Muñoz-Estrada
E-mail: rmunoze@udd.cl

Date of reception: 30-04-2025
Date of acceptance: 05-02-2026
DOI: 10.24875/AJI.25000029

Available online: 14-07-2026
Austral J. Imaging. (Engl. ed.). 2026;32(3):124-131
www.resochradi.com

Introduction

Transjugular intrahepatic portosystemic shunt (TIPS) is a validated procedure for reducing portal pressure and, consequently, associated complications. Its main indications include variceal (exsanguinating) hemorrhage, refractory ascites, hepatic hydrothorax, and Budd-Chiari syndrome.

The conventional technique is performed sequentially: it begins with catheterization of a hepatic vein via a jugular access, followed by the advancement of a rigid stylet to puncture a portal branch from this hepatic vein under fluoroscopic or endovascular ultrasound guidance. Once the portosystemic communication is established, a stent is implanted, completing the shunt[1-4].

The portal puncture likely represents the greatest technical challenge, as it is performed with a rigid needle, the direction of which can only be modified by displacing or rotating the entire assembly, without the option of achieving a controlled curvature. This limitation, coupled with the fact that the procedure is performed under fluoroscopic guidance and partially "blindly," without visualization of the portal vein to be punctured, contributes to a higher rate of technical failures, increased operative time, and higher radiation dose, with greater risk of complications[5-8].

To reduce these difficulties, we evaluated the technical feasibility, safety, and clinical outcomes of a variant technique that initially involves an ultrasound-guided transjugular percutaneous access, which, in a single transfixion puncture, connects a branch of the portal vein and a hepatic vein. At our institution, this technique was applied in patients for the creation of a TIPS (transjugular intrahepatic portosystemic shunt).

Materials and methods

Retrospective data were collected from patients who, after signing informed consent, underwent portosystemic shunting at our center between 2007 and 2024.

Procedures performed up to 2021 were carried out in an angiography ward using a Siemens Axiom Artis system. In subsequent years, procedures were performed using a Philips Azurion C20 FlexArm system. These procedures were performed by two interventional radiologists, both with more than 10 years of experience in this technique.

Technique

With the patient in the supine position and under anesthesia, a hepatic ultrasound is used to locate in the same plane an image of the selected portal vein and hepatic vein.

Both are then traversed with a 22G needle in real time. A 0.018" guidewire is inserted through the needle into the right atrium (Fig. 1), and then a 6 Fr introducer sheath is advanced into the portal vein.

Subsequently, access to the right internal jugular vein is obtained under ultrasound guidance, and a 14 Fr introducer sheath is advanced. A snare loop is advanced to the confluence of the hepatic veins, the 0.018" guidewire inserted percutaneously is captured and brought out through the jugular vein, achieving a through-and-through access (Fig. 2).

The hepatic tract is dilated with a 5 mm monorail balloon. From the jugular access point, a long 6 Fr introducer sheath is advanced to the portal access point. From this point, a second guidewire (0.035") is introduced into the peripheral portal venous system (splenic or superior mesenteric vein). The 6 Fr sheath containing the two guidewires is removed and reinstalled by the second guidewire up to the portal axis (Fig. 3).

Portal and systemic pressures (at the confluence of the hepatic veins) are measured to calculate the portosystemic pressure gradient. The portohepatic tract is dilated with a 5 mm balloon via the guidewire.

The 6 Fr sheath is exchanged for a 10 Fr sheath. Portography is performed with a graduated catheter to measure the estimated length of the stent. Subsequently, the stent is deployed, leaving the exposed/uncovered portion inside the portal vein and the covered portion in the hepatic tract up to the confluence of the hepatic veins (Fig. 4).

Finally, the percutaneous hepatic access tract is embolized with cyanoacrylate (Histoacryl®) (Fig. 5).

It should be noted that the 0.018" guidewire remains in place throughout the procedure for access safety and system stability (Fig. 6).

Data analysis

Data were collected from the AGFA Enterprise 8.3.2.060 RIS-PACS system. Clinical variables, including age, comorbidities, procedure indication, and associated complications, were recorded. For the technical analysis, pre- and post-procedure portosystemic pressures, as well as radiation doses (kerma air product [KAP] and fluoroscopy time [FT]), were recorded. Radiation levels were obtained from both data collected by the Qaelum Dose software and from transcripts written by the operator before the software's implementation at our center. The written data were subsequently digitized and analyzed.

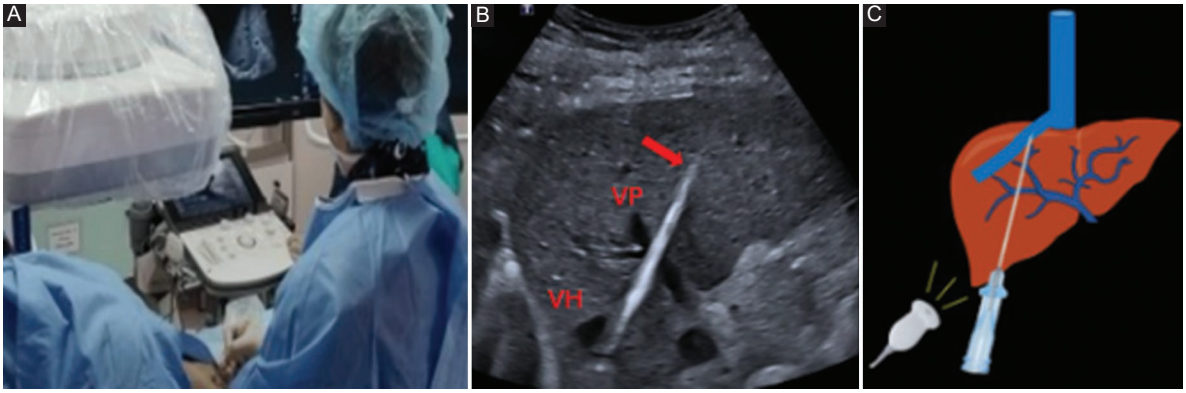

Figure 1. **A** and **B:** ultrasound-guided transhepatic needle puncture (arrow) of the selected portal vein (VP) and hepatic vein (VH). **C:** graphic representation.

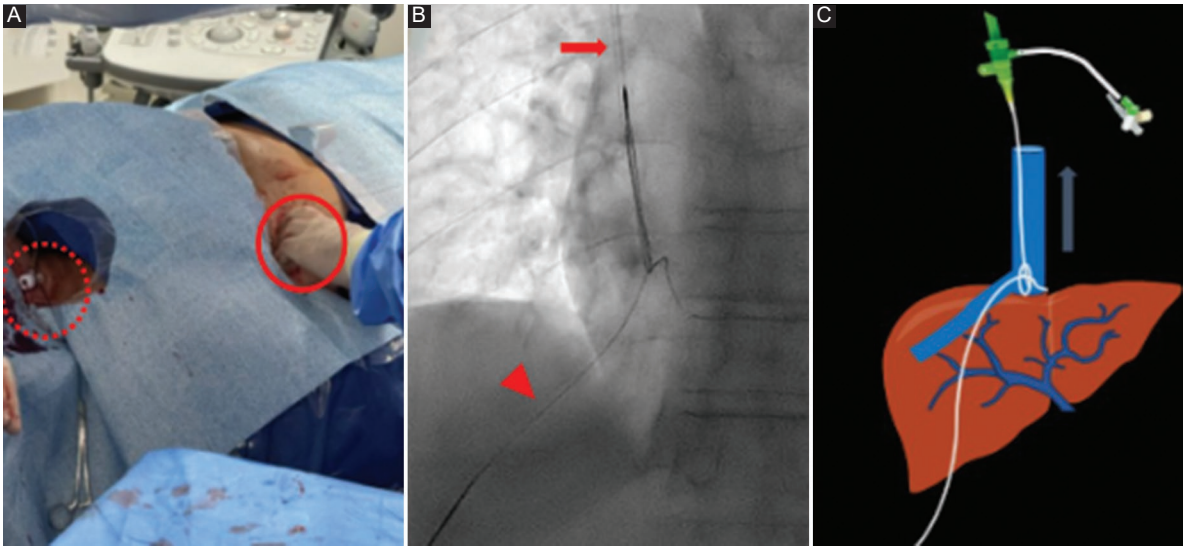

Figure 2. **A:** right jugular access (dotted circle) and percutaneous abdominal access (solid circle). **B:** snare loop (arrow) capturing the 0.018" guidewire (arrowhead). **C:** graphic representation.

Results

Clinical characteristics

During the 2007–2024 period, 27 procedures were performed on patients at the Clínica Alemana in Santiago. The most frequent comorbidity was liver cirrhosis, while the main clinical symptom indications were variceal hemorrhage and ascites. The main characteristics of the patients are summarized in table 1.

Success Rate

Technical success was defined as the effective creation of a portosystemic shunt, which was achieved in 100% of the cases using this technique variant. Regarding hemodynamic success, the studied cohort showed an average net reduction of 10 mmHg, representing an average decrease of 51% (Fig. 7). The portosystemic gradient after the procedure varied between 5 and 12 mmHg.

Number of needle insertion attempts

In all procedures performed with this technique, the portal vein was successfully catheterized in a single attempt.

Radiation dose

KAP and FT values were collected for all procedures performed between 2007 and 2024. The median

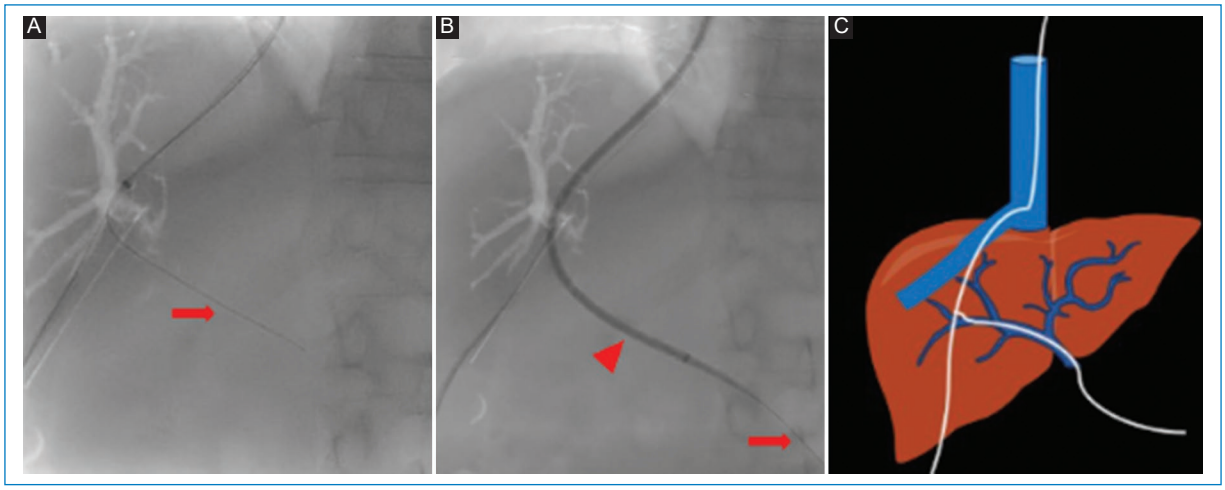

Figure 3. **A:** advancement of the 0.035" guidewire into the portal system, in this case toward the splenic vein (arrow). **B:** advancement via the guidewire (arrowhead). **C:** graphic representation.

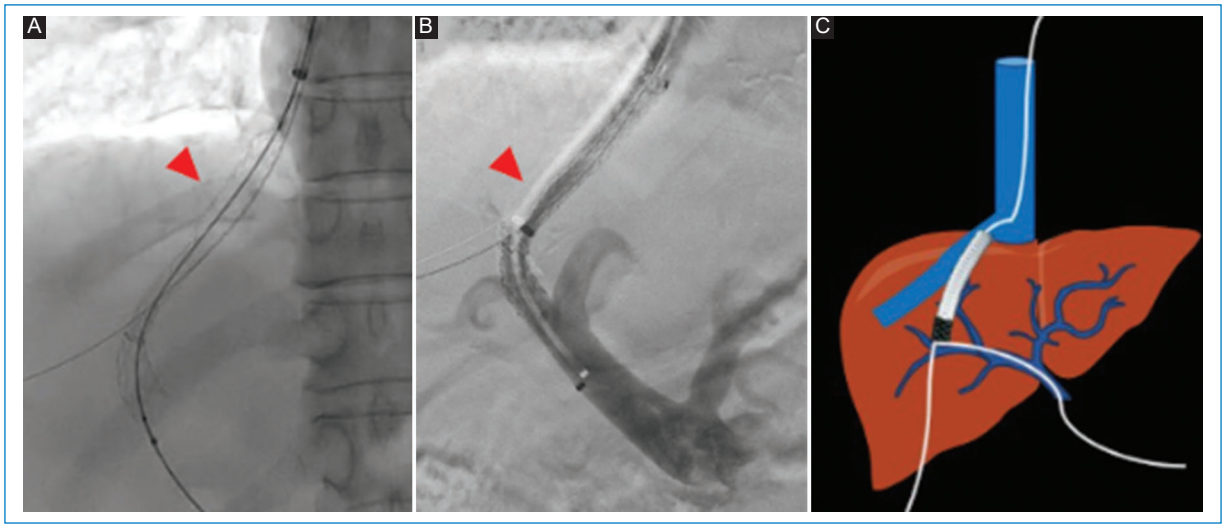

Figure 4. **A:** deployment of the stent (arrowhead). **B:** verification portography. **C:** graphic representation.

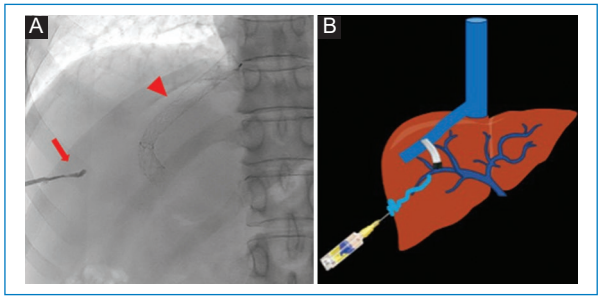

Figure 5. **A:** embolization path with cyanoacrylate (arrow) and stent already in place (arrowhead). **B:** graphic representation.

KAP was 120 Gy·cm² and the median FT was 19 minutes.

Complications

In this series, 2 patients (7%) experienced minor, self-limiting bleeding, without clinical repercussions or the need for specific treatment.

Regarding functional complications, 1 patient (4%) developed right heart failure and 6 (22%) developed hepatic encephalopathy; of these, 2 (7%) required

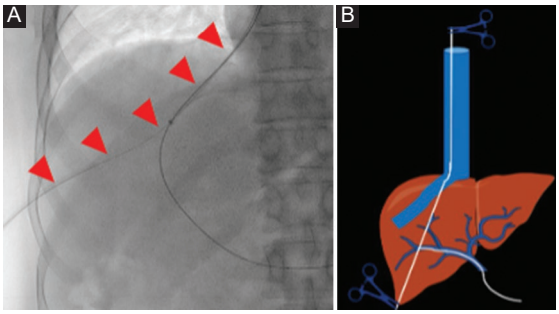

Figure 6. **A:** 0.018" guidewire (arrowheads). **B:** graphic representation.

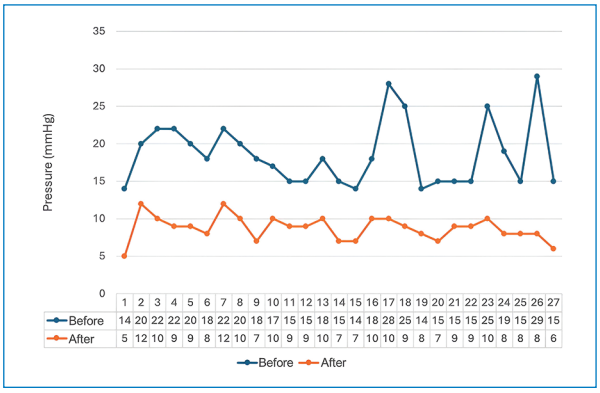

Figure 7. Comparative graph showing portosystemic pressure gradient values before and after the procedure.

prosthesis calibration, while the remaining patients were managed conservatively.

Patency over time

Only 3 patients (11%) presented with TIPS dysfunction during follow-up, all secondary to thrombosis. All required reintervention, with resolution via percutaneous repair. None of the three patients mentioned required a third intervention.

Table 1. Clinical characteristics of the patients

N° of patients	Age range	Comorbidity	Clinical symptom indication
27	16-83 years (mean: 53 years)	Chronic liver damage: 23 Myeloproliferative syndrome: 3 Coagulopathy: 1	Variceal hemorrhage: 11 Ascites: 10 Budd-Chiari malformation: 4 Portal vein thrombosis: 1 Preoperative: 1

Discussion

Advantages of access

The critical step in the conventional TIPS procedure is the puncture of both venous systems (aiming to access a portal vein branch from a hepatic vein) under fluoroscopic guidance[5-9]. In this conventional approach, the operator relies on a two-dimensional image, which does not allow for determining precise needle depth or positioning.

The rigidity of the puncture device limits the range of maneuverability and the ability to achieve controlled curvature, as this can only be modified by displacing or rotating the entire assembly. This contributes to the intervention being partially "blind," and success depends largely on the operator's skill and experience, and partly on chance, in estimating the exact position and direction of the needle. This challenge is greater in patients with liver cirrhosis due to the distortion of vascular anatomy and parenchymal rigidity, which can lead to multiple attempts to catheterize the portal vein. This, in turn, increases the procedure time, radiation exposure, and complication rate[7-9].

To improve visualization during the procedure, various fluoroscopic alternatives have been implemented, such as a simultaneous portography[5,10-13]. However, these options do not resolve the problem of device rigidity, which continues to limit the procedure's accuracy. Therefore, a detailed understanding of the anatomical relationship between the hepatic veins and the portal vein becomes the most crucial factor for accurately guiding the needle, minimizing the risk of complications, and reducing radiation dose. Generally speaking, fewer attempts to access the portal vein result in a safer procedure.

The ultrasound-guided *single-needle-pass* transhepatic puncture technique was initially described by Raza et al.[7], who in 2006 reported a 73% technical success rate (11 of 15 patients), suggesting that significant anatomical distortion due to advanced cirrhosis limited its applicability. Subsequently, Liang et al.[8] expanded the use of this variant to cases of complex anatomy in which the conventional transjugular approach had failed, achieving a 100% technical success rate in a series of 6 patients. Our institutional experience with 27 cases using real-time ultrasound for direct and simultaneous visualization of portal and hepatic vein puncture aligns with the feasibility

demonstrated by Liang et al.[8], but in a larger cohort, achieving 100% technical success and portal vein catheterization on the first attempt in all patients, which optimizes safety, reduces radiation exposure, and minimizes procedure time. This reinforces the technique's usefulness not only as a rescue alternative in challenging anatomies but also as a safe and reproducible primary approach in experienced hands, overcoming the anatomical limitations described in initial series using similar techniques.

Hemodynamic success

In hemodynamic terms, the consensus described in the literature establishes a target portosystemic gradient ≤ 12 mmHg[1,3,4,11]. In our cohort, portosystemic gradients after the procedure fluctuated between 5 and 12 mmHg, therefore all were considered to have met the hemodynamic success criterion.

Stability and safety

The 0.018" guidewire remains in place throughout the entire procedure (Fig. 6). It is inserted percutaneously through the right upper quadrant of the abdomen, passing continuously through the liver, portal vein, hepatic vein, and superior and inferior vena cava, until it reaches the right jugular vein, where it exits through the skin in the ipsilateral cervical region. This path ensures a stable and continuous working line throughout all phases. The constant presence of the guidewire offers advantages in safety and efficiency by acting as a reliable reference that allows the path to remain correctly aligned throughout the procedure. If an element shifts at any point, the established working line allows for quick and safe repositioning of the element without the need to reconstruct the access.

Radiation dose and contrast use

The procedure time and fluoroscopy duration significantly influence radiation exposure, and their prolongation increases the risk for both the patient and the operator. It should be noted that the conventional technique uses fluoroscopy as the primary imaging method.

The median KAP (120 Gy·cm²) and FT (19 minutes) in our series are below the levels reported in the American College of Radiology DIR-Fluoro study, published in 2023, which provided reference standards for daily practice in interventional radiology procedures[14]. This suggests dose optimization, attributable to the complementary use of ultrasound (a non-ionizing imaging method) for the direct, real-time localization of vascular structures.

This observation is consistent with that reported by Cam et al.[9], who, although they evaluated a different technical variant than the one described in this series, also demonstrated that incorporating ultrasound as a guidance tool significantly reduces radiation exposure (median of 125.6 Gy·cm² versus 351.7 Gy·cm² in the conventional technique). Thus, this technique shares the benefit of reducing the frequency of fluoroscopic acquisitions, limiting itself to posteroanterior projections and avoiding oblique projections to estimate the needle position.

Another advantage of this variant is the potential reduction in the volume of contrast medium used.

Although this variable was not quantified in our series, experience indicates that a more direct and precise puncture avoids additional maneuvers (such as repeated portography). This perception is supported by what Cam et al.[9] described, who documented a statistically significant reduction in contrast volume in ultrasound-guided procedures (average: 67.9 vs. 87.1 ml), validating the hypothesis that precise access decreases the need for contrast medium.

Cost and stent positioning considerations

Although a formal cost analysis is not available, this technique variant presents a potential cost savings by requiring fewer instruments than the conventional procedure, which could reduce the overall cost, an aspect that is especially relevant in centers with limited resources and in healthcare systems with high demand.

This variant also allows for real-time, direct visualization of the intraparenchymal path between the portal vein and the hepatic vein (Fig. 8), facilitating the selection of the appropriate stent size.

Complications and patency

Complications associated with TIPS are infrequent events and can be related to both the technique itself and the pathophysiological consequences of creating a portosystemic shunt. In our cohort, the observed complications were minor, and their overall incidence falls within the ranges reported in the literature. From a procedural point of view, minor and self-limiting bleeding, such as that which occurred in 2 patients (7%), usually resolves spontaneously and is often not systematically reported in the literature. Regarding functional

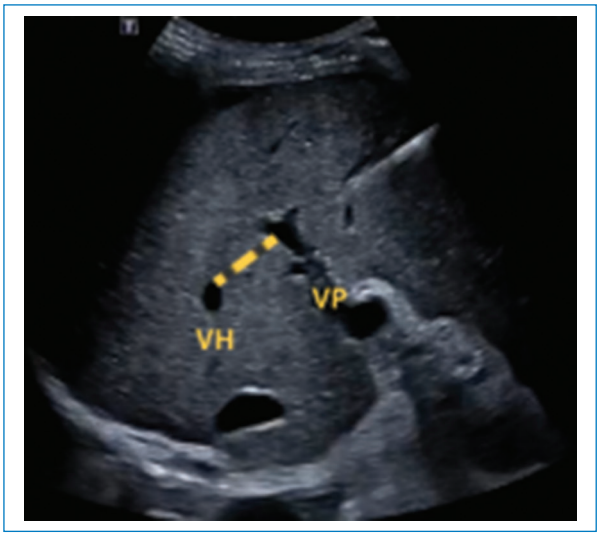

Figure 8. Ultrasound estimation of the distance (yellow dashed line) between the portal vein (VP) and the hepatic vein (VH).

complications arising from the shunt, the incidence of hepatic encephalopathy in 6 patients (22%) is close to the lower limit of the reported range (30-50% of cases)[4,15], being disabling in approximately 8%. Of these, only 2 patients (7%) required stent calibration, while the rest were managed conservatively. Right heart failure occurred in only one patient (4%), consistent with the maximum reported incidence of 20%[4].

Regarding durability, the use of polytetrafluoroethylene-coated stents has improved shunt functionality over time, reporting patency rates of 80-90% per year. In our cohort, only coated stents were used, and the TIPS dysfunction rate was 11% (3 patients), due to thrombosis, consistent with current evidence[16]. All cases of dysfunction required reintervention with percutaneous angioplasty. It is possible that the thrombosis in the described cases was related to a baseline prothrombotic state, given that one of the patients had polycythemia *vera* (PV) and another had essential thrombocythemia (ET).

Limitations

The limitations are inherent to a retrospective study, which does not allow for attributing causality. The sample size is small (n = 27) and there was no control group, so it cannot be definitively stated that the technique is superior. The procedural data come from a single center and were performed by two highly experienced operators, so the findings may not be generalizable to centers with less advanced technology or experience.

Conclusions

The ultrasound-guided transperitoneal transhepatic percutaneous technique for TIPS creation is safe and effective in our institutional experience, allowing a reduction in puncture times and radiological exposure.

Funding

The authors declare that they have not received funding.

Conflicts of interest

The authors declare no conflicts of interest.

Ethical considerations

Protection of human subjects and animals. The authors declare that no experiments on humans or animals were performed for this research.

Confidentiality, informed consent, and ethical approval. The authors have obtained approval from the Ethics Committee for the analysis of routinely collected and anonymized clinical data; therefore, individual informed consent was not required. Relevant ethical recommendations have been followed.

Declaration on the use of artificial intelligence. The authors declare that no generative artificial intelligence was used in the writing or creation of the content of this manuscript.

References

1. Lee EW, Eghtesad B, García-Tsao G, Haskal ZJ, Hernández-Gea V, Jalaeian H, et al. AASLD Practice Guidance on the use of TIPS, variceal embolization, and retrograde transvenous obliteration in the management of variceal hemorrhage. Hepatology. 2024;79:224-50.
2. European Association for the Study of the Liver; Bureau C, Larrue H, Cortes-Cerisuleo M, Miraglia R, Procopet B, Rudler M, et al. EASL Clinical Practice Guidelines on TIPS. J Hepatol. 2025;83:177-210.
3. Ferral H, López-Benítez R. The history of the transjugular intrahepatic portosystemic shunt. Semin Intervent Radiol. 2023;40:19-20.
4. Brooks MD, Maingard J. Transjugular intrahepatic portosystemic shunts. En: Mauro MA, Murphy KPJ, Venbrux AC, Morgan RA, eds. Image-guided interventions. 3rd ed. Philadelphia: Saunders; 2020. p. 639-44.
5. Gaba RC, Khiatani VL, Knuttinen MG, Omene BO, Carrillo TC, Bui JT, et al. Comprehensive review of TIPS technical complications and how to avoid them. AJR Am J Roentgenol. 2011;196:675-85.
6. Shah RP, Sze DY. Complications during transjugular intrahepatic portosystemic shunt creation. Tech Vasc Interv Radiol. 2016;19:61-73.
7. Raza SA, Walser E, Hernández A, Chen K, Marroquin S. Transhepatic puncture of portal and hepatic veins for TIPS using a single-needle pass under sonographic guidance. AJR Am J Roentgenol. 2006;187:248-52.
8. Liang HL, Liu WC, Huang JS, Chen MCY, Lai KH, Pan HB, et al. TIPS in patients with cranial porta hepatis: ultrasound-guided transhepatic portohepatic-portocaval puncture in a single-needle pass. AJR Am J Roentgenol. 2011;196:914-8.
9. Cam I, Gencturk M, Shrestha P, Golzarian J, Flanagan S, Lim N, et al. Ultrasound-guided portal vein access and percutaneous wire placement in the portal vein are associated with shorter procedure times and lower radiation doses during TIPS placement. AJR Am J Roentgenol. 2021;216:1291-9.

10. Sinha I, Goldman DT, Patel RS, Nowakowski FS. Advanced techniques for accessing the portal vein during transjugular intrahepatic portosystemic shunt creation. Semin Intervent Radiol. 2023;40:79-86.
11. Dariushnia SR, Haskal ZJ, Midia M, Martin LG, Walker TG, Kalva SP, et al. Quality improvement guidelines for transjugular intrahepatic portosystemic shunts. J Vasc Interv Radiol. 2016;27:1-7.
12. Richard J, Thornburg B. New techniques and devices in transjugular intrahepatic portosystemic shunt placement. Semin Intervent Radiol. 2018;35: 206-14.
13. Zemel G, Becker G, Bancroft JW, Benenati JF, Katzen BT. Technical advances in transjugular intrahepatic portosystemic shunt creation. Radiographics. 1992;12:615-22.
14. Jones AK, Wunderle KA, Fruscello T, Simanowith M, Cline B, Dharmadhikari S, et al. Patient radiation doses in IR procedures: the American College of Radiology dose index registry-fluoroscopy pilot. J Vasc Interv Radiol. 2023;34:544-55.e11.
15. Trivedi S, Lam K, Ganesh A, Hasnain Y, Hassan W, Herren J, et al. Hepatic encephalopathy after transjugular intrahepatic portosystemic shunt creation. Semin Intervent Radiol. 2023;40:9-14.
16. Goessmann H, Schuffenhauer V, Kandulski A, Weigand K, Jung EM, Uller W, et al. Retrospective evaluation of early thrombosis in transjugular intrahepatic portosystemic polytetrafluoroethylene-coated shunts under 2-day postinterventional heparinization. Sci Rep. 2022; 12:11893.

AUSTRAL JOURNAL OF IMAGING
REVISTA CHILENA DE RADIOLOGÍA

PERMANYER

Check for updates

REVIEW ARTICLE

Epiploic appendagitis: the great imitator in acute abdominal pain

Apendagitis epiploica: la gran simuladora en el dolor abdominal agudo

Natalia Tobajas-Ramos, Ana Goñi-Navarro, Andrea Senovilla-Ardid, Ma. Beatriz Fernández-Lago, Amalia Aranaz-Murillo, and Julián García-Maroto*

Radiology Department, Hospital Universitario Miguel Servet, Zaragoza, Spain

Abstract

Epiploic appendagitis is an infrequent cause of acute abdominal pain, often mistaken for appendicitis, diverticulitis, or cholecystitis. It results from the torsion and ischemia of the colon's epiploic appendages, leading to localized inflammation. Differential diagnosis is crucial, as its symptoms may overlap with other conditions. Appendicitis is associated with fever and leukocytosis, which are generally absent in epiploic appendagitis. Diverticulitis typically presents with colonic wall thickening on tomography, whereas epiploic appendagitis appears as an oval fat-density lesion with a hyperdense rim (ring sign) and an inflamed fatty center. Other conditions such as mesenteric lymphadenitis and omental epiploitis should also be considered. Treatment is conservative, based on anti-inflammatory drugs and analgesia, with resolution in 7-14 days. Proper identification prevents unnecessary surgeries and allows for appropriate management, highlighting the importance of imaging diagnosis in emergency settings.

Keywords: *Epiploic appendagitis. Differential diagnosis. Computed tomography. Ultrasonography. Abdominal pain.*

Resumen

La apendagitis epiploica es una causa infrecuente de dolor abdominal agudo, a menudo confundida con apendicitis, diverticulitis o colecistitis. Se produce por la torsión e isquemia de los apéndices epiploicos del colon, lo que genera inflamación localizada. El diagnóstico diferencial es clave, ya que sus síntomas pueden solaparse con otras afecciones. La apendicitis se asocia con fiebre y leucocitosis, generalmente ausentes en la apendagitis epiploica. La diverticulitis suele presentar engrosamiento parietal del colon en la tomografía, mientras que la apendagitis muestra una lesión ovalada de grasa con un borde hiperdenso (signo del anillo) y un centro graso inflamado. Otras entidades como la linfadenitis mesentérica y la epiploitis omental también deben considerarse. El tratamiento es conservador, con antiinflamatorios y analgesia; se resuelve en 7-14 días. Su correcta identificación evita cirugías innecesarias y permite un tratamiento adecuado. Destaca la importancia del diagnóstico por imagen en urgencias.

Palabras clave: *Apendagitis epiploica. Diagnóstico diferencial. Tomografía computarizada. Ecografía. Dolor abdominal.*

***Correspondence:**
Natalia Tobajas-Ramos
E-mail: nataliatobajasramos19@gmail.com

Date of reception: 12-03-2025
Date of acceptance: 20-07-2025
DOI: 10.24875/AJI.25000018

Available online: 14-07-2026
Austral J. Imaging. (Engl. ed.). 2026;32(3):132-141
www.resochradi.com

Introduction

Epiploic appendagitis is an uncommon cause of acute abdominal pain. It originates from the inflammation of the epiploic appendages, small fat projections covered by serosa that protrude into the peritoneal cavity arranged in two parallel rows and distributed along the entire colon, especially in the sigmoid colon. Interestingly, these epiploic appendages are usually absent in the rectum and their physiological function is still not fully understood, although it is believed that they protect against local inflammation or act as fat storage in situations of malnutrition.[1-3] The difficulty with this entity is its chameleon-like appearance, since it can mimic various common diseases such as appendicitis or diverticulitis, among others, which makes its diagnosis crucial to avoid unnecessary treatments and surgeries.[4] In fact, until a few years ago, the diagnosis of appendagitis was exclusively surgical, and only 2.5% of cases were correctly identified before the operation, all due to the lack of imaging techniques.[1]

The rarity of this disorder, its omission in differential diagnoses, its unique appearance on imaging techniques and the problems of its medical treatment makes knowledge of it important for emergency radiologists. The aim of this article is to review this chameleon-like condition and the differential diagnoses with which it may be confused.

Anatomy and epidemiology

Anatomically there are usually about 50-100 epiploic appendages and on imaging tests they are usually not seen if there is no pathology.[4,5] The epiploic appendages are between 1 and 2 cm thick, 0.5 to 5 cm long and are larger on the left side of the colon than on the right side.[6] Each epiploic appendage is composed of two arteries and a single vein, which is the one that thromboses more easily[7] (Fig. 1). Therefore, primary epiploic appendagitis consists of inflammation of these appendages caused by torsion of the appendage leading to ischemia or thrombosis of the vein that drains the appendage[1] (Fig. 2). There is a secondary form associated with other inflammatory processes in the abdomen or pelvis, the most frequent of these being diverticulitis.[4,6]

The incidence of epiploic appendagitis is 8.8 million people per year and it is four times higher in males, with a mean age of 44 years. On the other hand, it is a very rare entity in children.[3,8] Also, it is more frequently associated with obese people or those who have lost weight in a short time.[1] Other associated factors are performing intense exercise or the presence of an intra-abdominal hernia.[7]

Clinical symptoms and radiological diagnosis

The main clinical presentation of this disease is acute abdominal pain in the left lower hemiabdomen, afebrile, without nausea or vomiting. In addition, inflammatory markers are usually within normal values and there is usually no leukocytosis or elevated C-reactive protein (CRP).[1] When epiploic appendagitis occurs on the left side (sigmoid) it may clinically mimic acute diverticulitis; on the other hand, if it occurs in the right lower quadrant, the clinical presentation could be mistaken for acute appendicitis.[9]

As we mentioned in the introduction, the diagnosis of this disease used to be made intraoperatively, but due to advances in new imaging techniques, a correct pre-surgical diagnosis can be made. The characteristics of this condition on computed tomography (CT) were first described in 1986 by Danielson et al.,[10] and became the reference standard[4] (Figs. 2 and 3).

However, ultrasound may be useful in selected patients, revealing a 1.5-3.5 cm non-compressible hyperechoic mass attached to the colonic wall surrounded by a hypoechoic rim without Doppler flow, with inflammatory changes around it,[1,5,7] as we can observe in figures 4 and 5. The absence of a Doppler signal due to lack of blood flow as a result of torsion in the epiploic appendagitis, as well as the lack of visualization of an inflamed diverticulum, are useful findings to differentiate epiploic appendagitis from acute diverticulitis.[3] Normally no changes are seen in the adjacent colonic wall.[5,6]

Specifically on CT, an ovoid fat density mass surrounded by a hyperdense halo (hyperattenuating ring sign) can be seen, representing the inflamed visceral peritoneal covering,[6] and a central hyperdense area is often seen corresponding to thrombosis of the central epiploic vein (central dot sign)[1,3] (Fig. 6). The central dot may have high attenuation because the infarcted tissue tends to calcify. This calcification may detach and appear as a free body in the peritoneal cavity, and it may adhere to a surface such as the spleen and be called a "parasitized epiploic appendage".[5,6] These findings are characteristic of epiploic appendagitis and

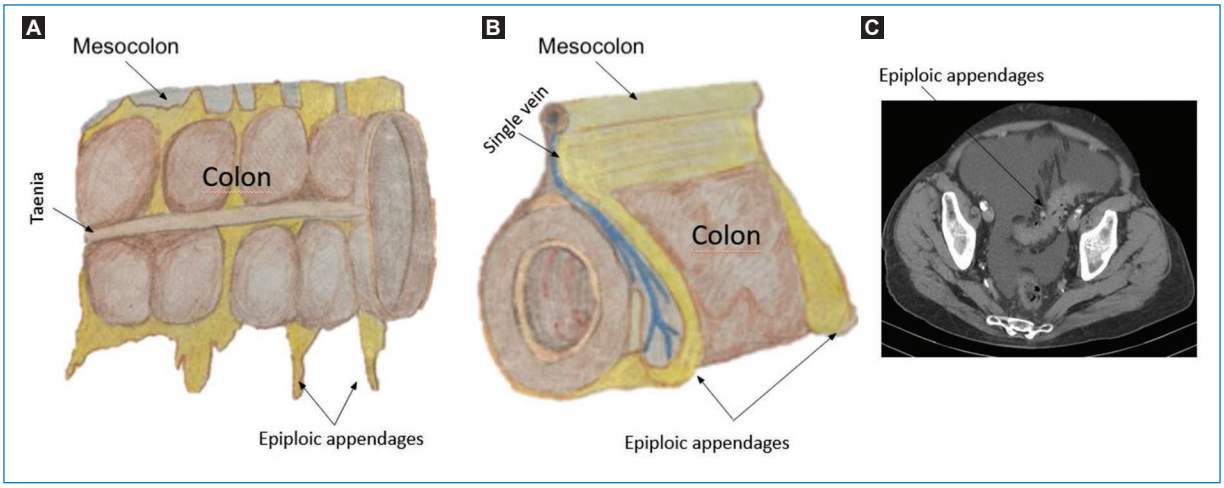

Figure 1. **A** and **B:** explanatory diagram of the anatomy of the epiploic appendages and their vascularization by means of a single vein. **C:** axial CT image where the epiploic appendages are identified in a male with ascites (barely visible in normal situations, without ascites).

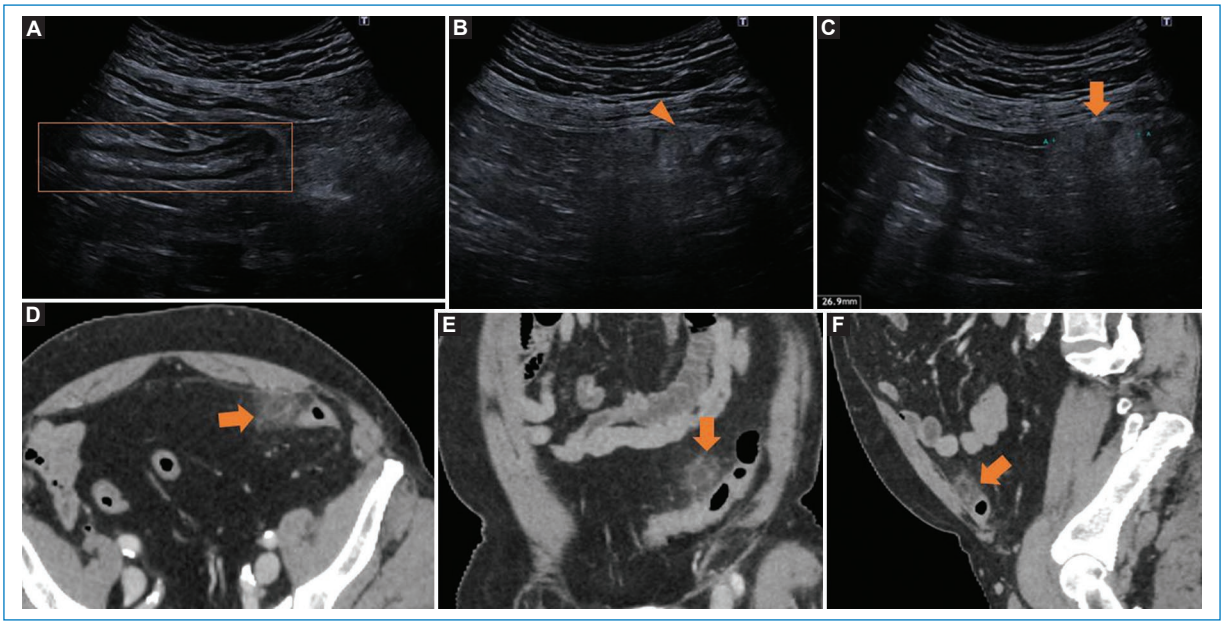

Figure 2. A 72-year-old male who presents to the emergency department for pain in the left iliac fossa. He has neither fever, nor nausea nor vomiting. As personal history he has hypertension, type 2 diabetes, obesity and dyslipidemia. **A:** ultrasound where descending colon without diverticula is observed. **B** and **C:** ultrasound in which focal hyperechogenicity of the fat adjacent to the colon is identified (arrows). **D:** Axial oblique CT. **E:** Coronal oblique CT. **F:** Sagittal oblique CT. Focal inflammatory changes of the fat adjacent to the colon are identified, round in morphology, with a peripheral hyperdense ring-shaped image and a central linear image (visible in reconstruction **D**), compatible with the thrombosed vein, all in relation to epiploic appendagitis in the sigmoid (arrows).
CT: computed tomography.

help us in its diagnosis, but they are not pathognomonic.[4] In addition, the absence of central dot signs and hyperattenuating ring sign does not exclude the diagnosis of acute epiploic appendagitis.[6]

Magnetic resonance imaging is not an imaging test used systematically in the diagnosis, but it may be used in pediatric and pregnant patients, with findings similar to those that we found on CT.[2,3]

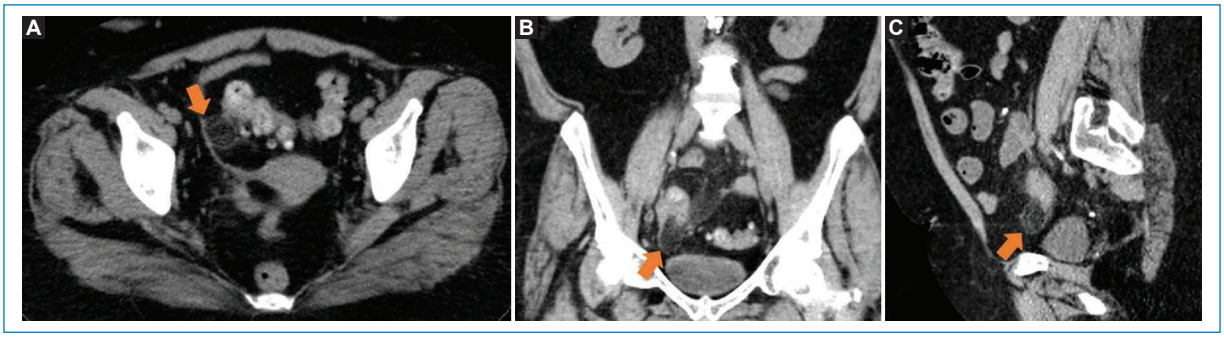

Figure 3. A 59-year-old female with the following history: hypertension, dyslipidemia, type 2 diabetes, colonic polyposis and multiple lacunar infarcts, who presents to the hospital emergency department referred by her primary care physician for hypogastric pain since yesterday morning. On examination the abdomen is soft and depressible. Painful on palpation in the meso- and hypogastrium, as well as in the right iliac fossa. Negative Blumberg. Preserved peristalsis. Negative bilateral fist-percussion. Clinical analysis highlights C-reactive protein at the upper limit of normal, without other remarkable findings. An inconclusive ultrasound was performed and was limited by abdominal wall fat, without identifying the cecal appendix. **A-C:** axial, coronal and sagittal abdominal computed tomography respectively was performed, where an ovoid 25 × 18 mm image is seen in the pelvis, of fat density and encapsulated, associated with inflammatory changes (arrows). Sigmoid diverticula without associated inflammatory signs. Findings compatible with epiploic appendagitis.

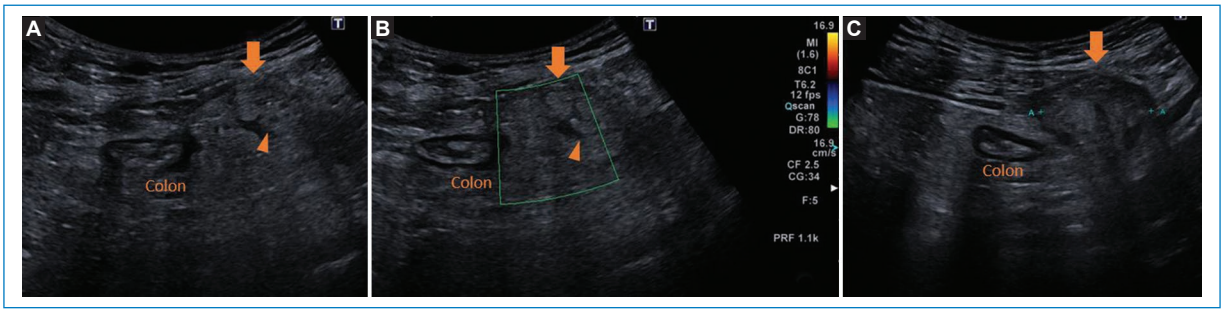

Figure 4. A 48-year-old male who presents to the emergency department for acute pain in the left iliac fossa, without fever, nausea or vomiting. **A-C:** an ultrasound was performed whose findings were a non-compressible hyperechoic image (arrows) without internal vascularization **(B)** and with a thin hypoechoic line in its interior (arrowhead), whose diagnosis was epiploic appendagitis.

Differential diagnoses

Primary epiploic appendagitis on the right side is often mistaken for acute appendicitis or right-sided diverticulitis, whereas primary epiploic appendagitis on the left side is often mistaken for sigmoid diverticulitis.[6]

Other entities that may give similar clinical manifestations are pancreatitis, omental infarction and mesenteric panniculitis. They have been included in table 1.[3,8]

Diverticulitis

Diverticula are hernias of the mucosa and submucosa through the muscular layers of the wall in areas of weakness of the intestinal wall[6] (Fig. 7). Diverticulitis occurs when a diverticulum is obstructed by feces or undigested food particles, with subsequent focal inflammation, localized ischemia and perforation. This condition is the most frequent complication of diverticular disease.[11] Diverticula can be found in any part of the colon, but they are predominant in the descending colon and sigmoid, so diverticulitis usually appears as acute abdominal pain localized in the left iliac fossa (LIF), being the most common cause of pain in the left lower quadrant.[5]

Analytically, the white blood cell count and inflammatory markers are usually significantly more altered than in epiploic appendagitis and, in addition, these patients are usually older than those with epiploic appendagitis,

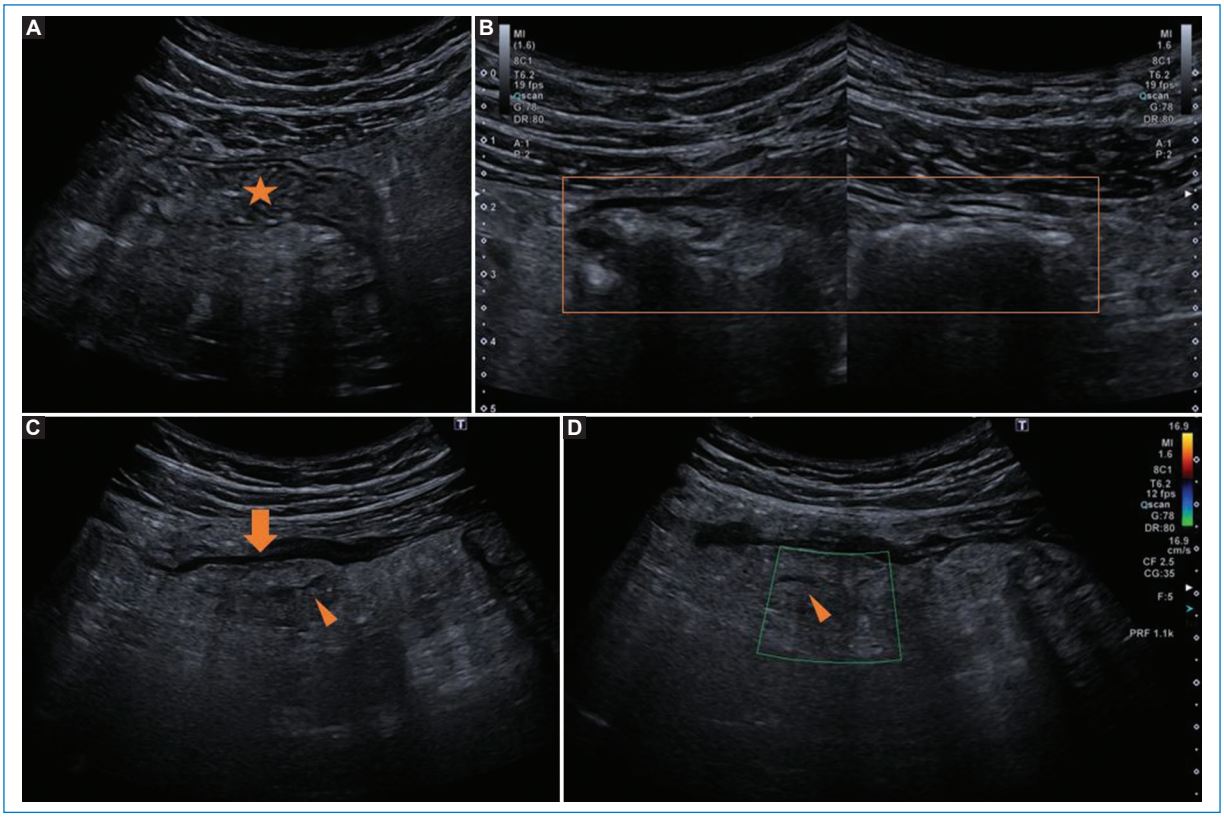

Figure 5. A 47-year-old male referred to the emergency department by his primary care physician for stabbing pain in the left hemiabdomen for 4 days, partially relieved with Nolotil. Without diarrhea or constipation, nor nausea or vomiting. Globulous and distended abdomen, slightly depressible, painful in the flank and left hemiabdomen, negative Blumberg, tympanism and somewhat increased peristalsis. Clinical analysis highlights a mild leukocytosis (12,400 leukocytes, neutrophils 7,500, lymphocytes 3,000, monocytes 1,600), with the rest of the analysis normal.
A-D: abdominal ultrasound is performed, showing normal bowel loops (star), colic frame without diverticula (square), with inflammatory changes of the fat adjacent to the sigmoid (arrow), without Doppler vascularization and with a central hypoechoic line (arrowhead), compatible with epiploic appendagitis.

presenting a greater probability of nausea and vomiting associated with pain.[6]

CT is the reference method in the evaluation of acute diverticulitis and the American College of Radiology (ACR) recommends CT with intravenous contrast as first-line imaging in patients with suspected acute diverticulitis because of its high sensitivity and specificity.[5,11] However, ultrasound may be performed in selected patients with uncomplicated acute diverticulitis, when laboratory parameters are not elevated and the clinical symptoms and examination do not suggest complication. On ultrasound we will see hyperechoic thickening of the colon wall (most frequently sigmoid) with abundant Doppler flow and visualization of inflamed oval formations (diverticula)[5] (Fig. 8).

Characteristic CT findings of diverticulitis include an ill-defined or blurred diverticulum with inflammatory changes and stranding of the adjacent fat, with mild wall thickening (generally < 5 mm). It usually affects a long segment of colon, more than 5 cm, and congested mesenteric vessels that irrigate the affected segment ("centipede sign").[5,6] Taken together, all the findings (wall thickening, increased pericolic fat density and a small amount of pericolic fluid) suggest a process of uncomplicated diverticulitis.[11]

CT findings of complicated acute diverticulitis include extraluminal free air, abscess, free intra-abdominal fluid, fistula and bleeding that may lead to peritonitis, with thickening and enhancement of the peritoneal layers being observed[11] (Fig. 9). Although there are several classifications to stratify findings in acute diverticulitis and clinical, radiological and surgical treatment,[5] in our hospital by consensus we use the modified Hinchey classification.

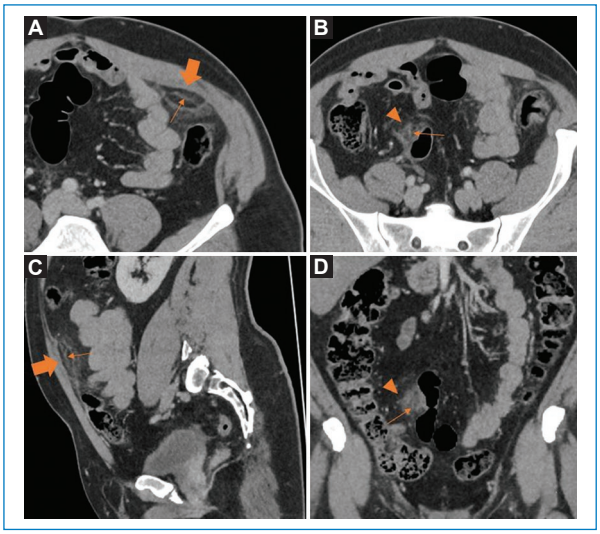

Figure 6. A 47-year-old male referred to the emergency department by his primary care physician for stabbing pain in the left hemiabdomen. On examination, firm abdomen with guarding on palpation in the left flank, with normal clinical analysis highlighting minimal leukocytosis and C-reactive protein at the upper limits of normal. Computed tomography is requested because of clinical symptoms suggestive of diverticulitis. Oblique axial reconstructions: upper at the level of descending colon **(A)** and lower, at the level of sigmoid **(B)**. **C:** oblique sagittal reconstruction centered at the upper level. **D:** coronal reconstruction centered at the lower level, at the level of the sigmoid. Two ovoid lesions with inflammatory changes and fat hyperechogenicity are visualized at the antimesenteric border of the descending colon (arrow) and sigmoid (arrowheads) with hyperattenuating halo and central dot sign (thin arrows) compatible with epiploic appendagitis in two locations.

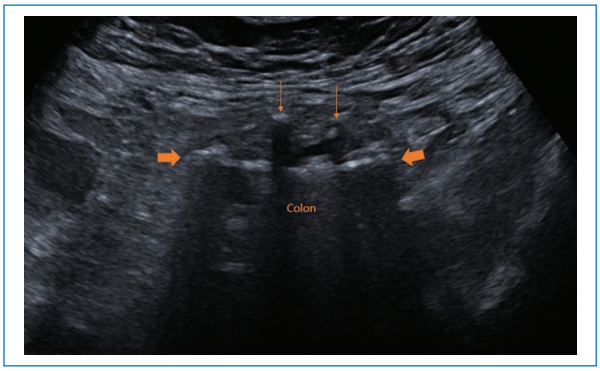

Figure 7. Ultrasound showing two diverticula in the descending colon (thin arrows), herniations of the mucosal and submucosal layer through the wall of the colon (hyperechoic, thick arrows).

Inflammation of the acute diverticulitis may extend to secondarily affect the epiploic appendages, with the consequent increased difficulty of diagnosis.[7] Thickening and involvement of the colonic wall is usually much greater in acute diverticulitis than that described in epiploic appendagitis.

Acute appendicitis

Acute appendicitis is the most frequent cause of acute abdominal pain requiring surgical treatment.[6] It is characterized by an acute stabbing periumbilical pain that radiates to the right lower quadrant, unlike epiploic appendagitis, which is normally located in the LIF, although the clinical symptoms according to the position of the cecal appendix may confuse the diagnosis. In addition, these patients have other associated clinical symptoms different from those of epiploic appendagitis such as fever, nausea, vomiting, guarding or abdominal rigidity and elevated inflammatory markers.[9]

On ultrasound, enlarged caliber (> 6 mm) of the cecal appendix, parietal hyperemia, increased echogenicity of periappendiceal fat and increased Doppler flow may be observed. CT will show a dilated fluid-filled appendix (> 6 mm) with thickening of the appendiceal walls (> 3 mm), hyperdensity of the periappendiceal fat and in one third of patients an appendicolith may be found inside it, which increases the probability of perforation[6] (Fig. 10). Reactive inflammation may extend to the adjacent cecum and signs of appendiceal perforation include abscess, extraluminal air, extraluminal appendicolith and focal defect in the enhanced appendiceal wall.[9]

Omental infarction

The greater omentum is a large peritoneal fold that originates from the greater curvature of the stomach and the beginning of the duodenum. It is composed of connective tissue, fat and lymphatics.[3] Omental infarction occurs due to an interruption of the arterial blood supply to the greater omentum, possibly due to omental torsion, venous insufficiency due to trauma or spontaneous thrombosis of the omental veins and may be primary or secondary.[6,7,12]

Secondary omental torsion is usually observed in adults with a predilection for males, although there are also cases in the pediatric population. Underlying causes of secondary torsion include omental mass,

Table 1. Summary and schematic table of the most likely differential diagnoses

Disease	Quadrant	Gender	Age	Main clinical symptoms	Additional data
Acute appendicitis	Right lower	Males	2nd decade	Periumbilical pain radiating to the right iliac fossa, guarding, peritonism	Leukocytosis, elevated CRP; clinical and ultrasound diagnosis
Omental infarction	Right lower	Both	Any age	Localized acute pain in the right quadrant	Risk factors: obesity, trauma, previous surgery, heart failure
Mesenteric adenitis	Right lower	Both	2-5 years	Intermittent pain, periumbilical or in the right iliac fossa	Ultrasound diagnosis: enlarged mesenteric lymph nodes
Cholecystitis	Right upper	Both	Adults	Right upper quadrant pain radiating to shoulder or back, nausea, fever	Leukocytosis, elevated bilirubin and alkaline phosphatase; positive ultrasound
Meckel's diverticulum	Right lower	Males	< 2 years	Abdominal pain, severe rectal bleeding	Diagnosis with Tc-99m scintigraphy
Diverticulitis	Left lower	Both	Older adults	Left iliac fossa pain, fever, vomiting, rectal bleeding	Increase in acute-phase reactants; CT with diverticular inflammation
Epiploic appendagitis	Left lower	Males	2nd decade	Pain in the left iliac fossa	Risk factors: obesity, sedentary lifestyle, rapid weight loss; diagnosis by CT
Renal lithiasis	Both	Both	Young adults	Nausea, vomiting, hematuria, colicky pain	Diagnosis by ultrasound or CT; conservative treatment if < 10 mm
Mesenteric panniculitis	Both	Both	Older adults	Nonspecific abdominal pain, nausea, early satiety	Imaging diagnosis: CT shows densities in the mesentery
Colitis	Both	Both	Elderly (ischemic); young (ulcerative)	Abdominal pain, diarrhea, fever	Diagnosis by colonoscopy; biopsy confirms diagnosis
PID (ovarian pathology)	Both	Females	Sexually active females	Fever, pelvic pain, vaginal discharge	Leukocytosis, elevated CRP; positive vaginal culture

PID: pelvic inflammatory disease; CRP: C-reactive protein; CT: computed tomography.

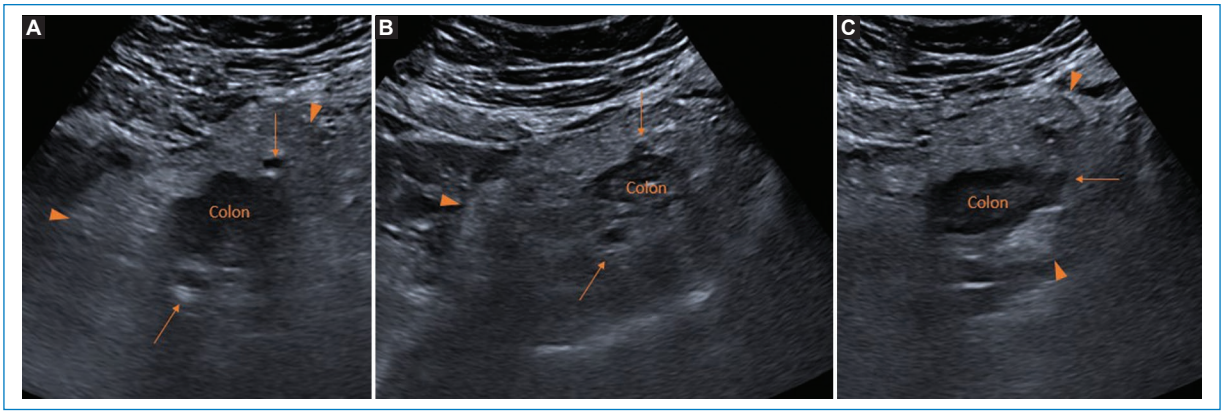

Figure 8. A 58-year-old female without remarkable history, presents for abdominal pain in the LIF, without nausea, vomiting or diarrhea. On examination, soft and depressible abdomen, with focal pain to fingertip in the LIF, which partially improves with analgesia. Clinical analysis was performed with results within normal limits and ultrasound was requested to rule out acute diverticulitis without suspicion of complication. **A-C:** abdominal ultrasound centered on the LIF, multiple diverticula are identified (thin arrows) with inflammatory changes and marked hyperechogenicity of the adjacent fat (arrowheads), without drainable collections. Antibiotic treatment with amoxicillin/clavulanate was prescribed for one week and follow-up by her primary care physician. LIF: left iliac fossa.

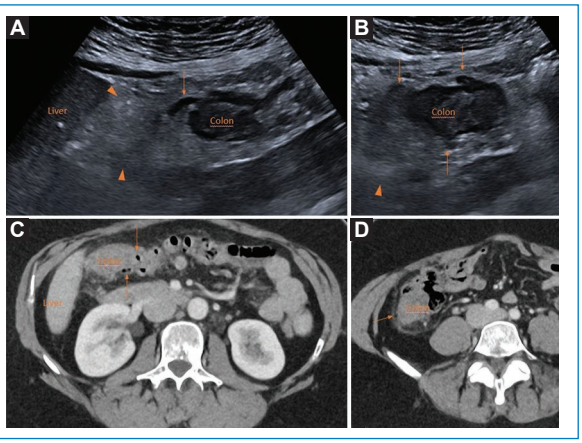

Figure 9. A 44-year-old female who presents to the emergency department because for 3 days she has had pain at the level of the right hemiabdomen more localized in the RIF with chills without measured fever. She was assessed 24 hours prior in the emergency department, for the same reason without analytical alterations and with response to analgesia. She currently has pain that does not subside with analgesia, elevated leukocytosis and C-reactive protein. On examination, pain in the RIF and right flank that increases with decompression. Ultrasound is requested to rule out appendicitis. **A** and **B:** ultrasound centered on the right hemiabdomen, showing multiple diverticula with inflammatory changes (thin arrows), thickening of the ascending colon wall and marked hyperechogenicity of the adjacent pericolic fat (arrowheads). As this is an extensive right-sided diverticulitis, complementary abdominal CT with contrast in venous phase is performed. **C** and **D:** axial CT slices centered on the ascending colon. Extensive right-sided diverticulitis is confirmed (thin arrows) without signs of complication. The patient is admitted with antibiotic treatment and intravenous analgesia with favorable evolution.
RIF: right iliac fossa; CT: computed tomography.

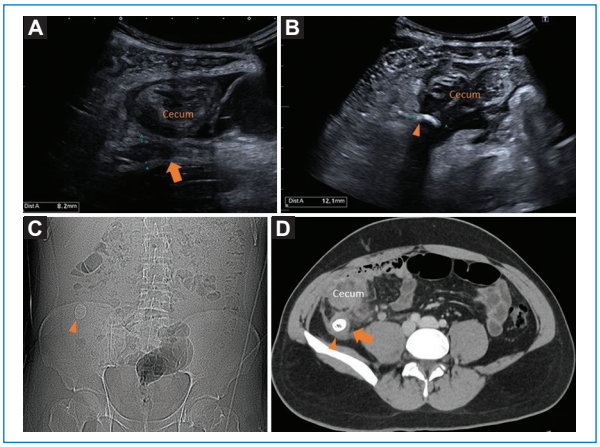

Figure 10. A 25-year-old male with abdominal pain in the right iliac fossa of one week's evolution. Nausea without vomiting. Afebrile. Positive Murphy sign on examination, without signs of peritoneal irritation. C-reactive protein 1.88, leukocytes 14,000. Ultrasound is requested to rule out biliary involvement. **A** and **B:** ultrasound where significant parietal thickening of cecum and terminal ileum is visualized, with a 15 mm hyperechoic image with acoustic shadow adjacent to the cecum suggesting appendicolith (arrowhead) in a possible thickened appendix difficult to approach (arrow). **C** and **D:** the study is completed with computed tomography, where a thickened cecal appendix is confirmed (diameter greater than 26 mm, arrow) in retrocecal location, with a bulky 18 mm appendicolith in the middle third of the appendix (arrowhead), visible on scout image **(C)**.

hernia, omental adhesions due to previous surgery, trauma and congestive heart failure.[3,13] However, most cases of omental infarction are idiopathic, primary. Obesity has been implicated as a predisposing condition in both children and adults.[3,6]

Torsion of the omentum is more common on the right side than on the left, due to greater length and mobility of the right-sided omentum together with lower vascularization, so pain is usually more focused in the right iliac fossa (RIF).[6,13] Clinical symptoms overlapping with other right lower quadrant conditions often prevents a definitive evaluation.[9]

CT is considered the reference method in diagnosis (Fig. 11). The characteristic finding on CT is a "mass-like" fat density in the mesentery with internal hyperattenuated streaks arranged in a concentric pattern giving a whirlpool appearance. This sign is characteristic, since it represents the twisted vascular pedicle and is not seen in other diseases of the omentum. In addition, unlike epiploic appendagitis, it is an irregular mass larger than 3 cm without hyperattenuating rim or central dot sign and does not contact with the surface of the colon (Fig. 12).[3,12]

Treatment may be conservative with oral analgesics, nonsteroidal anti-inflammatory drugs and/or prophylactic antibiotics. However, if conservative treatment fails due to intractable pain, peritoneal signs or complications, such as abscesses or intestinal obstruction due to the persistence of infarcted omental tissue, laparoscopy may be performed to provide rapid symptomatic relief.[9]

Treatment

Epiploic appendagitis is a self-limited process and can be treated conservatively with nonsteroidal anti-inflammatory drugs or opioid analgesics, depending on the magnitude of the pain, and it generally

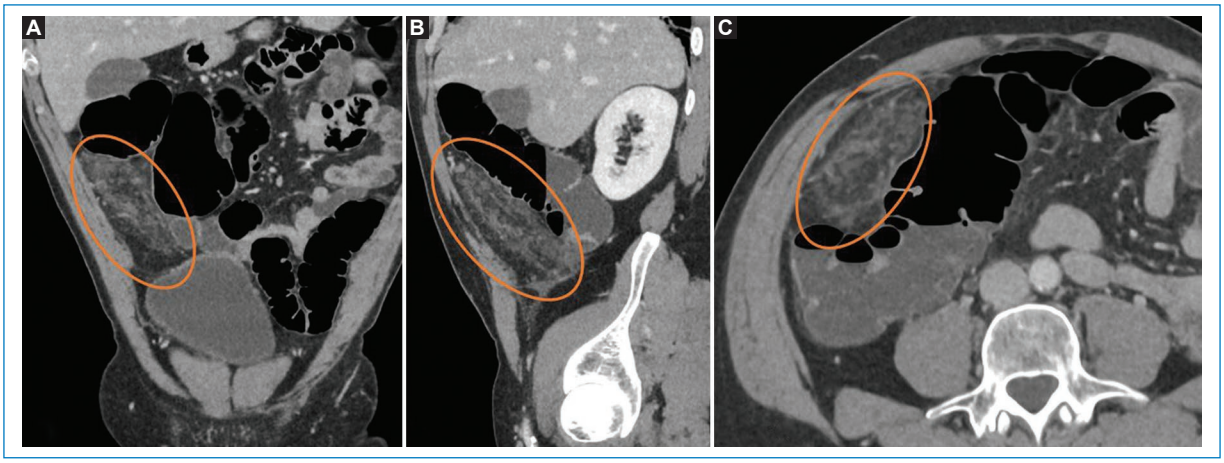

Figure 11. A 53-year-old male, without medical history, who presents for abdominal pain of 8/10 intensity of 24 hrs evolution. On physical examination: soft abdomen in left hemiabdomen, with abdominal guarding in the right iliac fossa and hypogastrium. Computed tomography is requested due to non-visualization of the cecal appendix on ultrasound. **A:** coronal reconstruction. **B:** sagittal reconstruction. **C:** axial slice. Inflammatory involvement in the right iliac fossa-right flank, in contact with the antimesenteric border of the ascending colon wall, pseudo-encapsulated appearance, trabeculated and with mass effect, in relation to omental infarction. No thickening of the colon wall is visible.

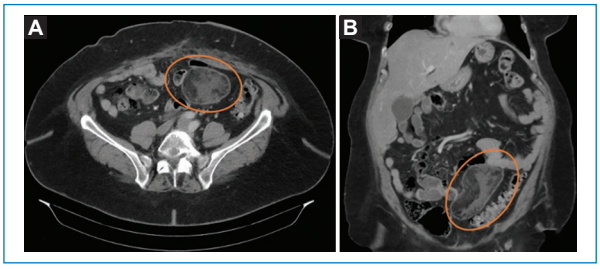

Figure 12. A 57-year-old female with history of type 2 diabetes, obesity, pulmonary embolism and squamous cell carcinoma originating in an ovarian teratoma, treated by total hysterectomy with bilateral salpingo-oophorectomy, omentectomy and pelvic and para-aortic lymphadenectomy. She presented to the emergency department for abdominal pain secondary to an incarcerated ventral hernia. She underwent urgent surgery with hernioplasty and dermolipectomy.
A and **B:** postoperative computed tomography, performed because of persistent abdominal discomfort, revealed a well-encapsulated fatty lesion of approximately 12 × 8 cm in the anterior abdominal cavity, with inflammatory changes suggestive of omental infarction (circles).

resolves in 7 to 14 days. However, radiological findings on CT do not resolve until 6 months after the onset of symptoms, with reduction in size or complete resolution.[4,7] Follow-up with imaging techniques is not necessary.[5]

Conclusions

Epiploic appendagitis, although uncommon, constitutes a crucial differential diagnosis in acute abdominal pain. Its correct identification, based on characteristic radiological findings such as the hyperattenuating ring sign and the central fatty dot on CT, is fundamental to avoid unnecessary surgical interventions. Early and precise diagnosis, guided by adequate radiological interpretation, allows for an effective conservative treatment and ensures a prompt recovery of the patient. The relevance of the radiologist in the emergency setting is highlighted.

It should be remembered that:

- Epiploic appendagitis is an uncommon cause of acute abdominal pain, frequently mistaken for appendicitis or diverticulitis due to the similarity of the clinical symptoms.
- Radiological diagnosis, particularly by CT, is key to identifying characteristic findings such as the hyperattenuating ring sign and the central fatty dot.
- A correct diagnosis prevents unnecessary surgical interventions, which reduces risks and costs associated with treatment of the patient.
- Treatment of epiploic appendagitis is conservative in most cases, by means of analgesics and anti-inflammatory drugs, without the need for hospitalization.

– The precision and experience of the radiologist are essential to differentiate this disease from other abdominal emergencies and ensure appropriate treatment.

Funding

The authors declare that they have not received funding.

Conflicts of interest

The authors declare no conflicts of interest.

Ethical considerations

Protection of human subjects and animals. The authors declare that no experiments on humans or animals were performed for this research.

Confidentiality, informed consent and ethical approval. The authors have obtained approval from the Ethics Committee for the analysis of routinely collected and anonymized clinical data; therefore, individual informed consent was not required. Relevant ethical recommendations have been followed.

Declaration on the use of artificial intelligence. The authors declare that no generative artificial intelligence was used in the writing or creation of the content of this manuscript.

References

1. Patel M, Haider I, Cheung A. Primary epiploic appendagitis: a mimicker of abdominal pain. Clin Med Res. 2023;21(3):159-62. http://dx.doi.org/10.3121/cmr.2023.1837
2. Giannis D, Matenoglou E, Sidiropoulou MS, Papalampros A, Schmitz R, Felekouras E, et al. Epiploic appendagitis: pathogenesis, clinical findings and imaging clues of a misdiagnosed mimicker. Ann Transl Med. 2019;7(24):814. http://dx.doi.org/10.21037/atm.2019.12.74
3. Lazaridou E, Aslanidi C, Mellou V, Athanasiou S, Exarhos D. Intraperitoneal focal fat infarction: the great mimicker in the acute setting. Emerg Radiol. 2021;28(1):201-7. http://dx.doi.org/10.1007/s10140-020-01830-0
4. Giambelluca D, Cannella R, Caruana G, Salvaggio L, Grassedonio E, Galia M, et al. CT imaging findings of epiploic appendagitis: an unusual cause of abdominal pain. Insights Imaging. 2019;10(1):26. http://dx.doi.org/10.1186/s13244-019-0715-9
5. Bodmer NA, Thakrar KH. Evaluating the patient with left lower quadrant abdominal pain. Radiol Clin North Am. 2015;53(6):1171-88. http://dx.doi.org/10.1016/j.rcl.2015.06.005
6. Almeida AT, Melão L, Viamonte B, Cunha R, Pereira JM. Epiploic appendagitis: an entity frequently unknown to clinicians--diagnostic imaging, pitfalls, and look-alikes. AJR Am J Roentgenol. 2009;193(5):1243-51. http://dx.doi.org/10.2214/AJR.08.2071
7. Singh AK, Gervais DA, Hahn PF, Sagar P, Mueller PR, Novelline RA. Acute epiploic appendagitis and its mimics. Radiographics. 2005;25(6):1521-34. http://dx.doi.org/10.1148/rg.256055030
8. Porras LE, Barasoain MA, Ríos MV, Botija A GM, Solé DC. Omental infarction, unusual cause of abdominal pain. Andes Pediatr. 2022;93(3):434-9. http://dx.doi.org/10.32641/andespediatr.v93i3.3830
9. Patel NB, Wenzke DR. Evaluating the patient with right lower quadrant pain. Radiol Clin North Am. 2015;53(6):1159-70. http://dx.doi.org/10.1016/j.rcl.2015.06.004
10. Danielson K, Chernin JR, Amberg JR, Goff S, Durham JR. Epiploic appendagitis: CT characteristics. J Comput Assist Tomogr. 1986; 10:142-3.
11. Tiralongo F, Di Pietro S, Milazzo D, Galioto S, Castiglione DG, Ini' C, et al. Acute colonic diverticulitis: CT findings, classifications, and a proposal of a structured reporting template. Diagnostics (Basel). 2023;13(24). http://dx.doi.org/10.3390/diagnostics13243628
12. Mansoor A, Shaukat R. Inguinal hernia leading to omental torsion: role of CT in differentiating from other clinical mimics - a case report and literature review. J Radiol Case Rep. 2023;17(11):8-17. http://dx.doi.org/10.3941/jrcr.v17i11.4722
13. Öztaş M, Türkoğlu B, Öztas B, Alakuş Ü, Meral UM. Rare causes of acute abdomen and review of literature: primary/secondary omental torsion, isolated segmental omental necrosis, and epiploic appendagitis. Ulus Travma Acil Cerrahi Derg. 2023;29(2):193-202. http://dx.doi.org/10.14744/tjtes.2022.28430

AUSTRAL JOURNAL OF IMAGING
REVISTA CHILENA DE RADIOLOGÍA

PERMANYER

Check for updates

CASE SERIES

Abdominopelvic neurogenic tumors: a case series and literature review

Tumores neurogénicos abdominopélvicos: serie de casos y revisión de la literatura

Fernando I. Vivanco-Concha[1], Jaime A. Zapata-Mercado[1], Marcelo I. Arias-Valenzuela[1], Nicolás G. Molina-Vásquez[1], and Giancarlo Schiappacasse-Faundes[2]*

[1]Faculty of Medicine, Clínica Alemana, Universidad del Desarrollo; [2]Abdominal Imaging Department, Clínica Alemana de Santiago. Santiago, Chile

Abstract

Neurogenic tumors of the abdomen and pelvis are rare neoplasms originating from nervous system cells, often located in the retroperitoneum, along the sympathetic plexus, in the adrenal glands, or in the pelvic region. They are classified into three main types based on their cellular origin: sympathetic ganglionic, paraganglionic, and nerve sheath tumors. Although they are typically found incidentally in imaging studies, radiology plays a key role in diagnosis and management. Magnetic resonance imaging is the most useful modality due to its high contrast resolution, allowing precise delineation of tumor margins and evaluation of adjacent tissue involvement. Computed tomography and positron emission tomography are valuable for assessing tumor extent and potential metastasis, particularly in cases of suspected malignancy. While definitive diagnosis requires histopathological analysis, proper clinical-imaging correlation improves diagnostic accuracy. Radiological follow-up is essential for detecting recurrences and optimizing therapeutic management, enhancing clinical outcomes and reducing recurrence rates.

Keywords: *Paraganglioma. Ganglioneuroma. Neuroblastoma. Schwannoma. Malignant peripheral nerve sheath tumor.*

Resumen

Los tumores neurogénicos del abdomen y la pelvis son neoplasias raras que se originan en células del sistema nervioso, localizándose frecuentemente en el retroperitoneo, a lo largo del plexo simpático, en las glándulas suprarrenales o en la región pélvica. Se dividen en tres tipos principales según su origen celular: ganglionares simpáticos, paraganglionares y de la vaina nerviosa. Aunque suelen descubrirse como hallazgos incidentales en estudios por imágenes, la radiología desempeña un papel crucial en su diagnóstico y seguimiento. La resonancia magnética es la herramienta más útil, debido a su alta resolución de contraste, que permite una delimitación precisa de los márgenes tumorales y la evaluación de la invasión a estructuras cercanas. La tomografía computada y la tomografía por emisión de positrones son útiles para evaluar la extensión y posibles metástasis, especialmente en casos de sospecha de malignidad. Aunque el diagnóstico definitivo requiere análisis histopatológico, una adecuada correlación clínico-imagenológica mejora la precisión diagnóstica. El seguimiento mediante imágenes es esencial para detectar recidivas y optimizar el manejo terapéutico, mejorando los resultados clínicos y reduciendo las tasas de recurrencia.

Palabras clave: *Paraganglioma. Ganglioneuroma. Neuroblastoma. Schwannoma. Tumor maligno de la vaina del nervio periférico.*

***Correspondence:**
Fernando I. Vivanco-Concha
E-mail: fvivanco@alemana.cl

Date of reception: 28-08-2025
Date of acceptance: 15-02-2026
DOI: 10.24875/AJI.25000063

Available online: 14-07-2026
Austral J. Imaging. (Engl. ed.). 2026;32(3):142-150
www.resochradi.com

Introduction

Neurogenic tumors constitute a rare group of neoplasms derived from cells of the nervous system[1]. Although their most common location is the posterior mediastinum, they can also occur in the retroperitoneum and pelvis. In the thorax, they represent approximately 4% of mediastinal lesions, predominantly in the paravertebral region[2]. In the abdomen, they are mainly located in the retroperitoneum, where they constitute between 10% and 20% of the primary retroperitoneal tumors, especially along the sympathetic plexus and in the adrenal glands[3-5]. In the pelvis, around half of these tumors are benign, usually appearing in middle-aged adults and have recurrence rates close to 20%[6].

Based on their cellular origin, they are classified into three groups:

1) tumors derived from sympathetic ganglion cells (ganglioneuroma, ganglioneuroblastoma, and neuroblastoma), 2) tumors from paraganglion cells (pheochromocytoma and paraganglioma), and 3) tumors of the nerve sheath (schwannoma, neurofibroma, and malignant peripheral nerve sheath tumor [MPNST])[1].

Diagnosis is based on clinical history and imaging findings obtained using computed tomography (CT) or magnetic resonance imaging (MRI), which allow for the evaluation of the lesion's location, shape, and internal characteristics[7]. However, definitive confirmation of the cell subtype and malignant potential requires histopathological analysis[8-10]. In this paper, we present a brief literature review, supplemented by a series of cases from our institution (Table 1).

Nerve sheath tumors

Peripheral nerve sheath tumors comprise a spectrum that includes schwannomas, neurofibromas, and MPNSTs. The latter represent 3-10% of soft tissue sarcomas and are associated with neurofibromatosis type 1 in up to 50% of the cases. On imaging, schwannomas tend to appear as well-defined masses, hypointense on T1 and markedly hyperintense on T2, with peripheral or septal enhancement after contrast administration, and minimal restriction on diffusion-weighted sequences. MPNSTs, on the other hand, show poorly defined borders, heterogeneous enhancement, central necrosis, and restricted diffusion, with possible extension along nerve pathways (Figs. 1-3).

Sympathetic ganglion tumors

Among the tumors derived from the sympathetic ganglion cell line are included ganglioneuroma, ganglioneuroblastoma, and neuroblastoma, differentiated according to their degree of cellular maturity. Ganglioneuroma is a benign, slow-growing lesion that appears on MRI as a well-defined mass, hypointense on T1-weighted images, hyperintense on T2-weighted images, with progressive enhancement and minimal restriction on DWI. The neuroblastoma, more common in childhood, exhibits infiltrative behavior, with remodeling of adjacent bone structures, foraminal involvement, heterogeneous enhancement, and marked diffusion restriction (Figs. 4 and 5).

Paraganglion tumors

The paragangliomas are extra-adrenal neuroendocrine neoplasms located along the sympathetic chain. On CT and MRI, they appear as well-defined, hypervascular masses with intense and homogeneous enhancement, although they may show cystic or necrotic areas. On positron emission tomography (PET) with 18F-fluorodeoxyglucose (18F-FDG) they typically show increased uptake, with a variable standardized maximum uptake value depending on the degree of metabolic activity. Mesenteric and retroperitoneal presentations with characteristic enhancement and high tracer uptake have been described (Figs. 6-8).

Mixed or unclassifiable tumors

Some neurogenic lesions present mixed or atypical elements, without a clearly malignant phenotype. These masses are usually located adjacent to structures such as the adrenal gland, with well-defined borders, progressive enhancement, and no signs of direct infiltration. Imaging characterization in these cases is essential to guide treatment (Fig. 9).

Discussion

Neurogenic tumors located in the abdomen and pelvis are rare, with the former constituting 10-20% of all primary retroperitoneal tumors, frequently located along the sympathetic paravertebral plexus and in the adrenal glands[4].

Tumors derived from sympathetic ganglion cells differ in their degree of cellular and extracellular maturation[8]. The ganglioneuroma is the tumor with the largest

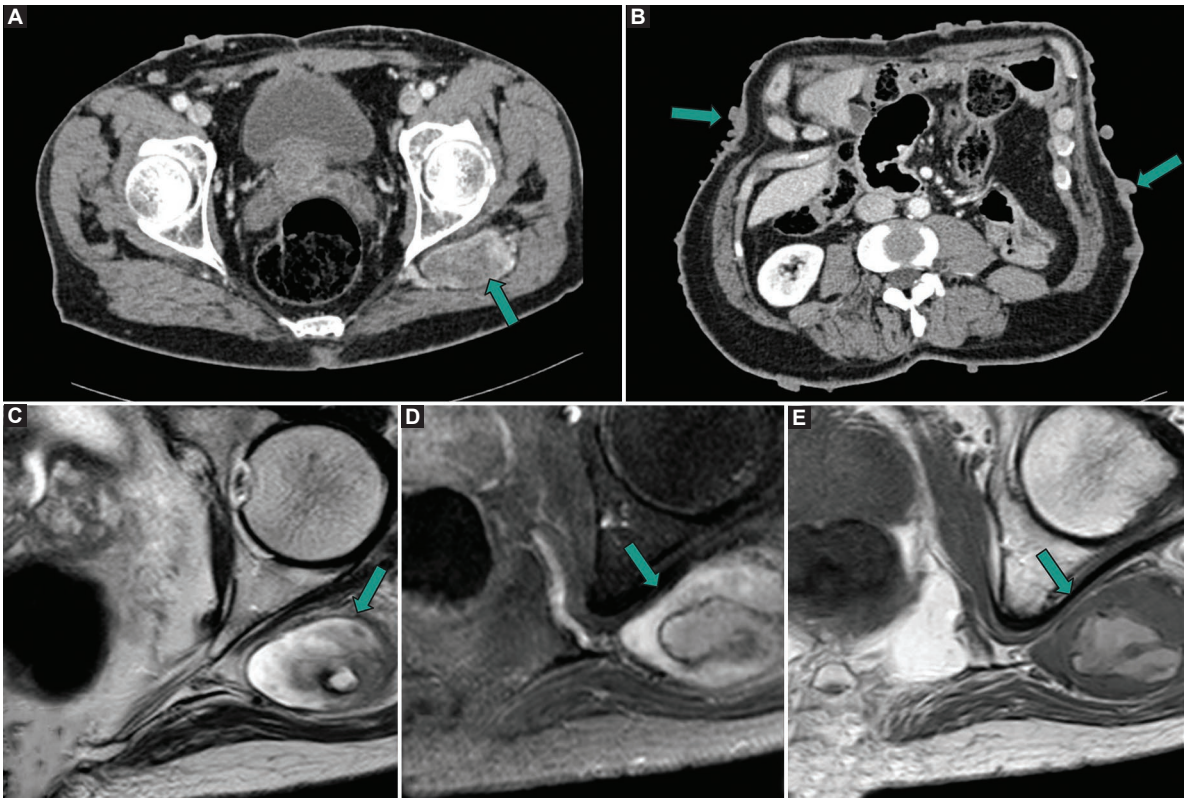

Figure 1. 66-year-old male. Abdominal computed tomography: a heterogeneous lesion with enhancement suggestive of originating from the left sciatic nerve (**A**) and multiple cutaneous neurofibromas (**B**) are observed. Pelvic MRI: lesion dependent on the sciatic nerve with high T2 signal (**C**), T1 enhancement with contrast (**D**), and a central region of high T1 signal suggestive of necrosis (**E**). Histological diagnosis of malignant tumor of the nerve sheath.

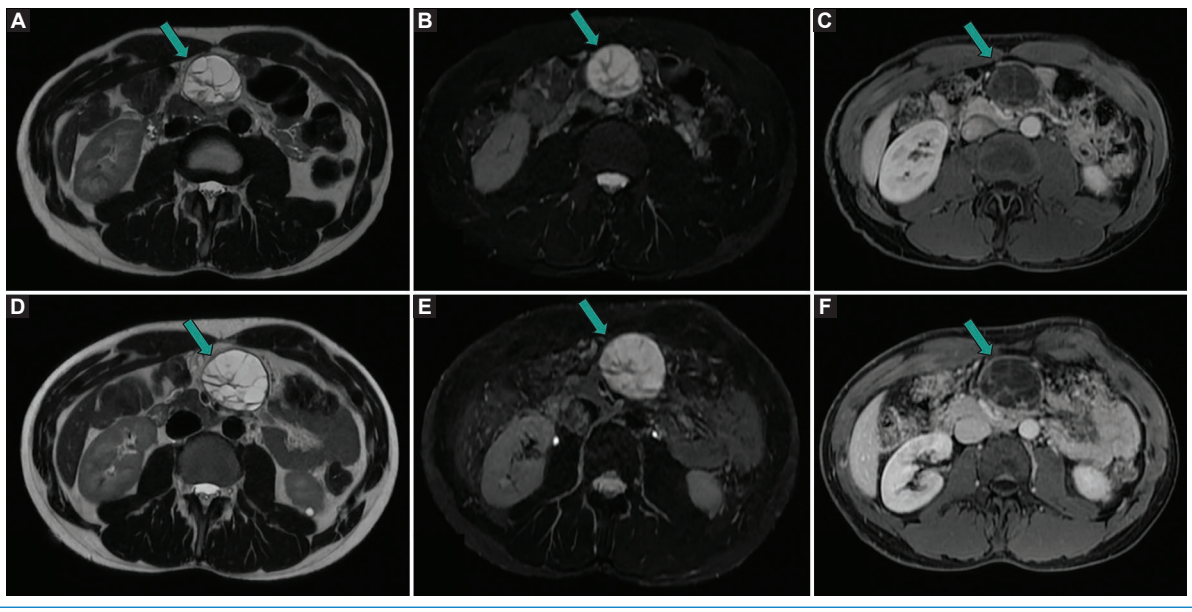

Figure 2. 30-year-old male. Abdominal MRI: cystic lesion of the mesentery with high T2 signal (**A** and **B**) associated with enhancement of its wall and septa with contrast (**C**). At the 6-month follow-up (**D-F**), approximately 25% growth of the lesion is observed. Histological diagnosis of cystic schwannoma of the mesentery.

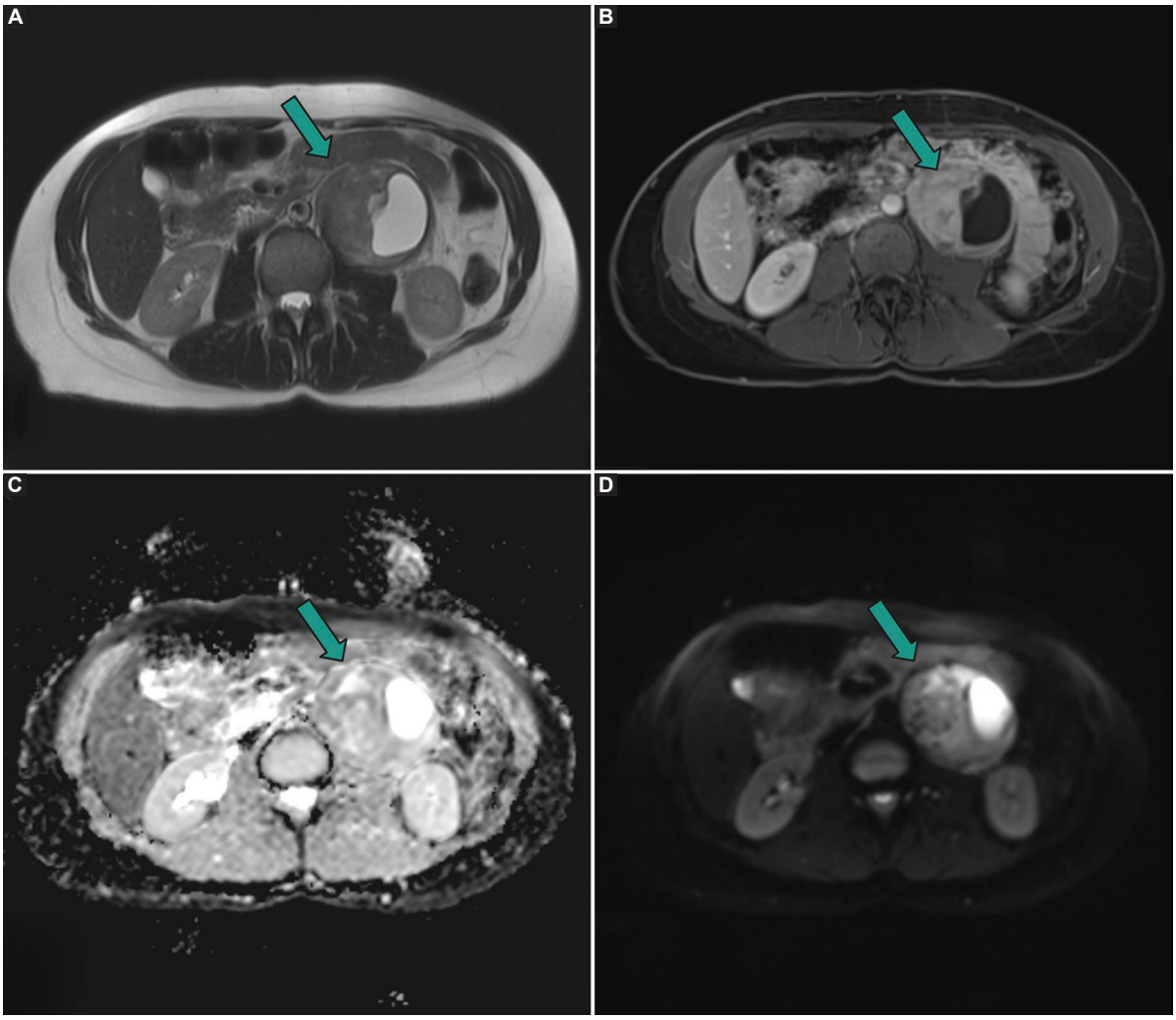

Figure 3. 37-year-old female. Abdominal magnetic resonance imaging: left retroperitoneal mass, adjacent to the abdominal aorta, of solid-cystic characteristic with a hyperintense component on T2 (**A**), heterogeneous enhancement with contrast medium (**B**) and without significant restriction on diffusion sequence (**C** and **D**). Histological diagnosis of retroperitoneal schwannoma.

mature component and the most benign behavior, followed by the ganglioneuroblastoma, with intermediate malignant potential, and finally the neuroblastoma, with a more immature component and the greatest malignant potential of the three[8]. Neuroblastoma is the most common tumor of the sympathetic nervous system and is one of the leading causes of malignancy in childhood, with a mean age at diagnosis of 17 months and exceptional cases reported in adulthood[11,12].

Tumors derived from paraganglion cells (pheochromocytoma and paraganglioma) originate from chromaffin cells and are differentiated by their anatomical location, with pheochromocytoma located in the adrenal gland and paraganglioma in extra-adrenal locations[13]. Their incidence is estimated at 2-8/1,000,000, with a peak between the third and fifth decades of life, and 20% of the cases occurring in the pediatric population[14]. When symptomatic, they manifest with symptoms secondary to the overproduction of catecholamines.

MPNST is rare, constituting 3-10% of soft tissue sarcomas, with a tendency toward local recurrence and metastasis[15]. Risk factors include the presence of neurofibromatosis type 1[16]; 25-50% of MPNST cases occur in individuals with this condition, and in addition, patients with plexiform neurofibromas have an increased risk of malignant transformation[17]. Another known risk factor for the development of MPNST is a history of radiotherapy, even 10-20 years after treatment.

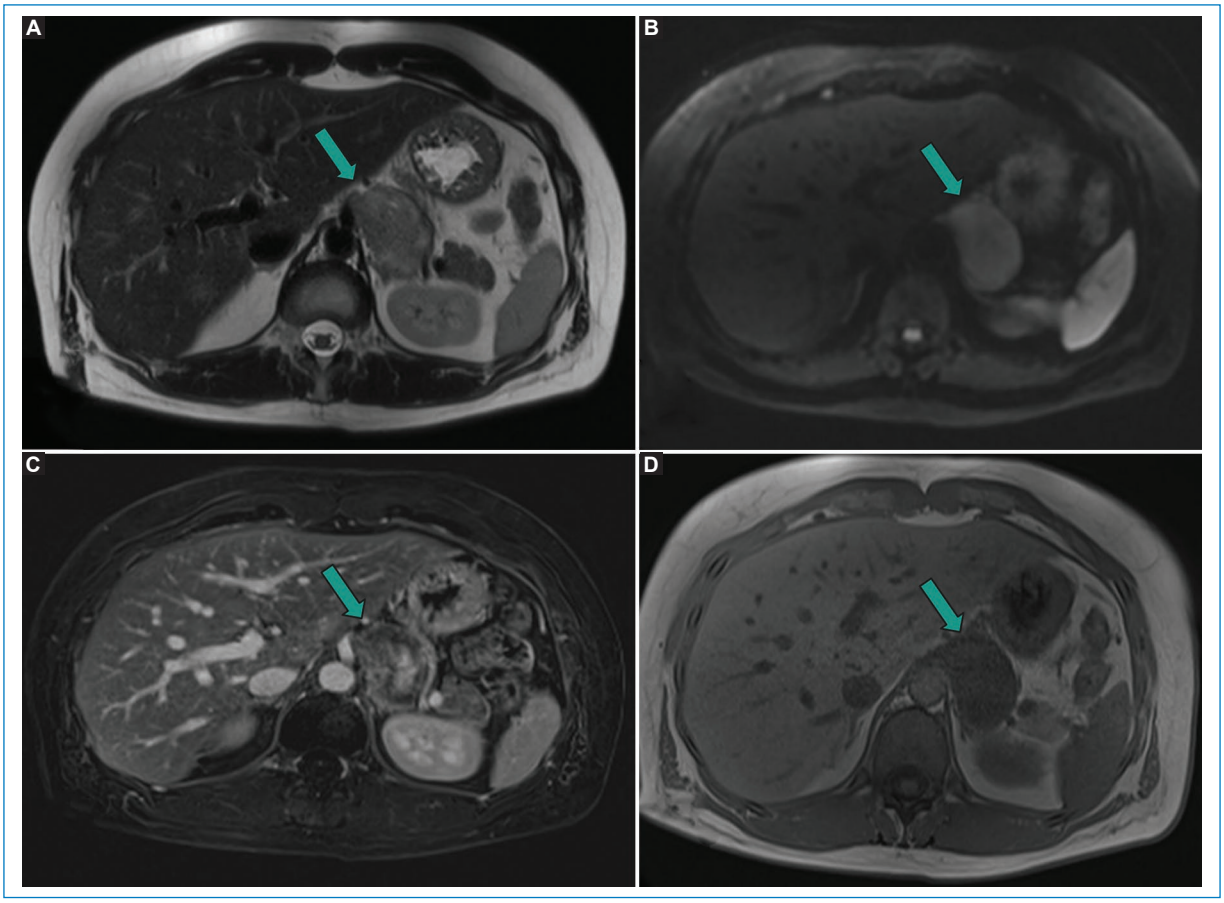

Figure 4. 30-month-old male. Abdominal MRI: lesion adjacent to the left adrenal gland, displacing it, showing low signal on T2 (**A**), minimal diffusion restriction (**B**), contrast enhancement and fat suppression (**C**), and low signal on T1 (**D**). Histological diagnosis of ganglioneuroma.

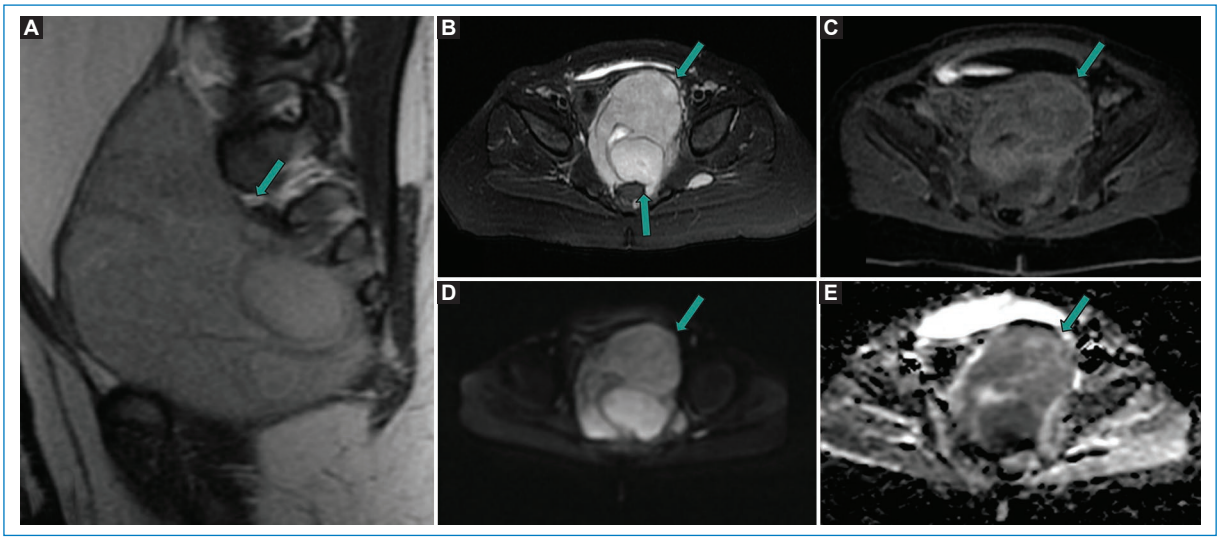

Figure 5. 16-month-old female. Pelvic MRI: presacral lesion causing involvement and remodeling of the neuroforamina, with moderate signal on T2, contrast enhancement (**A-C**), and restriction in the diffusion sequence (**D** and **E**). Histological diagnosis of neuroblastoma.

Table 1. Summary of the case series: epidemiological characteristics, clinical symptoms, histological diagnosis, and imaging findings

Patient	Clinical symptoms	Histological diagnosis	Main imaging findings
Male, 66 years (Fig. 1)	History of neurofibromatosis	MPNST	CT: Multiple cutaneous neurofibromas; well-defined lesion with heterogeneous enhancement, suggestive of sciatic nerve involvement MRI: ↑T2WI, ↓T1WI with a central area of high signal intensity and enhancement with IVC.
Male, 30 years (Fig. 2)	Abdominal pain and palpable mass	Cystic schwannoma of the mesentery	MRI: Complex cystic lesion at the root of the mesentery; ↑T2WI, subtle enhancement in septa and capsule with IVC.
Female, 37 years (Fig. 3)	Study of retroperitoneal lesion visualized on preventive ultrasound	Retroperitoneal schwannoma	MRI: Left retroperitoneal mass of solid-cystic nature with heterogeneous enhancement with IVC.
Male, 30 months (Fig. 4)	Study of abdominal mass	Ganglioneuroma	MRI: ↓T2WI, ↓T1WI, minimal diffusion restriction and heterogeneous enhancement with IVC.
Female, 16 months (Fig. 5)	Study of abdominal pain	Neuroblastoma	MRI: Presacral lesion with involvement and remodeling of the neuroforamina. ≈ T2WI, diffusion restriction and heterogeneous enhancement with IVC
Female, 68 years (Fig. 6)	Asymptomatic, study of mesenteric nodule	Mesenteric paraganglioma	18F-FDG PET: pelvic mesentery nodular lesion with well-defined margins, with areas of cystic appearance and heterogeneous enhancement after IVC and tracer uptake
Male, 59 years (Fig. 7)	Asymptomatic, study of retroperitoneal nodule	Retroperitoneal paraganglioma	18F-FDG PET: retroperitoneal nodular lesion with homogeneous enhancement after IVC and hypermetabolic activity
Male, 29 years (Fig. 8)	Study of adrenal incidentaloma	Adrenal pheochromocytom, retroperitoneal paragangliomas	DOTATATE PET: hypervascular lesions in the right adrenal gland, in the retroperitoneum in a retrocaval position and anterior to the psoas muscle, showing increased radiotracer uptake.
Female, 48 years (Fig. 9)	Asymptomatic, study of nodule visualized on ultrasound	Neurogenic tumor with ganglionic elements, without elements of malignancy	CT: well-defined nodular lesion adjacent to the right adrenal gland without involvement of the gland, heterogeneous and progressive enhancement with IVC

IVC: intravenous contrast; 18F-FDG: 18F-fluorodeoxyglucose; PET: positron emission tomography; MRI: magnetic resonance imaging; CT: computed tomography; MPNST: malignant peripheral nerve sheath tumor.

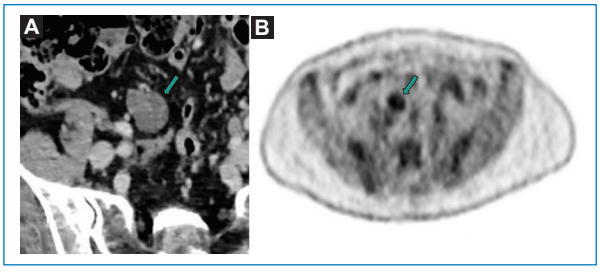

Figure 6. 68-year-old woman. Positron emission tomography with 18F-fluorodeoxyglucose: isolated mesenteric nodular lesion showing mild heterogeneous enhancement of the intravenous contrast agent (**A**) and hypermetabolic activity with tracer uptake (**B**). Histological diagnosis of mesenteric paraganglioma.

Furthermore, although rare, schwannomatosis (autosomal dominant inheritance) predisposes to the development of peripheral nerve schwannomas[18].

There is agreement between what is presented in our case series and that described in the literature, where most patients are asymptomatic at the time of diagnosis and are an incidental finding in imaging studies ordered for another reason[1]. In more advanced stages, neurogenic tumors located in the abdomen and pelvis can present with abdominal pain, a palpable mass, and symptoms related to mass effect and compression of adjacent neurovascular structures[19]. The initial approach to suspected neurogenic tumors usually begins with ordering radiological studies. CT is a non-specific examination for characterizing these lesions. Transverse findings such as a lesion with well-defined margins, soft tissue density, heterogeneous enhancement after contrast administration, and, in some cases, the presence of calcifications can guide the diagnosis[20]. Furthermore, CT allows for good evaluation of the lesions margins, infiltration of adjacent structures, and the presence of distant metastases. However, in most cases, the study should be complemented with MRI or biopsy of the lesion, or both. In four cases in our series where CT was performed, the most frequent finding

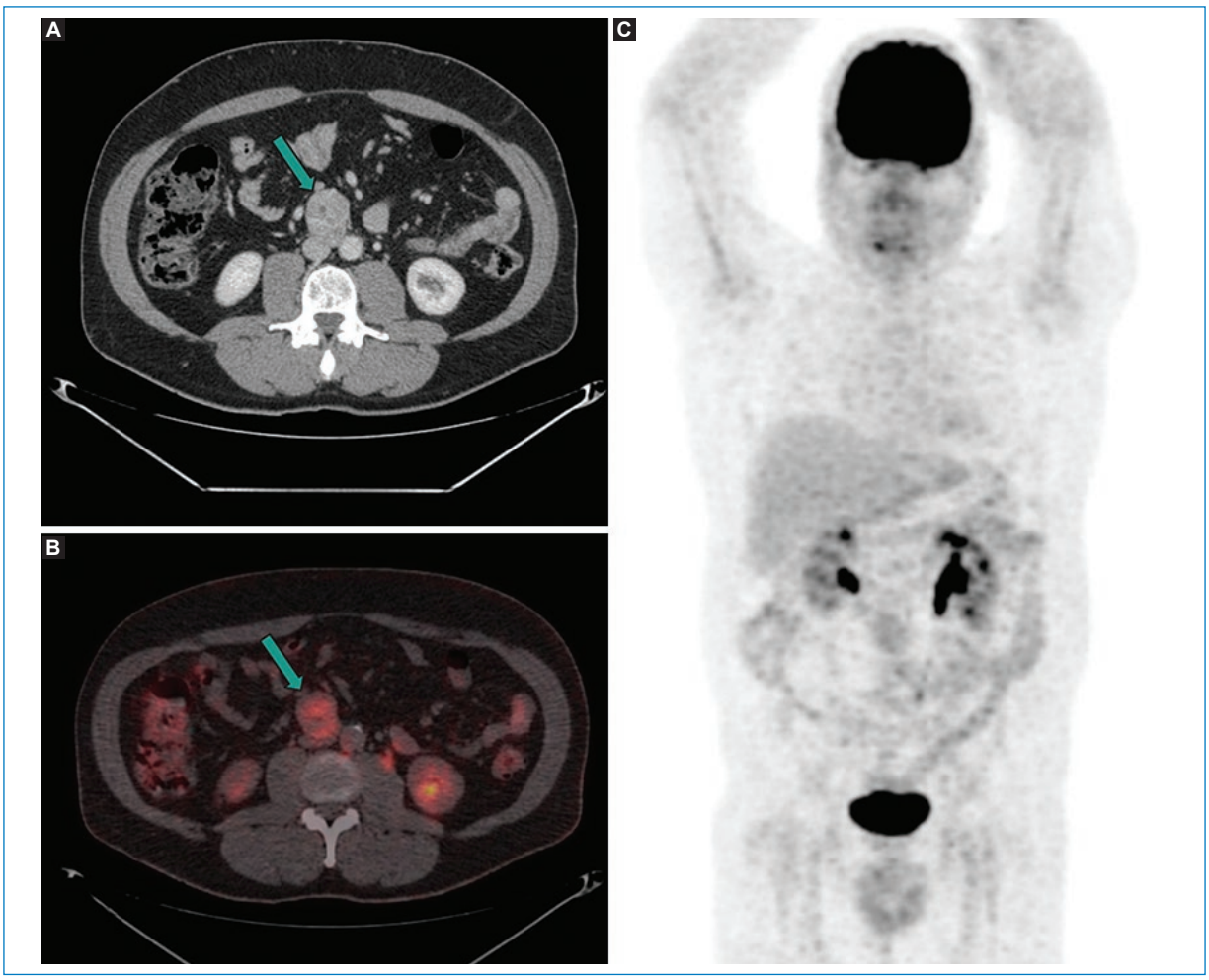

Figure 7. 59-year-old male. Positron emission tomography with 18F-FDG: retroperitoneal nodular lesion, anterior to the vena cava and abdominal aorta, with homogeneous enhancement after intravenous contrast administration (**A**) and tracer uptake (**B** and **C**). Histological diagnosis of retroperitoneal paraganglioma. 18F-FDG: 18F-fluorodeoxyglucose.

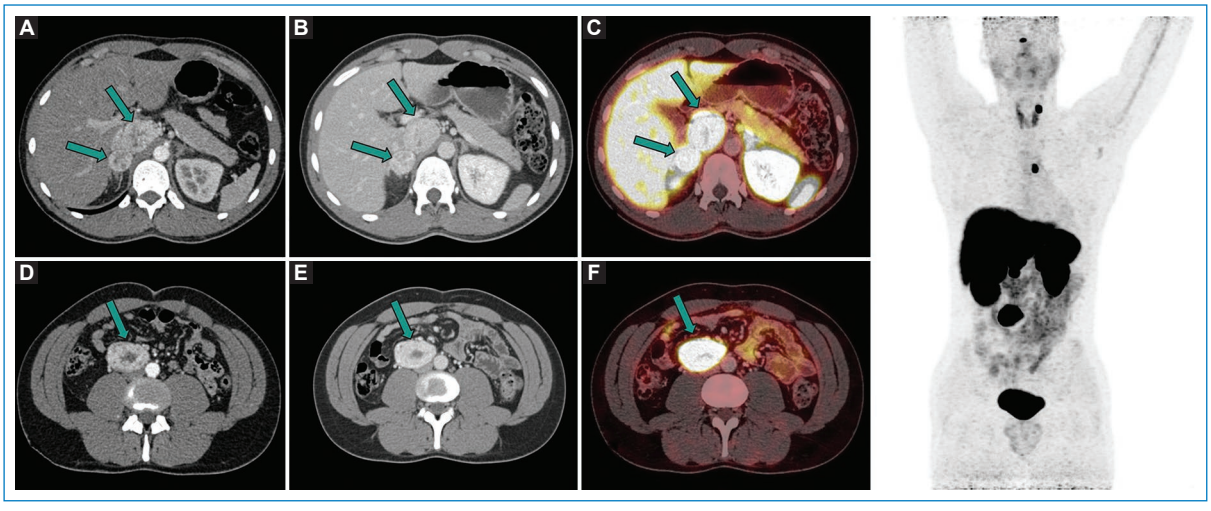

Figure 8. 29-year-old male. Positron emission tomography with DOTATATE: hypervascular lesions in the right adrenal gland and a retrocaval lesion adjacent to this (**A** and **B**), both of which present hypermetabolic activity with tracer uptake (**C**). A third lesion with similar characteristics is observed anterior to the psoas muscle (**D-F**). Histological diagnosis of adrenal pheochromocytoma and retroperitoneal paragangliomas.

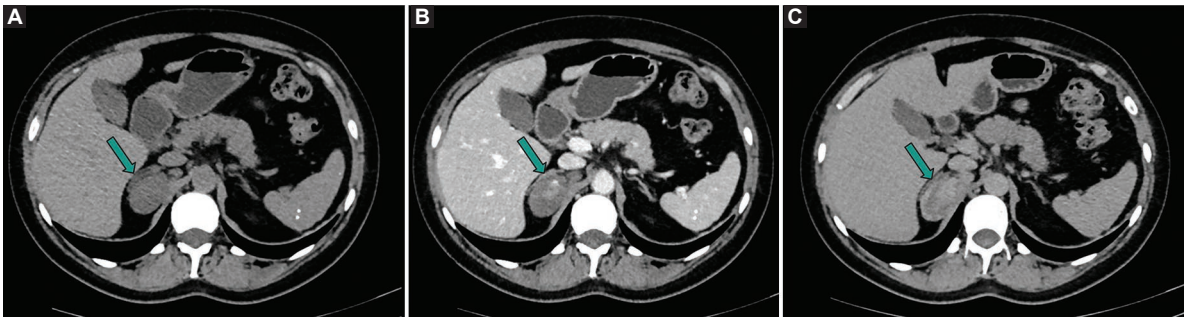

Figure 9. 48-year-old woman. (**A-C**): abdominal computed tomography with intravenous contrast: well-defined nodular lesion (arrow) adjacent to the right adrenal gland with heterogeneous and progressive enhancement. Diagnosis of neurogenic tumor with ganglionic elements, without elements of malignancy.

was a lesion with well-defined margins and heterogeneous enhancement after contrast administration.

Given its superior contrast resolution, MRI remains the imaging study of choice for evaluating tissue composition, delineating lesion margins, and assessing the degree of involvement of adjacent structures[21]. An overlap of imaging characteristics shared by the three cell lines of neurogenic neoplasms on MRI is described: presence of calcifications, high signal on T2-weighted images, cystic areas, potential for spinal canal invasion, bone erosion/remodeling, restricted diffusion on DWI/ADC, and variable enhancement patterns. In our series, the most common findings on MRI were high signal on T2-weighted sequences, varying degrees of diffusion restriction, and heterogeneous enhancement after contrast administration.

Treatment of the abdominal and pelvic neurogenic tumors depends on numerous factors, including histological type, tumor location and size, and the presence of associated complications. In general, complete surgical resection is the therapeutic standard, especially for lesions suspected of malignancy or that present with compressive symptoms. Radiotherapy and chemotherapy are reserved for malignant or unresectable tumors, such as MPNSTs and advanced neuroblastomas[16].

In the context of imaging follow-up, MRI is the preferred modality due to its high contrast resolution and good ability to assess postoperative changes, local recurrences, and metastases. In the lesions associated with type 1 neurofibromatosis, serial MRI allows monitoring of the progression of plexiform neurofibromas and the appearance of malignant transformation. From a functional perspective, 18F-FDG PET is useful in tumors with a high suspicion of malignancy, particularly for evaluating metastatic disease and residual metabolic activity. Additionally, PET with radiotracers targeting somatostatin receptors, such as 68Ga-DOTATATE, has proven useful in characterizing neurogenic tumors expressing these receptors, providing relevant information for staging and therapeutic management in selected cases. Finally, the integration of imaging studies with specific histopathological and genetic markers is crucial for a comprehensive and personalized evaluation of each patient[18].

Conclusion

Neurogenic tumors of the abdomen and pelvis present a diagnostic and therapeutic challenge due to their low incidence and the overlap of imaging characteristics between different subtypes. Clinical-imaging correlation is essential to guide the initial diagnosis, while histopathological confirmation remains the gold standard. The experience accumulated in our case series reaffirms the importance of meticulous imaging follow-up to optimize clinical outcomes and reduce recurrence rates.

Funding

The authors declare that they have not received funding.

Conflicts of interest

The authors declare no conflicts of interest.

Ethical considerations

Protection of human subjects and animal. The authors declare that no experiments on humans or animals were performed for this research.

Confidentiality, informed consent, and ethical approval. The authors have followed their institution's confidentiality protocols, obtained informed consent from all patients, and secured approval from the Ethics Committee. SAGER guidelines have been followed as applicable to the nature of the study.

Declaration on the use of artificial intelligence. The authors declare that no generative artificial intelligence was used in the writing or creation of the content of this manuscript.

References

1. Farma JM, Hassett JM, Poynter L. Benign neurogenic tumors. En: Bland KI, Büchler MW, Sarr MG, Garden OJ, Wong J, Poston GJ, et al., editores. General surgery: principles and international practice. London: Springer; 2022. p. 529-35.
2. Roden AC, Yi ES, Jenkins SM, Edwards WD, Aubry MC, Visscher DW, et al. The distribution of mediastinal lesions across multi-institutional, international radiology databases. J Thorac Imaging. 2019;34:93-102.
3. Shen SH, Xu Z, Zhao J, Wen L, Liu Q, Peng W. MR imaging features of benign retroperitoneal extra-adrenal paragangliomas. Eur J Radiol. 2017;89:192-8.
4. Sassa N, Shiraishi T, Fukuda T, Shimizu Y, Sato Y, Kinoshita H, et al. Retroperitoneal tumors: review of diagnosis and management. Int J Urol. 2020;27:1058-70.
5. Ducatman BS, Scheithauer BW, Piepgras DG, Reiman HM, Ilstrup DM. Malignant peripheral nerve sheath tumors: a clinicopathologic study of 120 cases. Cancer. 1986;57:2006-21.
6. Hamdy NA, Saafan T, Elshalakany AH, Fathy H, Abdelaziz M, Elshafei M, et al. Retrospective cohort study of the characteristics and outcome of surgical treatment of pelvic neurogenic and presacral tumors. BMC Surg. 2022;22:6.
7. Rha SE, Byun JY, Jung SE, Chun HJ, Lee HG, Lee JM, et al. Neurogenic tumors in the abdomen: tumor types and imaging characteristics. Radiographics. 2003;23:29-43.
8. Belakhoua H, Wacrenier A, Forest F, Péoc'h M, Guyétant S, Decouvelaere AV, et al. Diagnostic pathology of tumors of peripheral nerve. Diagn Histopathol (Oxf). 2021;27:263-71.
9. Sangster GP, Do D, Previgliano C, Heldmann M, Otrakji A, Vujic I. The gamut of primary retroperitoneal masses: multimodality evaluation with pathologic correlation. Abdom Radiol (NY). 2016;41:1616-30.
10. Scali EP, Chandler TM, Heffernan EJ, Coyle J, Harris AC, Chang SD. Primary retroperitoneal masses: what is the differential diagnosis? Abdom Imaging. 2015;40:1887-903.
11. Lonergan GJ, Schwab CM, Suarez ES, Carlson CL. Neuroblastoma, ganglioneuroblastoma, and ganglioneuroma: radiologic-pathologic correlation. Radiographics. 2002;22:911-34.
12. London WB, Castleberry RP, Matthay KK, Look AT, Seeger RC, Shimada H, et al. Evidence for an age cutoff greater than 365 days for neuroblastoma risk group stratification in the Children's Oncology Group. J Clin Oncol. 2005;23:6459-65.
13. Lee KY, Oh YW, Noh HJ, Lee YJ, Yong HS, Kang EY, et al. Extra-adrenal paragangliomas of the body: imaging features. AJR Am J Roentgenol. 2006;187:492-504.
14. Aygun N. Pheochromocytoma and paraganglioma: from epidemiology to clinical findings. Cancer Imaging. 2020;20:25.
15. Wasa J, Nishida Y, Tsukushi S, Shido Y, Sugiura H, Nakashima H, et al. MRI features in the differentiation of malignant peripheral nerve sheath tumors and neurofibromas. AJR Am J Roentgenol. 2010;194:1568-74.
16. Reilly KM, Kim A, Blakely J, Ferner RE, Gutmann DH, Legius E, et al. Neurofibromatosis type 1–associated MPNST state of the science: outlining a research agenda for the future. Neurology. 2017;88:e66-e75.
17. Bhaumik S, Hwang M, Wells K, Chhabra A, Soldatos T, Chalian M, et al. Early detection of transformation of plexiform neurofibromas to malignant peripheral nerve sheath tumors in neurofibromatosis type 1. J Pediatr Surg. 2015;50:622-5.
18. Kehrer-Sawatzki H, Cooper DN. The molecular pathogenesis of schwannomatosis, a paradigm for the co-involvement of multiple tumour suppressor genes in tumorigenesis. Hum Genet. 2016;135:129-48.
19. Simsek GG, Cayci M, Akyol M, Yilmaz I, Bektas M, Ozturk S, et al. Comprehensive clinicopathologic characteristics of intraabdominal neurogenic tumors: single institution experience. J BUON. 2021;26:843-9.
20. Rajiah P, Sinha R, Cuevas C, Dubinsky TJ, Bush WH, Kolokythas O. Imaging of uncommon retroperitoneal masses. Radiographics. 2011;31:949-76.
21. McCarville MB. What MRI can tell us about neurogenic tumors and rhabdomyosarcoma. Pediatr Radiol. 2016;46:869-75.

AUSTRAL JOURNAL OF IMAGING
REVISTA CHILENA DE RADIOLOGÍA

PERMANYER

Check for updates

CASE REPORT

First percutaneous cryoablation in Chile as an alternative treatment for renal cancer

Primera crioablación percutánea en Chile como alternativa de tratamiento en cáncer renal

Claudia Moya-Ochoa, Ma. Fernanda Eyssautier-Susarte, Loreto Lara-Pérez, Leonardo Álvarez-Aros, and Patricio Palavecino-Rubilar*

Radiology Department, Interventional Radiology Unit, Hospital Clínico, Universidad de Chile, Santiago, Chile

Abstract

Percutaneous cryoablation is a widely accepted minimally invasive technique for the treatment of renal cell carcinoma (RCC) at stage cT1a. It achieves oncologic outcomes comparable to partial nephrectomy, with high safety standards, reduced pain, and low complication rates. However, in Chile, its implementation has been limited due to high costs and lack of integration into healthcare systems. We report the case of a 71-year-old man with a history of surgically treated urothelial neoplasia, in whom a 12 mm left renal nodule compatible with cT1a RCC was incidentally detected during surveillance. Following multidisciplinary evaluation, curative percutaneous cryoablation guided by computed tomography (CT) was indicated. Three freeze-thaw cycles were successfully performed without immediate or delayed complications. Imaging follow-up at 3 and 6 months demonstrated complete ablation zone without pathological enhancement or evidence of local recurrence. This represents the first documented case of percutaneous cryoablation for cT1a RCC in Chile, marking a milestone in the adoption and implementation of this ablative technique in the country.

Keywords: *Cryoablation. Renal cell carcinoma. Interventional radiology.*

Resumen

La crioablación percutánea es una técnica mínimamente invasiva ampliamente aceptada mundialmente para el tratamiento del carcinoma de células renales (CCR) en estadio cT1a. Su uso ha obtenido resultados oncológicos comparables a la nefrectomía parcial con altos estándares de seguridad, menos dolor y baja tasa de complicaciones. Sin embargo, en Chile su implementación se ha visto limitada debido a su alto costo y falta de integración en los sistemas de salud. Presentamos el caso de un hombre de 71 años con antecedente de neoplasia urotelial operada, en quien, durante el seguimiento, se pesquisó incidentalmente un nódulo renal izquierdo de 12 mm, compatible con CCR cT1a. De forma multidisciplinaria se decidió tratamiento curativo con terapia crioablativa percutánea guiada por TC, realizándose tres ciclos de congelación-descongelación, sin complicaciones inmediatas ni tardías, y sin evidencia de recidiva en el control imagenológico a los 3 y 6 meses. Este representa el primer caso documentado de crioablación percutánea para CCR cT1a en Chile, marcando un hito en la adopción e implementación de esta técnica ablativa en el país.

Palabras clave: *Crioablación. Carcinoma de células renales. Radiología intervencionista.*

***Correspondencia:**
Claudia Moya-Ochoa
E-mail: cmoya@calvomackenna.cl

Date of reception: 17-10-2025
Date of acceptance: 21-02-2026
DOI: 10.24875/AJI.25000070

Available online: 14-07-2026
Austral J. Imaging. (Engl. ed.). 2026;32(3):151-154
www.resochradi.com

Introduction

Renal cell carcinoma (RCC) is one of the most common neoplasms worldwide, and its diagnosis has increased, especially in early stages, thanks to the widespread use and improvement of imaging studies. In the early stages of the disease, the main objective of treatment is to achieve a cure, preserving renal function and minimizing associated complications. Historically, radical nephrectomy has been the treatment of choice, having evolved to less invasive techniques such as partial nephrectomy, which has a high recurrence-free survival rate, although not without complications[1].

Percutaneous ablation represents a minimally invasive alternative that has gained widespread international acceptance, with fewer adverse effects and oncological outcomes comparable to traditional treatment[2]. Among these modalities, freezing ablation or cryoablation is characterized by the application of extremely low temperatures using a probe that induces the formation of ice crystals, capable of generating controlled freezing to cause direct and indirect tissue damage. It is estimated that the rapid cooling of tissues below -40°C produces cell death, affecting not only cell viability but also the tumor microenvironment. Furthermore, it allows visualization of the ablation area without interfering with or generating significant artifacts in the image, in addition to its anesthetic effect and the ability to generate a robust immune response[3].

In our country, its implementation has been particularly later compared to the global trend. Therefore, the objective of this article is to document the first case recorded in Chile of percutaneous cryoablation as an interventional technique in the management of RCC in early stages, contributing to the local experience with this therapeutic alternative.

Case report

A 71-year-old patient with a history of hypertension under treatment and a right ureterectomy for a low-grade, non-invasive papillary urothelial lesion and transurethral resection of the prostate in 2024. He underwent follow-up computed tomography urography (CT urography) where an incidental finding was a 12 mm exophytic lesion in the upper pole of the left kidney, with enhancement in the arterial and portal phases, without involvement of the excretory system or evidence of dissemination, consistent with T1a RCC (Fig. 1). The patient was evaluated by the interventional radiology team, and considering the facts and the patient's preferences, the characteristics of the lesion, and technical feasibility, in conjunction with the urology team, curative treatment with cryoablation therapy was decided upon.

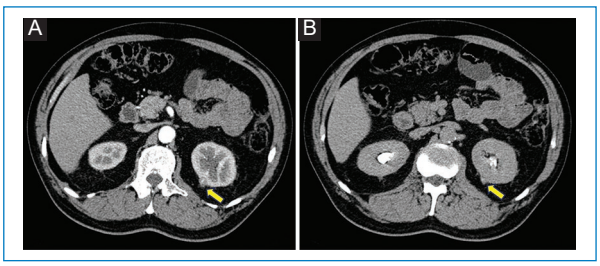

Figure 1. Axial CT scans of the abdomen. **A:** arterial phase, an exophytic lesion (yellow arrow) in the upper pole of the left kidney, posterior aspect, measuring 12 mm in diameter. **B:** in elimination phase, no involvement of the excretory system is observed.

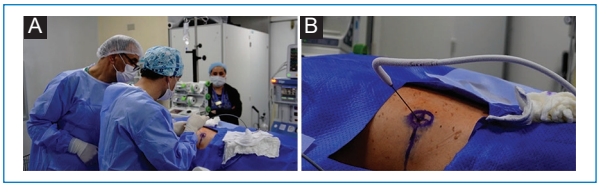

Figure 2. A: placement of the percutaneous cryoablation needle in a cT1a renal tumor guided by computed tomography. **B:** position of the percutaneous cryoablation needle in the skin during the freezing phase.

Procedure

In the prone position, under general anesthesia and guided by CT, the procedure was planned and the access site was marked on the skin (Fig. 2). A cryoablation needle (Boston Scientific IceRod™) was inserted, and three cycles of cryoablation were performed with passive thawing and ablation at 100% power for 10 minutes per cycle. Formation of an "ice ball" was observed covering the entire tumor on all planes with a 10 mm safety margin (Fig. 3).

Following the procedure, the patient recovered well, without pain or immediate complications, and was discharged after 24 hours of observation.

Clinical and imaging follow-up was performed at 3 and 6 months' post-procedure, with no delayed complications recorded. The patient progressed clinically asymptomatic, with preserved renal function. The follow-up CT scan revealed a renal scar at the ablation

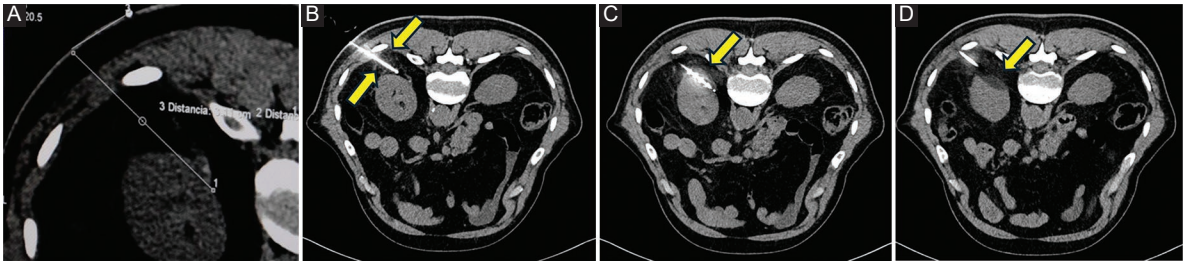

Figure 3. Axial computed tomography slices, in prone position. **A:** pre-procedure planning. **B:** positioning of the IceRod™ cryoablation needle, left posterior approach. **C:** final positioning control prior to the start of cryoablation cycles. **D:** hypodense image corresponding to the "ice ball" covering 100% of the tumor.

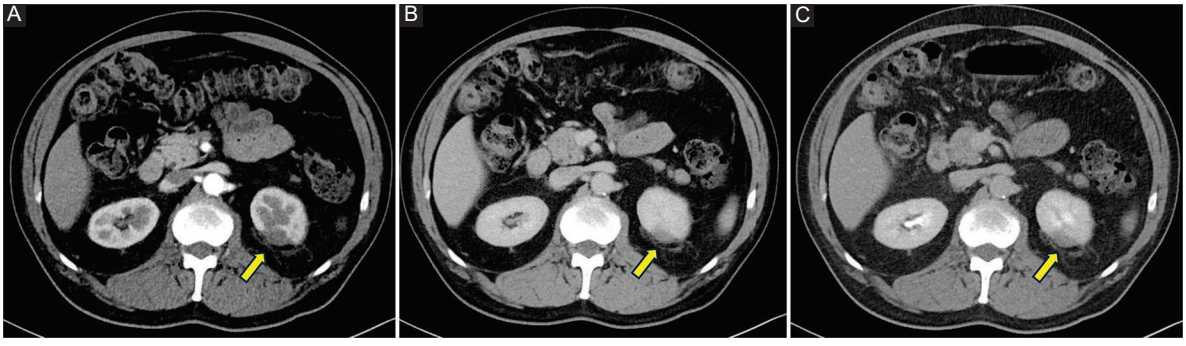

Figure 4. 3-month follow-up. **A-C:** arterial, venous, and delayed/late phases, respectively. A scar is observed in the upper third of the left kidney, without foci of nodular enhancement suggestive of recurrence or surrounding fluid collections.

site, characterized by a well-defined, hypodense area without foci of pathological enhancement or fluid collections, and without evidence of abdominopelvic spread (Fig. 4).

Discussion

Percutaneous ablation for the treatment of early-stage renal tumors has become established as a therapeutic alternative to conventional surgical management, supported by robust global scientific evidence.

A pivotal study published by Thompson et al. in 2015 in *European Urology*[4] compared the outcomes of percutaneous ablation and partial nephrectomy in 1803 patients with cT1aN0M0 renal tumors. The findings demonstrated comparable local recurrence and metastatic free survival rates between the two techniques.

Subsequent studies have confirmed that percutaneous ablation offers comparable oncological outcomes to those of partial or radical nephrectomy in appropriately selected elderly patients, with a lower complication rate. These studies highlight the efficacy of ablation in T1a renal tumors, with advantages in preserving the renal function and a significant reduction in perioperative morbidity, especially in high-risk surgical populations[5].

Other techniques, such as radiofrequency (RF) and microwave (MW) ablation, have also gained ground in the management of renal cell carcinoma (RCC). However, no significant differences in renal cancer-specific survival have been documented, and the characteristics, advantages, disadvantages, and costs of each modality must be considered[6].

Image-guided percutaneous cryoablation allows for precise monitoring of the ablation zone, facilitating the treatment of centrally located lesions near the ureter and collecting system with a lower risk of adverse events and less pain than MW or RF ablation. This, combined with the possibility of performing it under sedation, avoiding the risks associated with general anesthesia, and the ability to use multiple probes

simultaneously, facilitating the treatment of larger lesions, improves its versatility and efficacy[7].

Currently, the American Urological Association (AUA)[8] and the European Association of Urology (EAU)[9] guidelines recommend percutaneous cryoablation as a therapeutic option for cT1a renal tumors (< 4 cm) in patients with significant comorbidities or who are not candidates for surgical resection. However, its adoption in some countries, even developed ones, has been limited due to barriers such as the availability of the technology and its integration into healthcare systems[10].

Despite its late introduction in the country (Chile), this reported case and other cases recently treated in centers in Concepción and Temuco, represent a significant advance and lay the groundwork for expanding its use in our country, with the potential to be integrated into national oncology protocols.

Our initial experience with cryoablation in our local setting has been highly satisfactory, achieving effective local control of the renal tumor, without immediate complications, and with favorable results in short- and medium-term follow-up. These results are consistent with the internationally reported experience, reinforcing the viability and efficacy of the technique in our context.

Conclusion

Percutaneous cryoablation represents a therapeutic option for the management of renal tumors that is widely supported internationally, with results comparable to conventional techniques, and it is feasible to implement and expand its use in our country.

Acknowledgments

The authors would like to thank Dr. M. Borensztein of the Hospital Italiano de Buenos Aires; the interventional radiology team of the Hospital Clínico de la Universidad de Chile: MT. E. Boerr, MT. G. Arenas, RN. T. Medina; the interventional Technician in Higher-Level Nursing (*Técnico en Enfermería de Nivel Superior* - TENS in Spanish) specialists: C. Donoso and L. San-Juan; and the Boston Scientific team.

Funding

The authors declare that they have not received funding.

Conflicts of interest

The authors declare no conflicts of interest.

Ethical considerations

Protection of human subjects and animals. The authors declare that no experiments on humans or animals were performed for this research.

Confidentiality, informed consent, and ethical approval. The authors have followed their institution's confidentiality protocols, obtained informed consent from all patients, and secured approval from the Ethics Committee. SAGER guidelines have been followed as applicable to the nature of the study.

Declaration on the use of artificial intelligence. The authors declare that no generative artificial intelligence was used in the writing or creation of the content of this manuscript.

References

1. Kim SP, Thompson RH, Boorjian SA, Weight CJ, Han LC, Murad MH, et al. Comparative effectiveness for survival and renal function of partial and radical nephrectomy for localized renal tumors: a systematic review and meta-analysis. J Urol. 2012;188(1):51-7.
2. Nowak Ł, Janczak D, Łaszkiewicz J, Guziński M, Del Giudice F, Tresh A, et al. Clinical and oncological outcomes following percutaneous cryoablation vs. partial nephrectomy for clinical t1 renal tumours: systematic review and meta-analysis. Cancers (Basel). 2024;16(6):1175.
3. Erinjeri JP, Clark TW. Cryoablation: mechanism of action and devices. J Vasc Interv Radiol. 2010;21(8 Suppl):S187-S191.
4. Thompson RH, Atwell T, Schmit G, Lohse C, Kurup A, Weisbrod A, et al. Comparison of partial nephrectomy and percutaneous ablation for cT1 renal masses. Eur Urol. 2015;67(2):252-9.
5. Talenfeld AD, Gennarelli RL, Elkin EB, Atoria CL, Durack JC, Huang WC, et al. Percutaneous ablation versus partial and radical nephrectomy for T1a renal cancer: a population-based analysis. Ann Intern Med. 2018;169(2):69-77.
6. Morris CS, Baerlocher MO, Dariushnia SR, McLoney ED, Abi-Jaoudeh N, Nelson K, et al. Society of Interventional Radiology position statement on the role of percutaneous ablation in renal cell carcinoma: endorsed by the Canadian Association for Interventional Radiology and the Society of Interventional Oncology. J Vasc Interv Radiol. 2020;31(2):189-194.e3.
7. Allen BC, Remer EM. Percutaneous cryoablation of renal tumors: patient selection, technique, and postprocedural imaging. Radiographics. 2010;30(4):887-900.
8. Ljungberg B, Albiges L, Abu-Ghanem Y, Bedke J, Capitanio U, Dabestani S, et al. European Association of Urology Guidelines on renal cell carcinoma: the 2022 update. Eur Urol. 2022;82(4):399-410.
9. Campbell SC, Clark PE, Chang SS, Karam JA, Souter L, Uzzo RG. Renal mass and localized renal cancer: evaluation, management, and follow-up: AUA Guideline: Part I. J Urol. 2021;206(2):199-208.
10. Rosiak G, Franke J, Konecki D, Milczarek K, Ostrowski T, Nowaakowski R, et al. T1a renal cancer cryoablation - first experiences in Poland. Pol J Radiol. 2024;89:e453-e456.

AUSTRAL JOURNAL OF IMAGING
REVISTA CHILENA DE RADIOLOGÍA

PERMANYER

Check for updates

CASE REPORT

Optic nerve ischemia secondary to cosmetic procedures with botulinum toxin and platelet-rich plasma injection: report of two cases

Isquemia del nervio óptico secundaria a procedimientos estéticos con toxina botulínica e inyección de plasma rico en plaquetas: reporte de dos casos

*Laura C. Rodríguez-Fonseca[1], Jorge E. Izquierdo-Ordóñez[1], Daniel M. Varón-Orjuela[2], Carlos A. Castro-Galvis[3], and Juan S. Serna-Trejos[4]**

[1]Radiology Service, Universidad del Valle; [2]Neuroradiology Service, Clínica Imbanaco; [3]Medical Emergencies Service, Pontificia Universidad Javeriana; [4]Infectology Service, Clínica Colsanitas S.A., Clínica Sebastián de Belalcázar. Cali, Colombia

Abstract

Facial aesthetic injections have steadily increased; although most are safe, there are rare but devastating complications, as blindness and strokes due to retrograde embolization into the ophthalmic artery. Early clinical-radiological recognition and diffusion-focused imaging protocols are essential. Two cases are described. Case 1: 48-year-old woman with loss of left temporal hemifield after botulinum toxin and calcium hydroxyapatite injection. Angiography: nasal choroidal hypoperfusion consistent with ciliary branch occlusion. Magnetic resonance imaging (MRI): restriction on Diffusion-Weighted Imaging (DWI) and decreased Apparent Diffusion Coefficient (ADC) of the posterior intraorbital segment without FLAIR, consistent with hyperacute ischemia. She received methylprednisolone and follow-up. Case 2: 59-year-old woman with left amaurosis and facial paralysis after platelet-rich plasma injection. Examination: pale papilla and whitish retina. MRI: ischemia of the left optic nerve with muscle edema and two parietal/occipital cortical infarcts. Angiography: occlusion of the ophthalmic artery; NIHSS 0. Both cases support the embolic mechanism, underscoring the diagnostic value of DWI/ADC, the activation of urgent stroke protocols, and prevention based on anatomy, technique, and equipment.

Keywords: *Optic neuropathy ischemic. Retinal artery occlusion. Dermal fillers. Platelet-rich plasma. Adverse effects.*

Resumen

Las inyecciones estéticas faciales han aumentado de manera sostenida; aunque la mayoría son seguras, existen complicaciones poco frecuentes, pero devastadoras, como ceguera e infartos por embolización retrógrada hacia la arteria oftálmica. El reconocimiento temprano clínico-radiológico y los protocolos de imagen centrados en difusión son esenciales. Se describen dos casos. Caso 1: mujer de 48 años con pérdida del hemicampo temporal izquierdo tras inyección de toxina botulínica e hidroxiapatita cálcica. Angiografía: hipoperfusión coroidea nasal compatible con oclusión de rama ciliar. Resonancia magnética (RM): restricción en Diffusion-Weighted Imaging (DWI) y descenso de Apparent Diffusion Coefficient (ADC) del segmento intraorbitario posterior sin FLAIR, consistente con isquemia hiperaguda. Recibió metilprednisolona y seguimiento. Caso 2: mujer de 59 años con amaurosis izquierda y parálisis facial tras inyección de plasma rico en plaquetas. Examen: papila pálida y retina blanquecina. RM: isquemia del nervio óptico izquierdo con edema muscular y dos infartos corticales parietal/occipital. Angiografía: oclusión de arteria oftálmica; NIHSS 0. Ambos cuadros apoyan el mecanismo embólico y subrayan el valor diagnóstico de DWI/ADC, la activación de rutas urgentes tipo ictus y la prevención basada en la anatomía, la técnica y el material.

Palabras clave: *Neuropatía óptica isquémica. Oclusión de la arteria retiniana. Rellenos dérmicos. Plasma rico en plaquetas. Efectos adversos.*

Correspondence:
Juan S. Serna-Trejos
E-mail: juansantiagosernatrejos@gmail.com

Date of reception: 25-08-2025
Date of acceptance: 17-01-2026
DOI: 10.24875/AJI.25000062

Available online: 14-07-2026
Austral J. Imaging. (Engl. ed.). 2026;32(3):155-160
www.resochradi.com

Introduction

The use of facial fillers and botulinum toxin has grown steadily due to their apparent safety profile and quick results. In the United States, more than 1.2 million filler injections were performed in 2008 (≈ 200% increase compared to 1997), and although expected events (pain, edema, ecchymosis) are common, serious complications are rare in large clinical series; for example, 2,089 treatments with only 14 complications in 5 years (2 with hyaluronic acid, 6 with poly-L-lactic acid, and 6 with calcium hydroxyapatite).[1,2]

However, devastating complications do exist, such as blindness, ischemic strokes, and skin necrosis. Its fundamental mechanism is the retrograde embolization of filling material (or direct damage) to the ophthalmic artery and its branches through extensive anastomoses between the external and internal carotid territories (supratrochlear, supraorbital, dorsal nasal, etc.).[3] Among the ocular phenomena, central retinal artery occlusion (CRAO) and ophthalmic artery occlusion (OAO) are emergencies analogous to cerebral stroke. CRAO has an approximate incidence of 1/100,000 inhabitants per year (≈ 1/10,000 consultations) and a low rate of spontaneous functional visual recovery (17.7%); currently, there is no guideline-supported treatment, and the approach is aligned with that of acute stroke management.[4]

The strongest population-based evidence relating to iatrogenic OAO from facial injections comes from a Korean national survey (44 cases) that classified six angiographic patterns (ranging from diffuse retinal/choroid occlusions to localized occlusions and posterior ischemic optic neuropathy), with worst prognosis in the diffuse forms. The injected material influences the risk: autologous fat was associated with worse final visual acuity and a higher incidence of stroke than hyaluronic acid.[5]

Although generally considered “safe” because it is autologous, platelet-rich plasma can also cause irreversible blindness due to OAO immediately after injection into high-risk areas (glabella, nasolabial fold);[6] CRAO and choriocapillary occlusions with characteristic skin scarring have been documented.[3]

Clinical case 1

A 48-year-old woman, previously healthy, presented with visual loss in the temporal hemifield of her left eye, accompanied by headache, a few hours after receiving a facial injection of botulinum toxin and hydroxyapatite. Retinal evaluation with fluorescein angiography revealed nasal sectoral choroidal hypoperfusion consistent with posterior ciliary branch occlusion of the left eye, a finding that topographically explains the temporal visual field defect.

A brain and orbital magnetic resonance imaging (MRI) scan was requested. The images showed marked diffusion restriction in the posterior intraorbital segment of the left optic nerve and hyperintensity on Diffusion-Weighted Imaging (DWI) with a decreased Apparent Diffusion Coefficient (ADC) without correlation on FLAIR, a pattern characteristic of hyperacute optic nerve ischemia and without other parenchymal lesions (Fig. 1). Given the clinical symptoms-imaging concordance, methylprednisolone boluses were administered, and a close ophthalmological follow-up was indicated. The therapeutic objective was to mitigate axonal edema and control a possible inflammatory component, recognizing that the evidence of benefit is limited in optic nerve embolic ischemia.

Clinical case 2

A 59-year-old woman with no prior medical history presented with left-sided amaurosis and peripheral facial paralysis following facial application of platelet-rich plasma. The ophthalmological examination revealed ocular hypotony, conjunctival hyperemia, dyscoric pupil, pale and ischemic optic disc, and whitish retina in the posterior pole and mid-periphery, symptoms suggestive of occlusion of the left ophthalmic artery with extensive retinochoroidal involvement.

MRI of the orbits revealed acute ischemia of the left optic nerve along the entire intraorbital segment (restriction on DWI and descending ADC), with hyperintensity on T2/FLAIR and edema of the extraocular muscles (Fig. 2). Diffusion-weighted MRI of the brain showed acute infarctions in the left parietal and occipital lobes, with DWI/ADC signal without FLAIR translation, consistent with a hyperacute phase without objective cortical neurological deficit, with a score of 0 on the National Institutes of Health Stroke Scale (NIHSS) (Fig. 3). Fluorescein angiography confirmed occlusion of the left ophthalmic artery with optic nerve and retinal ischemia.

The diagnosis of ophthalmic artery occlusion due to retrograde platelet-rich plasma embolization, associated with subclinical cerebral infarctiions, was reported. Outpatient management was provided with vitamin C, sodium hyaluronate, and ophthalmic atropine, with follow-up by neurology and ophthalmology. At the 2-month follow-up, the corneal epithelial defect persisted, with stable functional evolution.

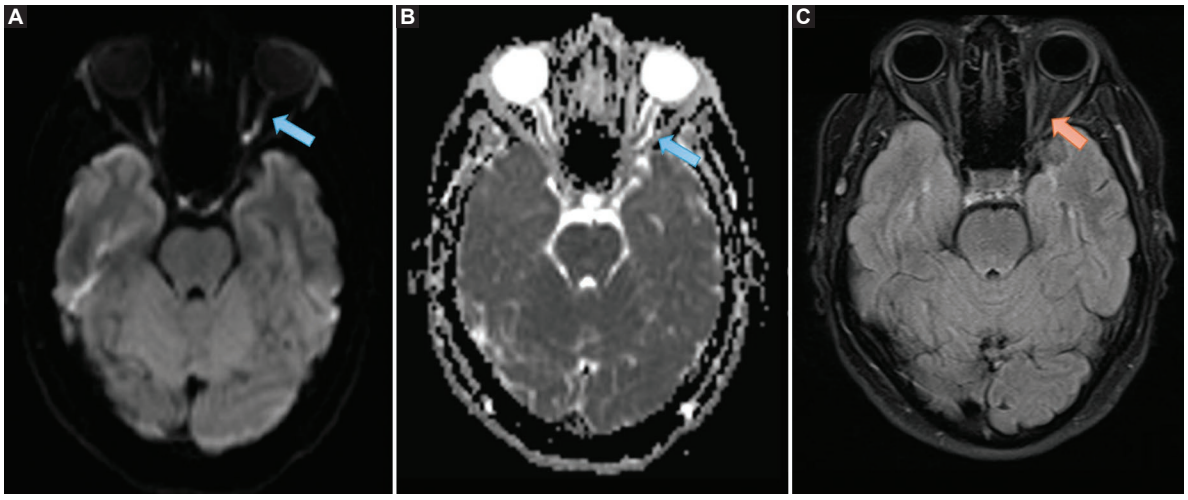

Figure 1. Lesion in the posterior region of the left intraorbital segment with restriction on DWI **(A)** diffusion sequences and ADC map **(B)**, without representation on FLAIR **(C)** sequence, consistent with optic nerve ischemia following a cosmetic procedure (arrow). The left optic nerve is visible **(C**, arrow). No other lesions were found in the remainder of the brain parenchyma.

Discussion

High-pressure injection can introduce the material into a facial artery (e.g., angular, supraorbital, supratrochlear, dorsal nasal) with retrograde flow toward the ophthalmic artery and subsequent embolization into the retina and choroid. The viscosity, cohesiveness, and particle size of the material influence the risk of embolization. This anastomotic network explains the vulnerability of the glabella, nasal dorsum, and periorbita.[3] Angiographic classification (OAO, generalized or localized posterior ciliary artery occlusions, CRAO, retinal artery branch occlusion, and posterior ischemic optic neuropathy) is useful for prognosis: diffuse occlusions are associated with worse initial and final vision, and less visual gain, than localized occlusions. In a Korean series, autologous fat was associated with diffuse OAO, worse visual outcomes, and more cerebral infarctions than hyaluronic acid.[5]

Ocular pain and decreased choroidal vascularity on optical coherence tomography have been proposed as markers for OAO with a poor visual prognosis; furthermore, in OAO due to fillers, all patients reported pain and showed a thinner and less vascular choroid. In some cases with hyaluronic acid, MRI may reveal ischemic optic neuropathy.[7,8] In CRAO, evidence regarding treatment remains limited, and there are no guideline-supported recommendations; initial management is similar to that for stroke and should prioritize urgent referral to centers with neurovascular protocols, considering the

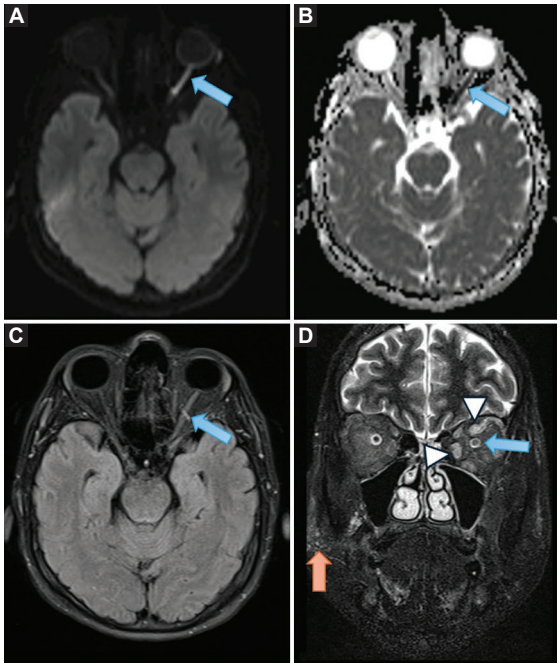

Figure 2. Lesion throughout the intraorbital segment of the left optic nerve, with restriction on DWI diffusion-weighted sequences **(A)** and ADC mapping **(B)**, and hyperintense on axial FLAIR **(C)** and coronal STIR **(D)** sequences compared to the contralateral optic nerve, consistent with an acute infarction of the left optic nerve (blue arrow), associated with hyperintensity of the intraorbital muscles related to edema (arrowhead). Punctate hyperintensities are observed in the right zygomatic subcutaneous tissue related to changes following platelet-rich plasma infiltration (orange arrow).

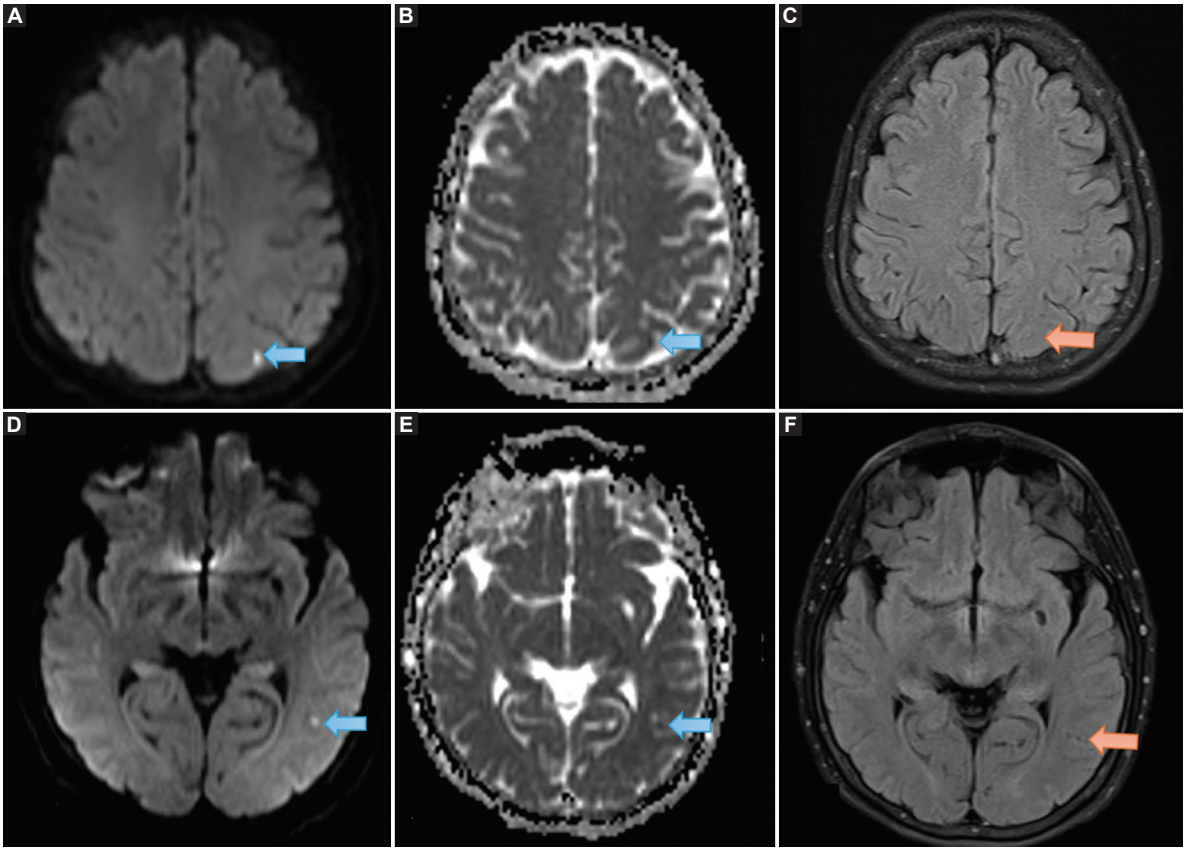

Figure 3. Lesions in the left parietal and occipital regions, presenting restriction on DWI diffusion sequences and ADC mapping (**A, B, D,** and **E**), without representation on FLAIR sequences (**C** and **F**), consistent with an acute ischemic event (orange arrows).

high future cardiovascular risk. In cutaneous vascular involvement due to hyaluronic acid (not intraocular), measures are recommended to restore blood flow (massage, heat, nitroglycerin) and early local hyaluronidase; these algorithms are empirical, and their applicability to the ocular territory is uncertain.[2] Reversibility of retinal artery occlusion is rare, which reinforces the diagnostic and therapeutic urgency.[3]

The glabellar and nasolabial areas are high-risk for injection-related retinal occlusions. Knowledge of the anatomy, technique (low pressure, aspiration, safe planes, microbolus), and material selection are key aspects.[7] The proliferation of non-specialized providers underscores the need for rigorous training and standardized protocols; anatomical consensus statements (although focused on botulinum toxin) emphasize muscular and bony reference points for safe and personalized injections.[2,9] Early recognition of cutaneous ischemia patterns (immediate blanching, intense pain, *livedo*) and facial "danger zones" reduces cases of necrosis and sequelae.[10] Despite its autologous nature, platelet-rich plasma can also cause OAO and CRAO with immediate blindness; in a series of four cases, three occurred with a glabellar injection and one in the nasolabial fold. This challenges the perception of "zero risk" and requires the same level of informed consent and technical caution as with other fillers.[3]

Integrating the clinical-imaging pattern (e.g., optical coherence tomography and MRI findings), the anatomical injection site, the type of material, and the chronology of symptoms will allow the discussion to be anchored in the literature: classifying the type of occlusion (diffuse or localized), arguing the prognosis, and supporting comprehensive management decisions (Fig. 4).

It is worth noting that a major limitation of our cases is the unavailability of angiographic images.

Conclusions

These cases necessitate a translational medicine approach that connects facial-orbital microvascular

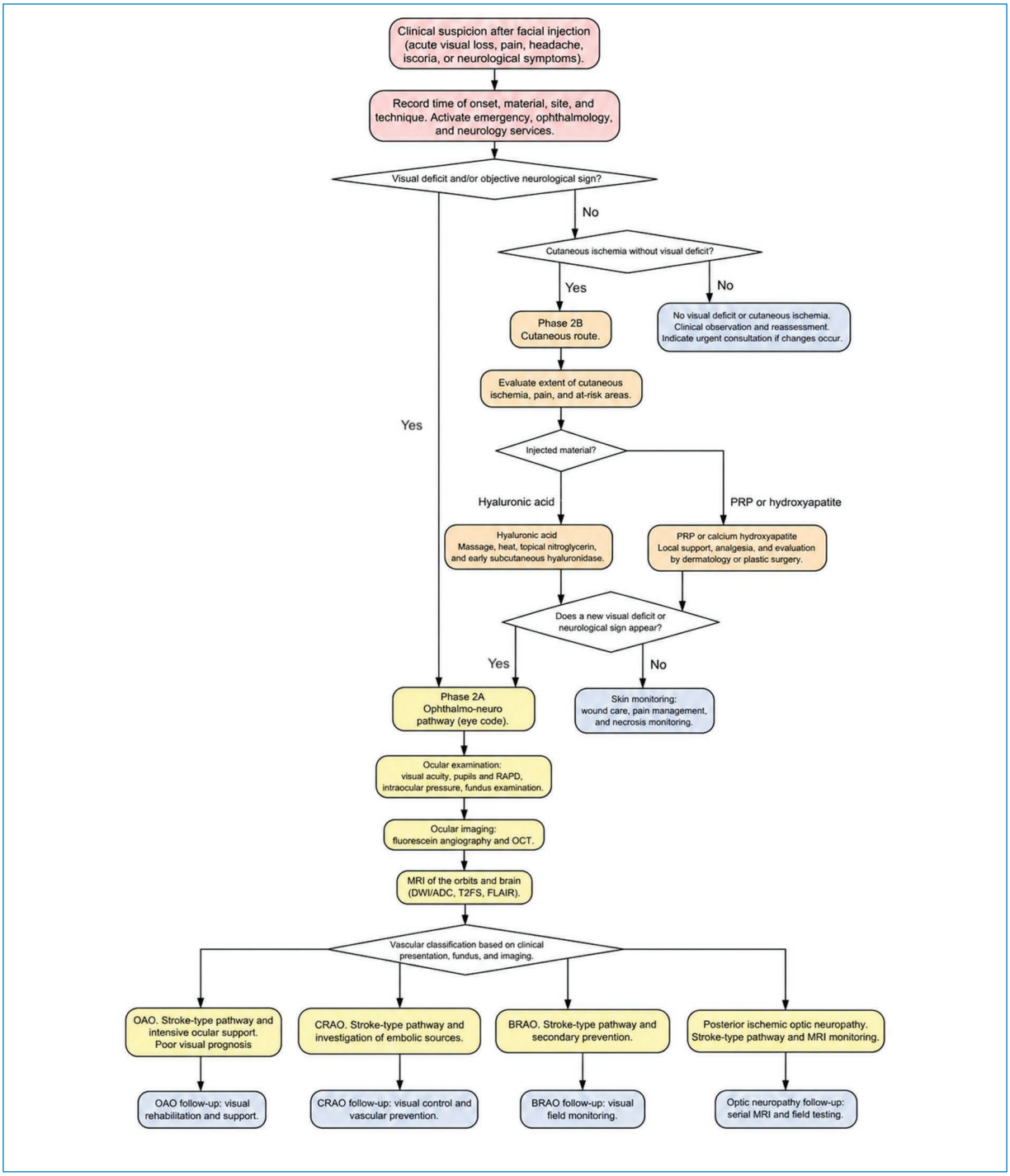

Figure 4. Algorithm for the clinical and imaging management of ocular and neurological complications following facial injections. A decision flowchart is presented for acute visual loss or the appearance of neurological signs after an aesthetic facial injection. It integrates initial triage with recording of the material and technique, ophthalmological evaluation (visual acuity, pupils/RAPD, intraocular pressure, and fundus examination), fluorescein angiography, and OCT, along with MRI of the orbits and brain (DWI/ADC ± FLAIR/T2FS), to classify vascular involvement as ophthalmic artery occlusion, central retinal artery occlusion, retinal artery branch occlusion, or posterior ischemic optic neuropathy, defining a stroke-type pathway for each condition. It also includes a cutaneous branch for ischemia without visual deficit, with differentiated management according to the injected material (hyaluronic acid versus PRP or calcium hydroxyapatite) and a clinical observation pathway when no visual or cutaneous findings are observed. RAPD: relative afferent pupillary defect; PRP: platelet-rich plasma; OCT: optical coherence tomography; OAO: ophthalmic artery occlusion; CRAO: central retinal artery occlusion; BRAO: branch retinal artery occlusion; MRI: magnetic resonance imaging.

anatomy with immediate clinical decisions. We propose integrating into the "eye code" pathway, a coordinated neuro-ophthalmological and neuroradiological evaluation, with specific MRI protocols for the optic nerve and skull, and simultaneous activation of the stroke team. Standardized informed consents should be obtained for cosmetic procedures, along with safety checklists by anatomical area and injection simulations in perfusion models to compare materials and gauges; furthermore, a multicenter registry will allow for estimating the incidence and risk factors, including platelet-rich plasma, and refining preventive strategies.

From a clinical practice perspective, we recommend the ultra-early recognition of critical ocular signs, direct referral to centers with advanced imaging capabilities, and interdisciplinary collaboration (dermatology, plastic surgery, emergency medicine, ophthalmology, neurology, and neuroradiology). In research, priority should be given to optic nerve perfusion studies, the development of accelerated sequences, and the controlled evaluation of selective or enzymatic endovascular procedures (when available), with functional outcomes for vision and brain function. This coordination reduces delays, optimizes prognostic stratification, and lays the groundwork for developing guidelines that harmonize aesthetic safety and neurovisual preservation.

Funding

The authors declare that they have not received funding.

Conflicts of interest

The authors declare no conflicts of interest.

Ethical considerations

Protection of human subjects and animals. The authors declare that no experiments on humans or animals were performed for this research.

Confidentiality, informed consent, and ethical approval. The authors have followed their institution's confidentiality protocols, obtained informed consent from all patients, and secured approval from the Ethics Committee. SAGER guidelines have been followed as applicable to the nature of the study.

Declaration on the use of artificial intelligence. The authors declare that no generative artificial intelligence was used in the writing or creation of the content of this manuscript.

References

1. Bailey SH, Cohen JL, Kenkel JM. Cosmetic medicine review article: etiology, prevention, and treatment of dermal filler complications. Aesthetic Surg J. 2011;31:110-21. doi: 10.1177/1090820X10391083.
2. Daines SM, Williams EF. Complications associated with injectable soft-tissue fillers: a 5-year retrospective review. JAMA Facial Plast Surg. 2013;15:226-31. doi: 10.1001/jamafacial.2013.798.
3. Karam EZ, Gan A, Muci Mendoza R, Martinez E, Perez E. Visual loss after platelet-rich plasma injection into the face. Neuro-Ophthalmology. 2020;44:371-8. doi: 10.1080/01658107.2020.1740936.
4. Madike R, Cugati S, Chen C. A review of the management of central retinal artery occlusion. Taiwan J Ophthalmol. 2022;12:273-81. doi: 10.4103/2211-5056.353126.
5. Park KH, Kim YK, Woo SJ, Kang SW, Lee WK, Choi KS, et al. Iatrogenic occlusion of the ophthalmic artery after cosmetic facial filler injections: a national survey by the Korean Retina Society. JAMA Ophthalmol. 2014;132:714-23. doi: 10.1001/jamaophthalmol.2013.8204.
6. Kassir M, Gupta M, Galadari H, Kroumpouzos G, Katsambas A, Lotti T, et al. Complications of botulinum toxin and fillers: a narrative review. J Cosmet Dermatol. 2020;19:570-3. doi: 10.1111/jocd.13266.
7. Park SW, Woo SJ, Park KH, Huh JW, Jung C, Kwon OK. Iatrogenic retinal artery occlusion caused by cosmetic facial filler injections. Am J Ophthalmol. 2012;154:653-62.e1. doi: 10.1016/j.ajo.2012.04.019.
8. Lucaciu A, Samp PF, Hattingen E, Kestner RI, Davidova P, Kohnen T, et al. Sudden vision loss and neurological deficits after facial hyaluronic acid filler injection. Neurol Res Pract. 2022;4:24. doi: 10.1186/s42466-022-00203-x.
9. Sundaram H, Huang PH, Hsu NJ, Huh CH, Wu WTL, Wu Y, et al. Aesthetic applications of botulinum toxin A in Asians: an international, multidisciplinary, pan-Asian consensus. Plast Reconstr Surg-Glob Open. 2016;4:1-16. doi: 10.1097/GOX.0000000000000507.
10. Kassir R, Kolluru A, Kassir M. Extensive necrosis after injection of hyaluronic acid filler: case report and review of the literature. J Cosmet Dermatol. 2011;10:224-31. doi: 10.1111/j.1473-2165.2011.00562.x.